Differential Scanning and Pressure Perturbation Calorimetric Studies on Proteins Confined in Mesoporous Molecular Sieves

DISSERTATION

zur Erlangung des akademischen Grades
Doktor der Naturwissenschaften
(Dr. rer. nat)

vorgelegt von
M. Sc. Shuang Zhao
aus Shenyang, China

eingereicht beim
Fachbereich Chemie
der Universität Dortmund

Dortmund 2007

Erster Gutachter:	Prof. Dr. R. Winter
Zweiter Gutachter:	Prof. Dr. J. P. Pohl

Tag der mündlichen Prüfung:

To my dear parents

and my beloved husband Xin

Table of Contents

Chapter 1

Introduction

Proteins perform most of the functions of living things, from metabolism to thinking. Textbooks usually show proteins naked, neglect fluctuations, and take little notice of the protein environment. Real proteins, however, are wiggling and jiggling, dressed by the hydration shell, and embedded in a cell or cell membrane. Biochemical reactions in living cells take place in media containing total concentrations of about 400 mg/mL of bio-macromolecules. In such physiological media, besides specific interactions and adsorption phenomena, also nonspecific interactions (such as steric repulsion) between macrosolutes, contribute significantly to the chemical potential and hence stability as well as reaction kinetics of the biomolecules [Ellis 2001, Zhou 2004a]. On the basis of the predictions of statistical thermodynamic models [Minton 2000a, Minton 2001, Zhou 2001], it is surmised that excluded volume effects due to the crowded nature within a cell may play a significant role in the stability, interaction, and function of biomacromolecules [Corma 1994]. (The influence of mutual volume exclusion upon the energetics and transport properties of macromolecules within a crowded, or highly volume-occupied, medium is termed 'macromolecular crowding' [Minton 2000b].) Thus, one might question the completeness of any result obtained by the reductionist approach where biomolecules are characterized in dilute solutions only.

How much of the difference between biochemical reactions *in vitro* and *in vivo* can be attributed to crowding depends upon the particular reaction and the microscopic environment in which the reaction is taking place? For a fairly simple fluid, for example hemolysate which contains primarily hemoglobin, it can be shown that volume exclusion is a dominating factor in this medium [Minton 2006]. However, in a more complex heterogeneous environment such as cytoplasm, crowding is probably just one of several non-specific factors affecting reaction rates and equilibria, such as weak non-specific associations with background molecules or

large structures leading to possible sequestration or adsorption of reactants and/or products. Nevertheless, in a crowded biological fluid, the effects of volume exclusion will always be present and play an important role in influencing macromolecular structure and function, independent of and in addition to the influences of other types of interactions. The ubiquity of this phenomenon in biological fluids has been compared to that of gravity [Minton 2006].

To understand the biochemical processes, which proceed in the living cell, the crowding conditions should be simulated in experiments *in vitro*, thus crowding agents should be added to the solution, or molecular confinement should be used to encapsulate protein. Studies used crowding agents to simulate macromolecular crowding *in vitro* were summarized by Chebotareva *et al.* [Chebotareva 2004]. In all cases, the addition of inert macromolecules (crowding agents) enhanced interaction, increased reaction rates, or shifted the equilibrium to association [Zimmerman 1993, Minton 2001, Hall 2003, Ralston 1990]. New methodical approaches have been developed to study macromolecular crowding. The measurement of sedimentation equilibrium is one of the most powerful methods for the quantitative estimation of macromolecular association in solution [Rivas 1999, Harding 1992, Rivas 2003]. The results obtained [Rivas 2001] provide direct evidence that excluded volume effects can significantly promote the self-assembly of proteins in macromolecularly crowded solutions. To imitate the conditions of molecular confinement, the sol-gel method of protein encapsulation into hydrated pores of silica gel matrix of silicic acid is also used [Eggers 2001a]. Theory predicts that such confinement will stabilize more compact protein structure. This prediction is confirmed by the fact that the thermostability of proteins (lysozyme, α-lactalbumin, apomyoglobin) in pores is significantly increased [Eggers 2001a]. The merit of this approach in studies of protein denaturation is that the undesirable aggregation of unfolded forms of protein molecules is excluded. However, sol-gels were found to be unsuitable for the immobilization of large biomolecules due to their broad pore size distribution [Dave 1994, Bhatia 2000].

The discovery of mesoporous silicate (MPS) molecular sieves opened up new possibilities in many areas of chemistry and material science [Kresge 1992, Zhao 1998a, Zhao 1998b, Yang 1998], including practicalities in studying macromolecular crowding. Microporous materials have a clear advantage over microporous zeolites and zeotype molecular sieves for the immobilisation and transformation of large organic molecules [Corma 1994, Reddy 1994]. For example, they fulfill many of the requirements for enzyme carriers such as high specific surface areas (up to ca. 1500 m^2/g), high specific pore volumes (up to ca. 1.5 cm^3/g), well-ordered pore structures with uniform mesopores adjustable in

diameter from about 15 to 300 Å, sufficient functional groups for enzyme attachment, hydrophilic/hydrophobic character, water insolubility, chemical and thermal stability, mechanical strength, suitable particle form, regenerability, and toxicological safety [Hartmann 2005]. The observation that some enzymes retain their functionality upon immobilization on ordered mesoporous supports triggered significant research activity in encapsulating enzymes as well as other bioactive components. Examples of a variety of biological molecules adsorbed onto ordered mesoporous silica and carbon materials were summarized by Hartmann [Hartmann 2005]. Immobilized enzymes in mesoporous materials have found applications in peptide synthesis [Xing 2000], pulp bio-bleaching [Sasaki 2001], biocatalysis [Deere 2003, Han 2002] and biosensors [Liu 1997a, Liu 1997b, Liu 2003, Heilmann 2003]. Most studies have been carried out using the hexagonal MCM-41-type/SBA-15-type material because of its easy availability and good reproducibility in synthesis and modification. Much less attention has been paid to MCM-48 [Kisler 2001a, Washmon-Kriel 2000].

To create more suitable biocatalysts, biosensors, or to separate proteins by using MPSs, it is of great importance to understand the factors that influence the immobilizing behaviour of proteins within MPSs. It has been found that two factors may greatly influence the immobilization properties of MPSs. The first is the size of the mesopore, or more specifically, the mesopore size with relative to the protein molecule size. Diaz and Balkus found that the amount of protein loading into mesoporous silica MCM-41 in a limited contact time decreased with increasing protein molecular weight [Diaz 1996]. This is expected if the pore size of the mesochannels are sufficiently large for ‘comfortable’ entrapment of biomolecules [Han 2002, Deere 2002]. Kisler *et al.* have demonstrated that the rate of adsorption in MCM-41 materials depends strongly on the adsorbing molecular size relative to the pore size for a range of biomolecules [Kisler 2001a]. The second factor that influences the immobilizing behaviour is the surface characteristics of the MPSs and proteins. The surface charges of MPSs and the proteins must be complementary, because it is generally accepted that the electrostatic interaction between protein and MPSs is one of the most important factors that influence adsorption and desorption [Wachmon-Kriel 2000, Han 2002, Deere 2002, Lei 2002, Kisler 2001b, Han 1999]. Some researchers studied the factors that may influence the surface properties of proteins, for example, the pH [Diaz 1996, Han 2002] and ionic strength [Deere 2002] of the protein solution. Takahashi *et al.* [Takahashi 2001] believe that MCM-41 and SBA-15 prepared with cationic and non-ionic surfactants, respectively, have different surface characteristics, and therefore different properties of adsorption. Lei *et al.* reported that suitable organically functionalized mesoporous hosts provide higher affinity for charged protein

molecules and the more favoured microenvironment results in exceptional immobilizing efficiency [Lei 2002]. Wright and coworkers have also investigated the adsorption and desorption property of SBA-15 functionalized by thiol, chloride, amine, and carboxyl groups and it has been found that the interactions of the enzyme-support depended strongly on the nature of the functional groups attached to the surface [Yiu 2001]. Fan reported that the amount and size of entrance in mesoporous materials may greatly influence the bioimmobilization behaviours of MPSs [Fan 2003a, Fan 2003b], and it has been revealed that for SBA-15 type MPSs, the morphology plays an important role in the immobilization ability [Lei 2004]. On the other hand, some protein adsorption behaviours have not been well understood. Deere *et al.* suggested that the hydrophobic interactions dominate rather than electrostatic interactions in the desorption process of cytochrome c (cyt c) from commercial Kieselgel silica [Deere 2002]. Lei *et al.* [Lei 2002] believed that there are electrostatic, H-bond, and hydrophilic interactions between protein and MPSs functionalized by amine and carboxyl groups. Czeslik and coworkers studied the adsorption of lysozyme (LYZ) at the silica/water interface: The attractive Coulombic interaction between LYZ molecules and the silica surface should lead to an exothermic adsorption process, but they found that the adsorption process was endothermic. Then they arrived at the conclusion that the attractive Coulombic interactions must be overcompensated by repulsive protein–protein interactions [Jackler 2002]. In the investigations of bioimmobilization within the same MPSs (*e.g.* SBA-15), their immobilization behaviours of similar proteins may be varied significantly according to different researchers [Takahashi 2000, Han 2002]. Thereby, there should exist other factors that have been ignored during former studies. Considering the large pore volume (~1.0 cm^3/g) of MPSs, the previously reported specific immobilization capacity of MPSs is still relatively low (<200 mg/g) [Han 2002, Lei 2002, Deere 2001, Takahashi 2001]. Furthermore, it often takes several hours, even four days for the immobilization of proteins to reach equilibrium [Deere 2002, Kisler 2001].

Based on simple models, the qualitative effects of confinement and crowding on the equilibria and rates of protein folding and binding were summarized by Zhou as follows [Zhou 2004b]: (1) confinement stabilizes proteins and may accelerate their folding significantly; (2) crowding is expected to have only a marginal effect on protein stability, but may accelerate folding; (3) crowding may significantly shift the binding equilibrium of proteins toward the bound state; as such it may contribute to protein aggregation and amyloid formation; (4) crowding significantly slows down protein diffusion; for diffusion-limited protein binding, this slowing down will moderate the positive effect of crowding in enhancing

the equilibrium probability near contact, and may even result in an overall decrease in the binding rate.

The stability of adsorbed enzymes should be discussed within two different concepts of enzyme stability: one is the intrinsic enzyme stability and the other is the operational enzyme stability. By definition, the intrinsic stability represents the stability of enzyme molecules themselves while the operational stability means the persistence of the enzyme activity during a process, *i.e.*, under conditions of use.

In general, the intrinsic stability of protein depends on temperature, pressure, its hydration capacity and solvent properties. The in-depth knowledge of the thermodynamical properties of proteins in solution that determine their stability and folding characteristics, has been a major issue of many research groups over the last decades [Fersht 1999, Timasheff 1993, Gregory 1995], as these form the basis for understanding the physiologival functions, and the use in drug designing and formulations of proteins. An important factor contributing to the stability of proteins is their relative affinity towards a particular reagent (co-solvent) in comparison to water or buffer solution. The use of co-solvents, such as glycerol, has been gaining much importance, primarily because of their ability to stabilize the folded protein through a mechanism, which may not involve direct contact, but rather alter the hydration layer around the protein. It has been proposed that the driving force for stabilization the protein conformation is a non-specific solvation effect in which the preferential exclusion of solvents from the protein surface arises from enhanced solvent ordering (structure makers) [Timasheff 1993, Gregory 1995, Brandts 1967, Pohl 1969]. In contrast, when denaturating co-solvents bind to proteins, water-protein and water-ligand interactions are replaced by relatively stronger ligand-protein interactions with a concomitant release of water molecules into the bulk phase. Furthermore, these compounds tend to reduce the solvent ordering (structure breakers) [Bennion 2003]. The structure-making and structure-breaking tendency of the protein's surface itself on protein-bound water has been discussed extensively by Lin *et al.* [Lin 2002]. Their results indicate that hydrophilic groups, such as charged or polar side chains of proteins, if they are exposed or come into contact with the surrounding water, show a the characteristic pattern of structure breakers with a large positive apparent expansion coefficient of the protein, in particular at low temperature, which decreases drastically with increasing temperature. On the contrary, apolar, hydrophobic amino acid side groups act in the reverse manner, as structure makers, by enhancing the space consuming hydrogen-bonded network structure of water, particularly at low temperature. This is accompanied by a decrease in solvent density around the hydrophobic groups. Aliphatic side chains, for example, are known

to have even negative apparent thermal expansion coefficients, α, at low temperatures (near 0 °C) with a large positive temperature coefficient [Lin 2002]. Increasing thermal energy, however, allows the water molecules to release from this expanded ordered solvation state. Hence, in general, for proteins in dilute aqueous solutions, the temperature dependent thermal expansion coefficient is drastically influenced by protein-water interactions and thus also by the accessible surface area (ASA) of the protein. Moreover, irrespective of whether co-solvents directly interact with or are rejected by the protein, they induce definite changes in the quantity of bound water and its associated properties [Lin 2002, Gekko 1981, Smith 1999, Timasheff 1998]. The stabilizing effect by a kosmotrope such as glycerol was assumed to be due to preferential hydration of the protein, *i.e.*, exclusion of the glycerol molecules from the surface of the protein, thus leading to marked increment in hydrated layers around the protein, which then causes an enhancement of protein stabilization. On the contrary, a chaotrope, such as urea, destabilizes the protein by direct ligand binding and restricts direct water contact with the protein surface. This preferential binding to the protein reduces the hydration level and also affects the peptide bonds causing the protein to approach a more disordered, random coil like state at high denaturant concentration.

The enzyme leaching from host materials can seriously affect the operational stability. In most studies with adsorbed enzymes, the operational enzyme stability was discussed rather than the intrinsic enzyme stability, due to the difficulties in dissecting the intrinsic enzyme stability from the results of operational enzyme stabilities. However, several recent papers discussed the improvement of intrinsic enzyme stability by confining enzymes in mesoporous materials [Ping 2003, Ping 2004]. This confinement can restrain enzyme unfolding or denaturation when it is located in a pore of similar dimensions or crowded by a high concentration of enzyme molecules in the same pore. The stabilization mechanism with adsorbed enzymes in mesoporous materials has been a topic of many studies, not only for practical applications, but also for scientific interests due to the resemblance of highly concentrated enzymes in mesoporous materials to the cellular environments containing high concentration of biomolecules [Minton 2001, Zhou 2001, Ping 2003]. Many factors are known to affect the stability of adsorbed enzymes in mesoporous materials. First, the pore size of mesoporous materials affects the adsorption behaviour and enzyme leaching [Diaz 1996, Takahashi 2000, Takahashi 2001, Yiu 2001, Fadnavis 2003, Fan 2003b, Jie 2004, Vinu 2004b]. Larger enzymes than the pore size of mesopores cannot be adsorbed into mesoporous materials. Size matching between pore size and the molecular diameter of enzymes plays a key role in achieving high enzymatic stability [Takahashi 2000, Takahashi 2001]. On the

contrary, mesoporous materials with large pore size usually end up with poor enzyme loading as well as poor enzyme stability by letting the adsorbed enzymes leach out very quickly from mesopores. The pore volume is also proven to determine the final amount of enzyme adsorption [Diaz 1996, Takahashi 2000, Vinu 2004a]. Second, the charge interaction is also important in determining the enzyme stability in mesoporous materials [Han 2002, Lei 2002, Vinu 2004a, Vinu 2004b]. The idea is simple: if the net surface charge of enzymes is opposite to the charge of the mesopores, it will not only expedite the enzyme adsorption, but may also lead to a stable enzyme system due to the attractive interaction between two opposite charges; on the other hand, when enzymes and mesopores have the same charge, both enzyme adsorption and stability are poor due to the repulsion between the enzymes and the internal surface of mesopores. The charge status of enzymes and mesopores can be controlled by changing the pH of buffer solution [Vinu 2004a, Vinu 2004b] and functionalizing mesoporous materials with amino or carboxyl groups [Lei 2002]. Finally, a hydrophobic modification is also known to affect the enzyme stability. Especially, lipase is stable and active in a hydrophobic environment, and Blanco demonstrated that strong hydrophobic interactions could enhance the stability of lipase in mesoporous silica functionalized with octyltriethoxysilane [Blanco 2004]. Various nanostructures for enzyme stabilization were reviewed by Kim [Kim 2006].

The model protein used in this work is ribonuclease A (RNase A). RNase A is a single-domain protein, a pancreatic enzyme that catalyzes the cleavage of single-stranded RNA, which consists of 124 amino acid residues with a molecular mass of 13.7 kDa. Bovine pancreatic RNase A is a nearly spherical (radius of gyration ca. 15 Å [Panick 2000]) basic protein with isoelectric point (PI) of 9.6. The protein structure is schematically shown in Fig. 1.1. This protein has traditionally served as a model for protein folding because it is small and stable and has a well-know native structure. The influence of various types of co-solvents on the expansivity as well as the denaturation temperature, relative volume and enthalpy change upon unfolding have been reported for this protein in bulk solution [Ravindra 2003b].

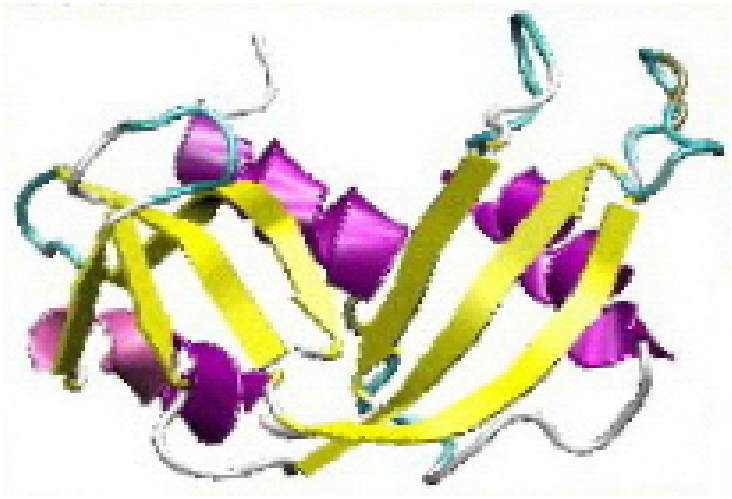

Fig. 1.1. Schematic drawing of the native structure of bovine pancreatic RNase A.

The rationale of this work was to gain insight into the effects of excluded volume and confinement on protein un/refolding and stability. We encapsulate the model protein RNase A in the 25 Å mesopores of MCM-48, 58 Å mesopores of SBA-15, 40 Å mesopores of C_{16}-MCM-41, and 30 Å mesopores of C_{12}-MCM-41 supports with glass wall structure and well-defined pores to create a confined hydrophobic microenvironment. There are only a few direct techniques, which are able to probe the physicochemical properties of proteins in silicate [Deere 2003, Nocek 2002, Bhatia 2000, Behrens 1993, Han 1999, Lei 2002, Weetall 1996]. In this work, the differential scanning (DSC) and pressure perturbation (PPC) calorimetric techniques are employed to evaluate the stability, hydration, and volumetric properties of the confined protein. Further influence of the solution pH and of the addition of co-solvents on the protein immobilization and on the thermal stability of the confined protein is also reported.

Chapter 2

Theory

2.1 Thermodynamic and volumetric properties of protein

In general, the intrinsic stability of proteins depend on temperature, pressure, its hydration capacity and solvent properties. The mechanism of unfolding may differ, however, for different treatments. For example, an important factor contributing to the stability of proteins is their relative affinity towards a particular reagent (co-solvent) in comparison to water or buffer solution. Denaturation by urea or GuHCl is accompanied by the binding of co-solvents to protein molecules [Dunbar 1997] in combination with non-specific effects due to modifications of the solvent [Vidugiris 1995]. The effect of pressure on the stability of proteins is due to the volume of the protein-solvent system being smaller in the unfolded state of the macromolecule than in its folded state. At higher temperatures, high entropy states are favoured. When it is above the unfolding temperature of the protein, ΔG of unfolding becomes negative because the entropy term ($-T\Delta S$) overcompensates the enthalpy part (ΔH). ΔS and ΔH themselves, however, are also dependent on temperature. They both increase with temperature, but the absolute value of the entropy term $-T\Delta S$ increases faster [Becktel 1987].

Proteins undergo a transition, or 'melting', between a structured, native and biologically active conformation (N) and an unstructured, denatured and inactive conformation (D) when temperature is increased in a physiologically relevant range. They share this behaviour with many other biological macromolecules (DNA, lipids *etc.*) and with organic polymers in general. If some property (signal) from the protein that reports on this conformational transition is followed, then a sigmoidal trace such as shown in Fig. 2.1 will be seen. When the structure of the protein is 'melted' in this way there are no changes to the covalent nature of the molecule. It is only non-covalent interactions that are perturbed and, in

many cases, if the protein is cooled down again, these interactions will reform spontaneously, yielding the active native conformation. Then, N and D are in reversible equilibrium with temperature as an intensive variable:

$$N \leftrightarrow D \tag{1}$$

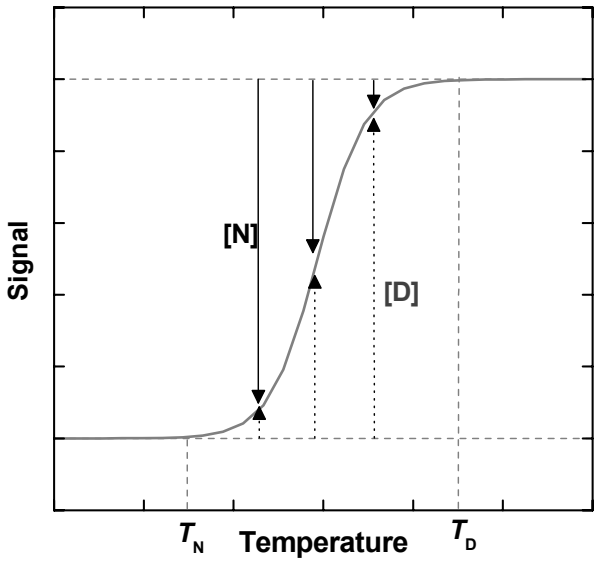

Fig. 2.1. Typical sigmoidal transition for the denaturation of a protein. Below T_N the protein is essentially native, above T_D the protein is denatured. Between these temperatures, the relative occupancy of each state is indicated by the length of the solid line and dot line arrows, respectively.

In Fig. 2.1, the proportions of N and D change as this equilibrium is driven toward D with increasing temperature can be seen. At any temperature, an equilibrium position, the equilibrium constant (K_{eq}), can be defined, which reflects the relative concentrations of N and D. On a logarithmic scale, this equilibrium constant is expressed in the standard Gibbs free energy change of unfolding, ΔG^0:

$$K_{eq} = \frac{[D]}{[N]} \tag{2}$$

$$\Delta G^0 = -RT \ln K_{eq} \tag{3}$$

with R, the gas constant, and T, the temperature in degrees Kelvin. The temperature at which the concentrations of D and N are equal is defined as the midpoint of the transition or melting temperature T_m. At this temperature, K_{eq} is equal to 1 and ΔG^0 is 0. The T_m is an important parameter for any protein since it indicates its thermal stability. Below this temperature, the concentration of the native protein is higher than the denatured one, while above the T_m, more

of the protein is denatured. The reason that proteins undergo this melting behaviour is because their native structures are stabilised by numerous interactions that are temperature dependent themselves. Stabilisation by enthalpy (ΔH) requires interactions involving bond making, structuring and reduction in internal energy, while stabilisation by entropy (ΔS) reflects disordering interactions and increasing the number of ways the system can be organised with the same energy. These terms are related to ΔG in the familiar equation:

$$\Delta G = \Delta H - T\Delta S \tag{4}$$

Combining Eqs. (3) and (4) and rearranging gives the van't Hoff Eq. (5) from which the variation in equilibrium constant with temperature can be plotted to yield the enthalpy and entropy change of thermal denaturation in a simple linear relationship ($\ln K_{eq}$ versus $1/T$):

$$\ln K_{eq} = -\frac{\Delta H}{RT} + \frac{\Delta S}{R} \tag{5}$$

The data in Fig 2.1 can be used to determine K_{eq} at temperatures in the transition region and from this evaluate ΔH and ΔS for the process.

To perform their biological functions, globular proteins should be in a water milieu and should also possess a unique tertiary structure with a sizeable core of water-inaccessible amino acid residues [Chothia 1984, Kuntz 1974, Richards 1992, Rupley 1991]. It must be noted, however, that there is a growing body of recent evidence suggesting that there are exceptions to these rules. Some proteins may be partially or fully functional in their so-called "natively unfolded" conformation [Uversky 2002a, Uversky 2002b, Uversky 2000, Wright 1999], while other proteins may retain significant enzymatic activity in a number of hydrogen-bonded non-aqueous liquids [Burova 2000, Klobanov 1997, Klibanov 2001, Knubovets 1999, Rariy 1997]. Notwithstanding, these observations are exceptions rather than a general rule. In native globular proteins, amino acid residues buried inside the solvent-inaccessible interior are tightly packed, although the packing is not perfect with ample intraglobular voids [Chotia 1984, Rashin 1986, Richards 1977, Richards 1985, Richards 1992, Richards 1994]. Nearly all these voids are made up of small cavities that cause native proteins to undergo dynamic fluctuations in structure [Gregory 1995, Richards 1992, Vanderkooi 1998]. In the course of these fluctuations, the size of intraglobular cavities varies owing to thermally activated vibrations of surrounding atoms. Such fluctuations (or mobile defects) facilitate the conformational dynamics of proteins, in particular, allowing the rotation of side chains [Chothia 1984].

Dynamic fluctuations of the protein between the nearly isoenergetic native-like subconformations cause fluctuations of the intrinsic volume. The mean-square fluctuations of the intrinsic volume, $\langle \delta V_M^2 \rangle$, in this case represent an effective, quantitative means of estimating protein dynamics. Significantly, δV_M, the mean amplitude of volume fluctuations, is uniquely related to the intrinsic coefficients of isothermal compressibility, β_{TM}, and thermal expansibility, α_M, of the protein molecule (Cooper 1976, Cooper 1984):

$$\left\langle \delta V_M^2 \right\rangle = k_B T V_M \beta_{TM} \tag{6}$$

$$\left\langle \delta U_M \delta V_M \right\rangle = k_B T V_M \left(T\alpha_M - p\beta_{TM} \right) \tag{7}$$

where k_B is Boltzmann's constant, T is the absolute temperature, p is the pressure, and δU_M is the mean amplitude of fluctuation of the intrinsic energy accompanying thermally activated subconformational transitions of the protein. Inspection of Eq. (6) and (7) reveals that the value of V_M can be used in conjunction with β_{TM} and α_M for quantitative characterization of the conformational dynamics of the protein as reflected in the values of δV_M and δU_M.

Much theoretical and experimental effort has gone into the thermodynamic, structural, and dynamic characterization of protein hydration, which represents a major determinant of the energetics of protein stability and recognition (Kuntz 1974, Rupley 1991). In this respect, volumetric measurements may provide useful and, in many respects, unique information about protein hydration. Interactions between solvent-exposed atomic groups of proteins and adjacent water molecules can cause the latter to exhibit thermodynamic properties distinct from those of bulk water. In particular, water of protein hydration is distinct from bulk water with respect to its partial molar volume, compressibility, and expansibility. Hence, these observables can be and have been used to discriminate between the populations of water of protein hydration and bulk water.

Protein hydration, as well as its packing and dynamics, generally changes in the course of protein folding and binding events. Consequently, volumetric measurements can be used in protein-recognition studies for identifying and quantifying changes in hydration, packing, and dynamics of a protein that are associated with its conformational transitions or complexation with other molecules. The importance of volumetric data for the thermodynamics of protein folding was already emphasized 20 years ago by Kauzmann [Kauzmann 1987], who explicitly stated that no thermodynamic theory of protein folding and other conformational transitions can be considered valid unless it provides rationalizations for both temperature-dependent (calorimetric) and pressure-dependent (volumetric) data.

Recently, it has been pointed out again that conformational fluctuations of proteins are also significantly influenced by the solvent properties [Fenimore 2002]. These fluctuations permit conformational motions, for instance, flips of the side chains and motions of the backbone, thus causing transitions among the various conformational substrates of proteins, which occur also in their native state and are essential for their function. It has been shown that the solvent fluctuations may even overwhelm the intrinsic fluctuations of the protein and its hydrations shell [Fenimore 2002]. Hence, the fluctuations in the hydration shell and of the (in particular) charged residues consequently are controlled by the solvent and produce volume, enthalpy and volume fluctuations in the protein. The hydration shell and amino acid residues thus couple the protein to the surrounding thermal bath, and the solvent is thus considered an active participant in protein dynamics and folding. It can be shown from Eq. (7) that the coefficient of thermal expansion of a protein system, α, is related to the magnitude of its thermally activated enthalpy (δH) and volume (δV) fluctuations as follows [Hill 1962, Chalikian 2003]:

$$\langle \delta H \delta V \rangle = k_{\mathrm{B}} T^2 V \alpha \tag{8}$$

This reveals that a larger value of α may indicate a larger magnitude of volume fluctuations, a large magnitude for enthalpy fluctuations, or both. Information on enthalpy fluctuations can be obtained directly from the heat capacity, C_p, as $\langle \delta H^2 \rangle = k_{\mathrm{B}} T^2 C_p$, and as mentioned previously in Eq. (6), information on the volume fluctuations can be obtained directly from the isothermal compressibility.

2.2 Measurements of thermodynamic and volumetric data

Not surprisingly, calorimetry, from the Latin, *calor*, meaning heat, and *metrium*, to measure, is the only way to determine directly the enthalpy change for denaturation of a protein. Ultra sensitive calorimeters, such as the MicroCal VP-DSC, suitable for accurately measuring enthalpies from fractions of mg of material are available. These instruments are simple to use, accurate and reliable, making calorimetric measurements of this type a routine part of any biophysical lab. They work by measuring the heat capacity, C_p, of a sample of protein solution while scanning up or down in temperature. C_p is simply the amount of energy required to raise the sample temperature some amount, normally 1 K and is related to enthalpy change in Kirchoff's law:

$$\Delta H = \int_{T_N}^{T_D} C_p \cdot \mathrm{d}T \tag{9}$$

The excess (differential) heat capacity of the protein is measured relative to a carefully matched solvent reference cell during the scanning and hence these types of instruments are known as differential scanning calorimeters (DSC).

The DSC measurement is similar to Fig. 2.1 except that now the property of the protein followed during the denaturation is its heat capacity. A conformational transition such as in Fig. 2.2 will be observed.

From Eq. (9) it is clear that to obtain the enthalpy change one must simply integrate the excess heat capacity function. Before doing this, one has to remove the instrumental baseline which is observed when both the sample and the reference cells contain solvent only. For technical reasons, the instrumental baseline does not give a zero excess heat capacity between the cells (dash line, Fig. 2.2). Having removed this instrumental contribution, one has to extrapolate the linear regions on either side of the transition peak, which represent the heat capacity of the native and denatured states of the protein, into the transition region and then merge them in relation to the progression through the transition. This is done with software routines. Finally, one can integrate the area under the resulting peak to give the excess energy that the DSC requires to denature the protein in the sample cell. Providing the concentration of the protein solution and the operational volume of the calorimeter cell, this energy can be converted to ΔH in calories or Joules *per* mol of protein. Normally one uses ΔH_{cal} to indicate that this is a directly measured calorimetric enthalpy change.

The DSC is a very sensitive instrument capable of measuring the very small changes in heat capacity associated with protein denaturation in a dilute solution. The heat capacity of the solvent exceeds that of the protein by many orders of magnitude. Thus, for the most accurate and reliable measurement one must eliminate this background heat capacity carefully by ensuring that the solvent of the protein sample and reference solutions are exactly matched in composition. Dialysis or chromatography is the best method with the final dialysate or column flow through used as the reference solution.

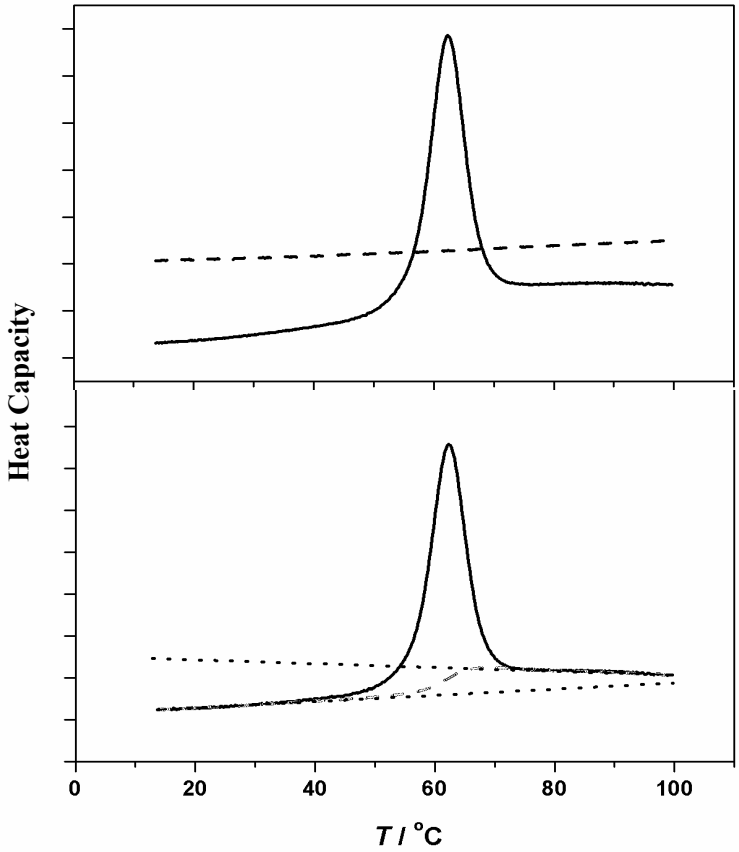

Fig. 2.2. DSC data for the denaturation of the RNase A measured at 5 mg/mL at 40 °C h^{-1} in a VP-DSC instrument. The instrumental baseline recorded with buffer is indicated as dashed line. The lower panel shows the data after 'buffer' subtraction and illustrates the process of baseline generation prior to integration of the peak.

Densimetric messurements can be used in studies for identifying and quantifying changes in hydration, packing, and dynamics of a protein that are associated with its conformational transitions or complexation with other moleculaes [Chalikian 1996, Chalikian 2001, Chalikian 2003]. However, densimetric studies often have not the sufficient sensitivity to reveal these changes in solvation properties or even volume changes upon unfolding of

proteins [Makhatadze 1990, Hinz 1994, Rösgen 2000]. Applying a relative new and efficient technique, called pressure perturbation calorimetry (PPC) [Bennion 2003, Makhatadze 1990, Ravindra 2003b, Heerklotz 2002, Kujawa 2001], determination of the thermal expansion coefficient and relative volume changes, $\Delta V/V$, upon unfolding of proteins in solution has advantages over densimetric measurements since its sensitivity is higher by more than one order of magnitude [Lin 2002, Kujawa 2001]. This high sensitivity is a prerequisite for such studies, as expansivity and volume changes upon unfolding, which can be either positive or negative, are usually very small ($\Delta V/V < 1$ %). The observed volume and expansitivity changes are correlated with further thermodynamic properties (ΔC_p, ΔH) obtained from differential scanning calorimetry (DSC). Taken together, these data lead to a deeper understanding of the solvation process of proteins in different co-solvents in their native and unfolded states. The basic theory of pressure perturbation calorimetry is as following:
The heat of a reversible process, dQ_{rev}, is related to the entropy change, dS, at the temperature T,

$$dQ_{rev} = T dS \tag{10}$$

Differentiation with respect to pressure, p, yields

$$\left(\frac{\partial Q_{rev}}{\partial p}\right)_T = T\left(\frac{\partial S}{\partial p}\right)_T \tag{11}$$

From $dG = V dp - S dT$, it follows that

$$\left(\frac{\partial S}{\partial p}\right)_T = -\left(\frac{\partial V}{\partial T}\right)_p \tag{12}$$

Eq. (11) can thus be rewritten as

$$\left(\frac{\partial Q_{rev}}{dp}\right)_T = -T\left(\frac{\partial V}{\partial T}\right)_p \tag{13}$$

The thermal expansion coefficient of volume V is defined as

$$\alpha_V = \frac{1}{V}\left(\frac{\partial V}{\partial T}\right)_p \tag{14}$$

and can thus be determined from an isothermal measurement of the heat consumed or released upon a small pressure change:

$$\alpha_V = -\frac{\Delta Q_{rev}}{TV\Delta p} \tag{15}$$

Moreover, the relative volume change $\Delta V/V$ at a phase or structural transition (*e.g.*, the unfolding of a protein), taking place in the temperature range from T_N to T_D can be obtained by

$$\frac{\Delta V}{V} = \int_{T_N}^{T_D} \alpha \cdot \mathrm{d}T \tag{16}$$

For two-component systems, such as biopolymer solutions, one has to extend these equations [Lin 2002, Kujawa 2001]. If the sufficiently dilute solution is composed of m_s grams of a solute dissolved in m_0 grams of solvent, the total solution volume V_{total} may be expressed as

$$V_{total} = m_0 V_0 + m_s \overline{V_s} \tag{17}$$

where V_0 is the specific volume of the pure solvent, and $\overline{V_s}$ is the partial specific volume of the solute in the solution. The partial volume of the solute includes not just its intrinsic volume, but also any volume changes induced as the result of interactions with the solvent. Differentiating Eq. (17) with respect to temperature at constant pressure yields

$$\left(\frac{\partial V_{total}}{\partial T}\right)_p = m_0 \left(\frac{\partial V_0}{\partial T}\right)_p + m_s \left(\frac{\partial \overline{V_s}}{\partial T}\right)_p \tag{18}$$

and after substituting the right hand side of Eq. (18) into Eq. (13) and (14), we obtain

$$\left(\frac{Q_{rev}}{\partial p}\right)_T = -T\left[m_0 \left(\frac{\partial V_0}{\partial T}\right)_p + m_s \left(\frac{\partial \overline{V_s}}{\partial T}\right)_p\right] = -T\left[m_0 V_0 \alpha_0 + m_s \overline{V_s}\,\overline{\alpha_s}\right] \tag{19}$$

where α_0 is the thermal coefficient of expansion of the solvent volume and $\overline{\alpha_s}$ is the thermal coefficient of the solute partial volume. The heat arising from pressure perturbation of the solution can thus be viewed as the sum of that arising from the perturbation of the solvent and from the perturbation of the solute in solution. Integration of Eq. (19) over a small pressure range Δp leads to

$$\Delta Q_{rev} = -T\left[m_0 V_0 \alpha_0 + m_s \overline{V_s}\,\overline{\alpha_s}\right]\Delta p \tag{20}$$

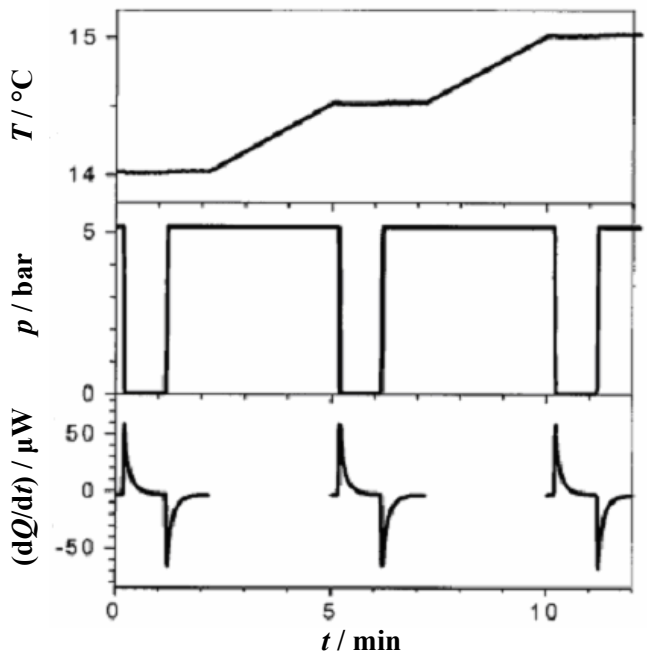

Fig. 2.3. Schematic diagram of a PPC experiment. The figure illustrates the time courses of the cell temperature, T, the pressure, p, and the compensation power (dQ/dt) upon 3 (out of typically 20–100) pressure jumps (downward and upward). Integration of dQ/dt yields two data points for $Q(T)$ at a given pressure change. (Adopted from [Heerklotz 2002].)

In a differential PPC experiment now (Fig. 2.3), with sample solution in the sample cell and buffer in the reference cell, both cells are subjected to the same Δp so that the net heat change ΔQ_{rev} will be equal to the difference between Eq. (20) for the sample cell and that for the reference cell. If the cells have an identical volume, then ΔQ_{rev} arises because the volume occupied by the solute in the sample cell, $m_{\mathrm{s}}\overline{V}_{\mathrm{s}}$, is replaced by solvation in the reference cell, *i.e.*,

$$\Delta Q_{\mathrm{rev}} = -T\left[m_{\mathrm{s}}\overline{V}_{\mathrm{s}}\overline{\alpha}_{\mathrm{s}} - m_{\mathrm{s}}\overline{V}_{\mathrm{s}}\alpha_0 \right]\Delta p \tag{21}$$

which then rearranges to

$$\overline{\alpha}_{\mathrm{s}} = \alpha_0 - \frac{\Delta Q_{\mathrm{rev}}}{T m_{\mathrm{s}}\overline{V}_{\mathrm{s}}\Delta p} \tag{22}$$

where the total mass of solute, m_{s}, is obtained by multiplying its concentration c_{s} [g/mL] with the cell volume, V_{cell} [mL]. If the solvent is pure or nearly pure water, α_0 can be obtained directly from density data in the literature. If the solvent contains moderately high

concentrations of electrolytes (buffer) and other solutes (co-solvents), which will generally be the case, α_0 will differ significantly from the value of pure water and must be determined in a separate PPC experiments, with buffer in the sample cell and pure water in the reference cell. The α_0 for buffer may then be obtained from α_w of pure water and the cell volume V_{cell} using

$$\alpha_0 = \alpha_w - \frac{\Delta Q_{rev}}{TV_{cell}\Delta p} \tag{23}$$

In the following, the partial specific value of the volume, $\overline{V_s}$, and the expansion coefficient, $\overline{\alpha_s}$, of the solute, will be replaced by their apparent values, denoted V and α, respectively.

2.3 Macromolecular crowding

A characteristic of the interiors of all cells is the high total concentration of macromolecules they contain. Such media are termed ‘crowded’ rather than ‘concentrated’ because, in general, no single macromolecular species occurs at high concentration but, taken together, the macromolecules occupy a significant fraction (typically 20–30%) of the total volume. This fraction is thus physically unavailable to other molecules. This steric exclusion generates considerable energetic consequences that are not generally appreciated. Biological macromolecules have evolved to function inside such crowded environments. For example, the total concentration of protein and RNA inside a cell of *Escherichia coli* is in the range of 300–400 g/L (Zimmerman 1991). An artist’s impression of this degree of crowding is shown in Fig. 2.4.

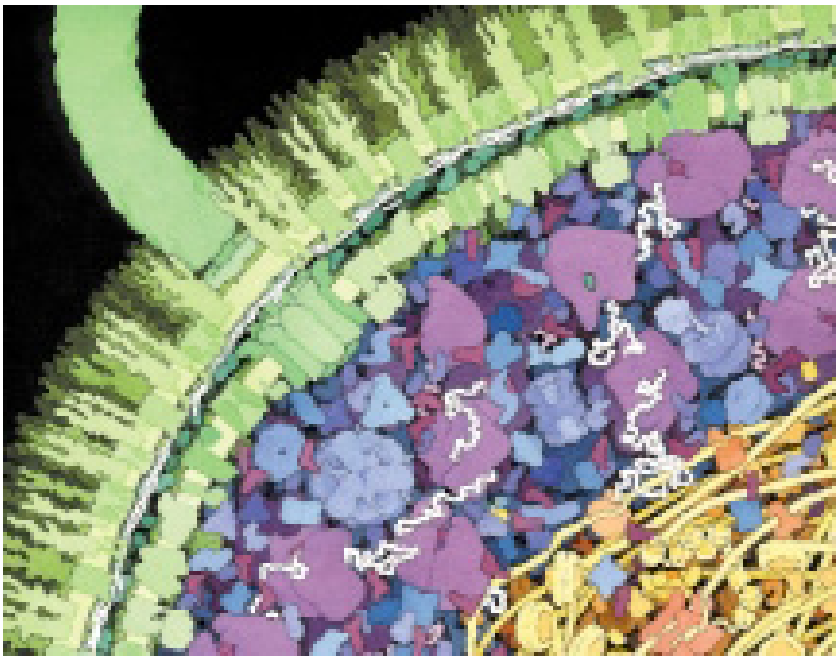

Fig. 2.4. Representation of the approximate numbers, shapes and density of packing of macromolecules inside a cell of *Escherichia coli*. Small molecules are not shown. (Adopted from [Hoppert 1999])

Molecular crowding is more accurately termed the excluded volume effect, because the mutual impenetrability of all solute molecules is its most basic characteristic. This nonspecific steric repulsion is always present, regardless of any other attractive or repulsive interactions that might occur between the solute molecules. Thus, crowding is similar to gravity – it cannot be avoided and organisms have to cope with its consequences.

The importance of the size of a molecule in determining the magnitude of the intracellular volume that is excluded to that molecule is so striking as to be counterintuitive,

but can be grasped from Fig. 2.5. The squares outline elements of volume containing spherical macromolecules (black) that occupy ~30% of the total volume, a value typical of intracellular compartments. The volume available to another molecule is defined as the fraction that can be occupied by the centre of that molecule. Obviously, if the introduced molecule is small relative to the macromolecules already present (Fig. 2.5a), it can access virtually all the space between these macromolecules – the volume available is depicted in yellow. However, if the introduced molecule is similar in size to that of the macromolecules (Fig. 2.5b), the available volume is much less than might be expected because the centre of that molecule can approach the centre of the other macromolecules to no less than the distance at which the surfaces of the two molecules meet; this distance is indicated by the open circle around each macromolecule. It follows that the centre of the added macromolecule can occupy only that part of the total volume that is exterior to any open circle. The volume available to the large molecule (Fig. 2.5b) is much less than that available to a small molecule (Fig. 2.5a), as can be seen by comparing the yellow areas. The available volume per macromolecule thus defines an effective concentration that can be much higher than the actual concentration in a crowded medium. The consequence of this is that effects of crowding on reaction equilibria and reaction rates are highly non-linear with respect to the sizes and concentrations of the interacting molecules.

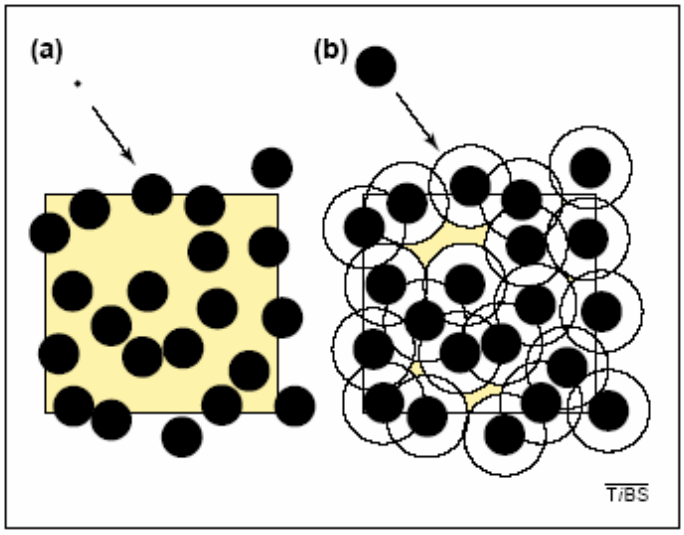

Fig. 2.5. The importance of size in volume exclusion. The squares define volumes containing spherical macromolecules occupying ~30% of the available space. (a) The centre of an introduced small molecule has access to virtually all of the remaining 70% of the space, indicated in yellow. (b) The centre of an introduced molecule similar in size to the macromolecules is excluded from most of this 70% as it cannot approach these macromolecules to a distance less than that indicated by the open circles. (Adopted from [Minton 2001].)

Volume may be excluded to a test particle by the surfaces of immobile structures as well as by individual background macrosolutes (Minton 1992, Giddings 1968), as illustrated in Fig. 2.6, which depicts a pore with square cross-section (this pore is one possible idealized representation of a small element of volume bounded by large macromolecular assemblies, such as interstices within a lattice of rodlike fibers or lamellar space between adjacent membrane surfaces). The center of a spherical test molecule whose diameter is comparable with the largest dimension of the pore (Fig. 2.6b) is excluded from the pink-colored region which in this instance represents a significant fraction of the total volume of the solution enclosed in the pore.

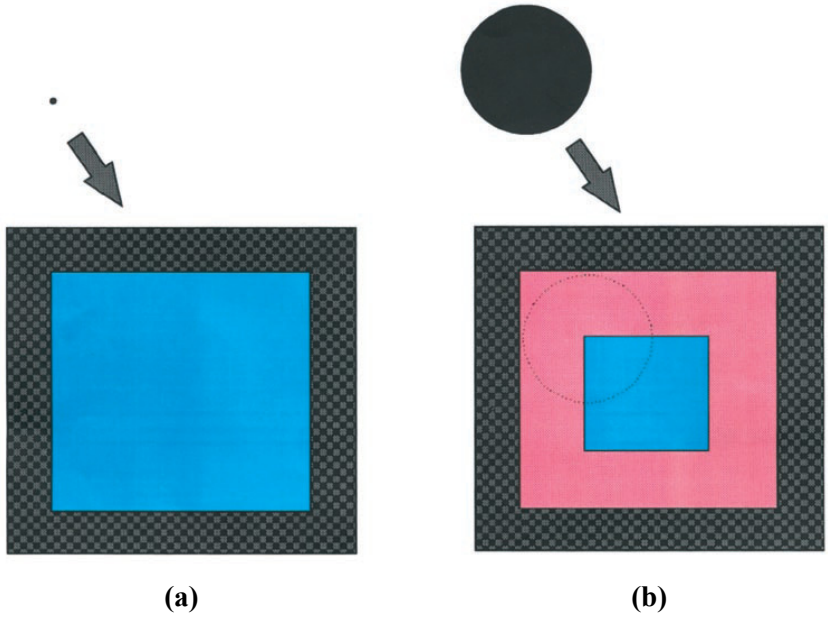

Fig. 2.6. Excluded (pink) and available (blue) volume in a pore of square cross-section. (a) volume available to a test molecule of infinitesimal size; (b) volume available to a test molecule of size comparable with pore dimensions.

There are two opposing effects of excluded volume on reaction rates (Minton 1998). If the overall rate of the reaction is limited by the rate with which a transition state complex decays to products, then crowding would be expected to enhance the relative abundance of the transition state complex and hence the forward reaction rate. Under these conditions, the forward rate constant may be increased by up to the equilibrium enhancement factor, depending upon details of the particular reaction. However, if the overall rate of the reaction is limited by the rate with which reactant molecules encounter each other through diffusional motion, then crowding, which retards diffusional motion (Ogston 1973, Muramatsu 1988), would be expected to lower the forward reaction rate. In the limit of high fractional volume occupancy, all association reactions are expected to be diffusion limited and hence slowed by

crowding (Zimmermann 1993). Hence, depending upon the nature of a particular reaction, one of two types of behaviour may be observed as the fractional volume occupancy of background molecules increases: the forward rate for a macromolecular association may decrease monotonically or may initially increase, pass through a maximum, and then decrease. A bimodal dependence of reaction rate on crowder concentration has been observed experimentally (Harrison 1986).

Macromolecular crowding and/or confinement by background molecules or structures can in principle affect the equilibrium and kinetics of any macromolecular reaction in which there exists a significant difference between the volume excluded to reactants and the volume excluded to products. Such reactions include self- or heteroassociation, condensation (crystallization, nucleation-controlled fiber formation), binding of macromolecules to specific surface sites, nonspecific surface adsorption, and protein isomerization, including folding/unfolding (Minton 1992, Minton 1981b, Zimmermann 1993, Ralston 1990, Minton 1995, Minton 2000a). Crowding may also affect enzyme-catalyzed reactions of small molecules if the mechanism of catalysis involves significant conformational change of the enzyme (Minton 1981a, Minton 1981b). Many such effects have indeed been observed experimentally. Most of the older observations were cited by Zimmermann (Zimmermann 1993), and some more recent observations are listed in Table 2.1.

For example, the application of crowding theory to protein aggregation makes two predictions:

• Crowding should favour aggregation because of its effect of increasing the thermodynamic activity of partially folded polypeptide chains. This effect will be greater for small polypeptides as for large polypeptides their diffusion is slowed and, thus, the encounter rate is reduced. In particular, crowding should enhance the aggregation of slow-folding chains, as fast-folding chains can internalize their hydrophobic surfaces before these can bind to those in other chains.

• Crowding should enhance the functional activity of chaperones by stimulating their association with partially folded chains; thus, these chains should have less time to encounter one another.

Some evidence for both these predictions was reported several years ago [v. d. Berg 1999].

Table 2.1: Some recent reports of experimentally observed crowding and confinement effects on macromolecular reactions (adopted from [Minton 2001]).

Observation	Magnitude
Enhancement of spectrin self-association by PEG, dextran [Cole 1994, Lindner 1995]	10-fold increase of equilibrium constant for association, K_{12}, in 20% dextran
Enhancement of actin polymerization by dextran and PEG [Lindner 1997]	3-fold decrease in solubility in 15% dextran
Enhancement of binding of HU protein to *E. coli* DNA by PEG and non-DNA binding proteins [Murphy 1994, Murphy 1995]	12% PEG increases affinity of DNA for HU by >10-fold
Stabilization of supercoiled conformations of DNA by PEG [Naimushin 2001]	
Sequestration of protein molecules in hydrated sol-gel glass stabilizes them with respect to thermal denaturation [Eggers 2001b]	Thermostability for a-lactalbumin increased by >25 °C
Self-association of fibrinogen induced by bovine serum albumin [Rivas 1999]	Doubling of weight-average molar mass in >5% bovine serum albumin
Enhancement by dextran of limited self-association of tubulin under conditions not permitting microtubule assembly [Minton 2001]	>2-fold increase in weight-average molar mass in 10% dextran
Enhancement of self-association of FtsZ by bovine serum albumin, hemoglobin [Rivas 2001]	2-fold increase in weight-average molar mass in 30% albumin or hemoglobin
Enhancement of unimolecular condensation of large linear DNA by PEG [Kidoaki 1999]	>10-fold increase in 2-state equilibrium constant at 18% PEG
Enhancement of productive refolding and assembly of GroEL by Ficoll 70 [Galan 2001]	>3-fold increase in recovery of ATPase activity in presence of >10% Ficoll
Reduction in solubility of deoxy sickle cell hemoglobin by dextran [Bookchin 1999]	~15-fold decrease in 21% dextran

2.4 Mesoporous molecular sieves for bioadsorption/immobilization and biocatalysis

The adsorption of proteins from solution onto solid surfaces has attracted much attention due to its scientific importance and application in many areas. In medical and food industries, it is essential to remove adsorbed proteins since even a small amount of deposited proteins may give rise to the subsequent adsorption of fibrous proteins leading to adverse biological consequences. Protein adsorption can also contribute to blood clotting and heart disease. The adsorption (immobilization) of proteins on inorganic materials is crucial because of the potential to improve the stability of enzymes under extreme conditions [Klibanov 1983]. The controlled adsorption of proteins is essential in the fields of enzymatic catalysis, biosensors, and disease diagnostics.

The discovery of mesoporous silicate molecular sieves opened up new possibilities in many areas of chemistry and material science [Kresge 1992, Zhao 1998a, Yang 1998]. The mesoporous inorganic hosts are obtained by hydrothermal synthesis and characterized by a regular arrangement of mesopores with a narrow pore size distribution. According to the IUPAC definition, pores with diameters between 2 and 50 nm are termed mesopores. Mesoporous materials are further characterized by high specific surface areas (up to ca. 1500 m^2/g) and specific pore volumes (up to ca. 1.5 cm^3/g), which renders them ideal candidates as hosts for biomolecules. Moreover, variation of the synthesis conditions enables the researchers to tailor the inorganic host so that the encapsulation of a variety of proteins, enzymes, and other biological molecules is feasible. These materials also fulfill many of other requirements for enzyme carriers such as sufficient functional groups for enzyme attachment, hydrophilic/hydrophobic character, water insolubility, chemical and thermal stability, mechanical strength, suitable particle form, regenerability, and toxicological safety. Mesoporous materials have a clear advantage over microporous zeolites and zeotype molecular sieves for the adsorption and transformation of large organic molecules [Corma 1994, Reddy 1994].

The observation that some enzymes retain their functionality upon immobilization on ordered mesoporous supports triggered significant research activity in encapsulating enzymes as well as other bioactive components. Examples of the variety of biological molecules that have been adsorbed onto ordered mesoporous silica and carbon materials were summarized by Hartmann [Hartmann 2005].

The starting point of intensive research in the area of mesoporous materials was the disclosure of the M41S family of silicate/aluminosilicate mesoporous molecular sieves by scientists from Mobil. Depending on the shape of the supramolecular template, hexagonal phase MCM-41 (Mobil Composition of Mater No. 41) [Kresge 1992, Beck 1992], cubic phase MCM-48 [Vartuli 1994] and lamellar phase MCM-50 [Dubois 1993] have been discovered (Fig. 2.7). They propose that the formation of these materials takes place by means of a liquid-crystal 'templating' mechanism, in which the silicate material forms inorganic walls between ordered surfactant micelles. Huo et al. synthesized a novel mesoporous molecular sieve with a three-dimensional cubic structure in highly acid media [Huo 1994]. The material is denoted SBA-1 (Santa Barbara Material No. 1) and possesses a cage-type structure with open windows. Highly ordered large pore mesoporous silicas SBA-15 with thick pore walls (ca. 3 nm) and a two-dimensional channel structure consisting of a hexagonal array of mesopores with diameters between 8 and 30 nm interconnected by micropores have been synthesized in 1998 [Zhao 1998a, Zhao 1998b]. Properties of the mesoporous molecular sieves selected in this study are listed in Table 2.2. MCM-41 possesses honeycomb arrays of nonintersecting uniformly sized channels with diameters ranging from 1.5 to 10 nm depending on the template used, the addition of auxiliary organics, and the synthesis parameters, *e.g.*, synthesis time, synthesis temperature, or postsynthetic treatments [Kresge 1992, Beck 1992]. MCM-48 is a cubic phase with $Ia\bar{3}d$ symmetry consisting of an enantiomeric pair of nonintersecting three-dimensional channel systems that are mutually intertwined. SBA-15 has an unfavourable ratio between pore diameter and wall thickness. This ratio is more favourable for MCM-41 despite its smaller wall thickness [Hartmann 2002].

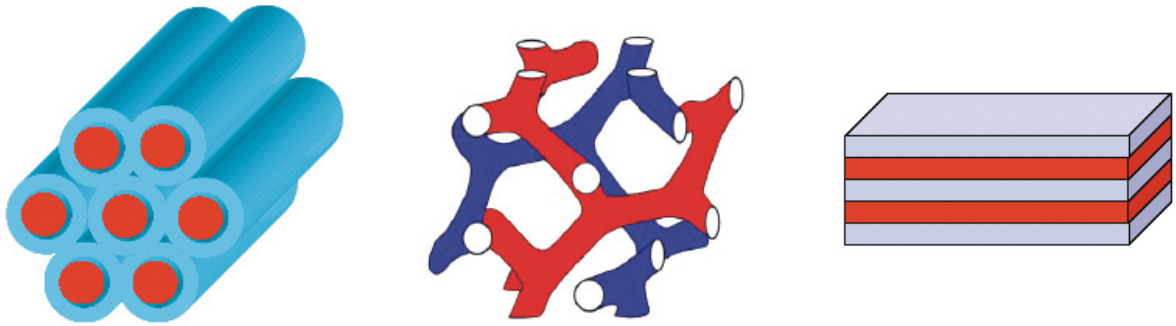

MCM-41 **MCM-48** **MCM-50**

Fig. 2.7. Schematic drawing of the mesoporous structures of the M41S family of materials.

Table 2.2: Properties of selected mesoporous molecular sieves.

	MCM-41	MCM-48	SBA-15
Pore structure	Hexagonal, nonintersecting, unidirectional	Cubic, nonintersecting, intertwined	Hexagonal, uniform, tubular (interconnected by micropores)
Template	Cationic surfactants possessing alkyl chains 8-22 carbons	Cationic surfactants possessing alkyl chains 8-22 carbons	Amphiphilic triblock copolymer P123 surfactant
Preparation condition	Alkaline	Alkaline	Acid
Space group	*p6mm*	$Ia\bar{3}d$	*p6mm*
Pore diameter / nm	2-5	1.5-3	5-10
Pore size distribution	Narrow	Narrow	Narrow but bimodal
Particle morphology	Spherical	Spherical	Rod-like
Mass transfer kinetics	Less favorable	More favorable	Less favorable
Reference	Kresge 1992 Beck 1992	Vartuli 1994	Zhao 1998a Zhao 1998b

2.5 Driving forces for protein adsorption at solid surfaces

The existence of a compact highly ordered structure of globular protein molecules in an aqueous environment requires that the decreased conformational entropy of the compact folded state (relative to that of the unfolded flexible coil-structure) is outweighed by the net enthalpy and entropy of the various structure-determining intra- and intermolecular interactions. These are electrostatic, hydrophobic, hydrogen bonding and van der Waals (dispersion) interactions. Because of the counteracting contributions, under most conditions the three-dimensional structure of a protein molecule is only marginally stable [Privalov 1979]. Introduction of a sorbent surface, which is more or less hydrophilic and which is usually electrically charged, causes a shift in the delicate balance of the interactions. This may lead to spontaneous adsorption, possibly accompanied by structural rearrangements in the protein molecule [Haynes 1994]. Whatever the mechanism of the process, protein adsorption under conditions of constant temperature T and pressure p only occurs spontaneously if the change in Gibbs energy G of the system is negative. According to Eq. (24) this can be realise by a decrease in the enthalpy H and/or an increase in the entropy S

$$\Delta_{ads}G = \Delta_{ads}H - \Delta_{ads}S \tag{24}$$

where G, H, and S may be expressed per mole of protein and Δ_{ads} indicates the change due to the adsorption process. The mechanism of protein adsorption can be explained in terms of the contributions to $\Delta_{ads}G$ from the major interactions that determined the overall adsorption process, *i.e.*, changes in the state of hydration, redistribution of charged groups (electrostatic interaction) and structural rearrangements in the protein molecules.

The presence of an interface provides a region where the protein can unfold without exposing hydrophobic residues to the aqueous phase. Such a structural alternation involves a reduction of intramolecular hydrophobic interaction. Because hydrophobic interactions in the interior of the protein molecule promote the formation of secondary structures such as α-helices and β-sheets, a reduction of these interactions may cause a decrease of such secondary structures. This could result in a substantial increase of conformational entropy of the adsorbing protein molecule.

When the surface of the sorbent and the protein are polar, their hydration is favourable. In that case, dehydration would oppose adsorption. If adsorption occurs, it is likely that some hydration water is retained between the adsorbed protein layer and the sorbent surface. However, if (one of) the contacting surface(s) (is) are hydrophobic, dehydration of (that) those

surface (s) would promote protein adsorption. It has been estimated that dehydration of hydrophobic surfaces results in a reduction in the Gibbs energy of 5-15 mJ/m^2 (which is mainly due to an entropy increase). For a protein molecule having a molar mass of 15 kD that adsorbs ca. 1 mg/m^2, it corresponds to a contribution to the Gibbs energy of adsorption ranging between -30 and -100 *RT* per mole of protein, which demonstrates that hydrophobic dehydration strongly contributes to spontaneous protein adsorption.

Both the protein molecule and the sorbent surface are generally electrically charged. In an aqueous environment these charged species are surrounded by counterions, which, together with the surface charge form the so-called electrical double layer. Close approach between the protein molecule and the sorbent surface implies overlap of the electrical layers and, hence, redistribution of ions. If one of the components carries a great excess of charge it would, upon adsorption, result in a considerable net amount of charge in the contact region between the protein layer and the sorbent surface. This non-aqueous, proteinaceous region has a low dielectric permittivity relative to that of bulk water and, therefore, accumulation of net charge in such an environment is energetically very unfavourable. A similar situation would result upon adsorption of a charged protein molecule on a sorbent surface that has the same charge sign. Nevertheless, even under such electrostatically adverse conditions, proteins often adsorb spontaneously. It has been reasoned [Norde 1978] and also experimentally verified [van Dulm 1981] that, simultaneously with protein adsorption, low-molecular-weight ions are transferred between the solution and the adsorbed layer to prevent charge accumulation in the contact region between the protein and the sorbent. Hence, ion association and ion pair formation is expected to occur in that region. Ion pair formation in the protein-sorbent contact region does not substantially contribute to $\Delta_{ads}G$ [Norde 1996]. However, if for other reasons, *e.g.* hydrophobic dehydration, ionic groups are forced to become located in a low-dielectric environment, ion-pairing will be strongly favoured.

Contributions from hydrogen bonding (other than accounted for the hydrophobic effect) and dipolar interactions are believed to have only a minor effect on protein adsorption affinity. The reason is that hydrogen bonds and polar interactions between groups at the protein and the sorbent surface, respectively, are formed at the expense of interactions between those groups and water molecules. Dispersive (or London-van der Waals) interactions hardly influence adsorption of proteins from an aqueous solution. The reason is that the Hamaker constant for proteins is only slightly larger than that for water [Nir 1977].

The amount of adsorbed protein can be influenced by the electrical charge, hydrophobicity, and the protein structure's stability. If global electrostatic interaction between

the protein and the sorbent surface would dominate the adsorption, the adsorbed amount would be a monotonic function of pH, decreasing at a negatively and increasing at a positively charged surface. It is quite generally observed for protein adsorption on solid surfaces that the adsorbed amount passes through a maximum near the isoeletric point of the protein-sorbent complex. This could be explained by an increased lateral electrostatic repulsion between charged protein molecules preventing the formation of close-packed monolayers. In addition, the pH influences the structural stability of (global) proteins and there is now convincing evidence that pH variation affects the extent of structural alternation that proteins undergo upon adsorption [Haynes 1994]: structural rearrangements are larger the further the pH deviates from the isoelectric point of the protein-sorbent complex. The adsorption saturation reflects an overall electrostatic interaction between the protein and the sorbent and the variation in the charge (and, thereby, in the structural stability) of the protein molecule has a stronger effect on the adsorption capacity than a variation in the sorbent charge density [Norde 1996]. Assessment of the influence of the hydrophobicity is generally difficult because a variation in hydrophobicity involves a change in chemical composition and, often, a change in the surface charge density. It is generally observed that the adsorption affinity increases with increasing surface hydrophobicity. Furthermore, as a rule, structural changes in the protein molecule are more strongly triggered at hydrophobic sorbent surfaces. Apart from the existence of hydrophobic patches at its exterior, the overall hydrophobicity of the protein molecule may be relevant to the adsorption behaviour. The overall hydrophobicity strongly influences the protein's structural stability, which, in turn, leads to more or less structural rearrangements in the adsorbing molecule, thereby affecting the adsorption affinity. Various observations, such as the influence of temperature, pH, ionic strength, *etc.*, on the amount adsorbed [Haynes 1994] and the reduction in biological activity suggest structural rearrangements in the adsorbed protein. Based on transmission circular dichroism (CD), a decrease of α-helix content was observed for protein adsorbed on ultrafine silica particles [Norde 1992]. The extent of helix reduction was shown to increase with decreasing native state stability of the protein and with decreasing coverage of the sorbent surface. A breakdown of ordered secondary structure leads to a higher conformational entropy of the protein. Isothermal titration calorimetry (ITC) with the same system reveals that the adsorption is endothermic so that the process is driven by an entropy increase [Norde 1992]. It seems that the gain in conformational entropy is more than sufficient to compensate for the unfavourable enthalpy change of adsorption. It has been concluded from the DSC studies [Steadman 1992, Norde 1996] that at a hydrophobic surface proteins have lost most of their

ordered structure, while at a hydrophilic surface the protein that has stronger internal coherence in solution retains most of its ordered structure whereas the less stable proteins lose their ordered structure almost completely. Thus, the influence of the structural stability of the protein on its adsorption behaviour is particularly prominent at hydrophilic surfaces.

Chapter 3

Experiment Section

3.1 Proteins and chemicals

The model protein used in this study is mainly bovine pancreatic ribonuclease A (RNase A). RNase A was purchased from Sigma Chemicals, Germany, and used without further purification.

Urea was obtained from Fluka, and glycerol from Merck. The chemicals were used without further purification. 10 mM of phosphate buffer (di-sodium hydrogen phosphate, anhydrous, from Merck) at various pH values was used for the experiments.

For the immobilization of denatured protein, 50 mM Tris-HCl buffer at pH 8.2 containing 1 mM ethylenediaminetetraacetic acid (EDTA) was used. Tris-HCl, EDTA and poly-ethyleneglycol (PEG) 3500 was from Sigma, dithiothreitol (DTT) from Sigma-Aldrich.

3.2 Preparation of the mesoporous molecular sieves

The mesoporous molecular sieves used in this study, MCM-48 [Gies 2003], MCM-41 [Kresge 1992, Beck 1992] and SBA-15 [Zhao 1998a, Zhao 1998b] are obtained by standard hydrothermal synthesis and calcinations methods and characterized by a regular arrangement of mesopores with a narrow pore size distribution.

The physical properties of the MPSs were characterized using transmission electron microscopy (TEM), X-ray powder diffraction (XRD) and nitrogen physisorption at 77 K. Pore size data were obtained from the adsorption branch of nitrogen physisorption isotherms using the Brunauer-Emmett-Teller (BET) model [Brunauer 1938] for MCM-41 and SBA-15, and the Barrett-Joyner-Halenda (BJH) model [Barrett 1951] for MCM-48. The *d*-spacing was determined from the first XRD reflection peak.

Rod-like SBA-15 possesses discrete rod-like morphology with uniform length (2–9 μm) [Yu 2002], while conventional SBA-15 has a fibrous macrostructure, extending tens of micrometres by stacking and coupling of rod-like SBA-15 (Fig. 3.1). More rapid (< 10 min to reach equilibrium) and higher-capacity (up to 533 mg/g) immobilization of enzymes within rod-like SBA-15 than conventional SBA-15 has been reported [Fan 2003a]. In this study, only rod-like SBA-15 was used to get optimized immobilization.

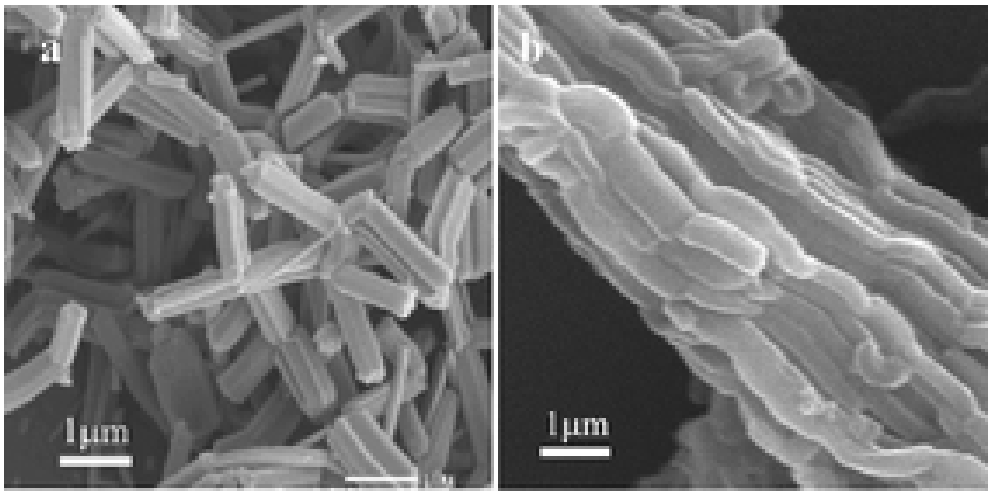

Fig. 3.1. SEM images of (a) Rod-SBA-15 and (b) Con-SBA-15 (Adopted from [Fan 2003a]).

The MCM-41 silica samples are denoted as C_n-MCM-41, where *n* indicates the number of the carbon atoms of the alkyl side chain of the surfactant which was employed in the synthesis. The characterization data for these materials are listed in Table 3.1. The silicas synthesized using above method were obtained from the lab of Prof. Dr. H. Gies, Institute of

Geology, Mineralogy & Geophysics**,** Ruhr-Universität-Bochum, Germany, and the lab of Prof. Dr. M. Hartmann, Institute of Physics, Universität Augsburg, Germany.

Table 3.1: Properties of the selected mesoporous molecular sieves.

	C_{12}-MCM-41	C_{16}-MCM-41	MCM-48	SBA-15
Average pore diameter / Å	30	40	25	58
Specific internal surface area / $m^2\ g^{-1}$	1135	1212	1150	910
Specific pore volume / $cm^3\ g^{-1}$	0.70	0.86	0.93	1.25
Particle size / nm	100-500	100-500	350-500	200-500 (diameter), 2000-9000 (length)

3.3 Immobilization of native protein

The immobilization took place inside a well-stirred compartment, where MPSs were brought into contact by injection into a protein solution of known concentration. Intense mixing allowed the process to take place under control. The acquired data were interpreted in terms of protein immobilization rates.

The mesoporous molecular sieve powder was suspended in protein solution in 10 mM phosphate buffer. The resulting dispersion was continuously stirred (for MCM-48 sample) or shaken (for MCM-41 and SBA-15 samples) at about 20 °C until equilibrium partitioning into the mesoporous system was reached (typically 4-96 h). The immobilization process is illustrated in Fig. 3.2. The amount of protein immobilized was calculated by subtracting the protein concentration determined by UV absorbance at 278 nm of the supernatant after centrifugation from that of the protein solution of the initial concentration. For the test of protein leaching from the mesoporous molecular sieves, the protein-entrapped solid was recovered by centrifugation, washed with buffer until no palpable amount of protein was observed in the washing buffer, then re-suspended in buffer and stirred at 20 °C for 24 h. The amount of RNase A leached from mesoporous molecular sieves was determined by measuring the UV absorbance at 278 nm of the supernatant after centrifugation.

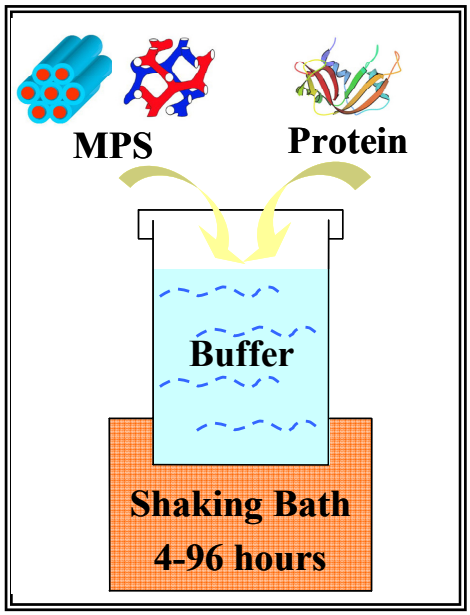

Fig. 3.2. Schematic illustration of the immobilization method: The MPS powder was suspended in protein solution in buffer. The resulting dispersion was continuously shaken or stirred at about 20 °C until equilibrium partitioning into the mesoporous system was reached (typically 4-96 h).

3.4 Immobilization of denatured protein

RNase A was denaturized in Tris-HCl buffer containing 8 M urea and 30 mM dithiothreitol (DTT). The resulting protein solution (30 mg/mL) was incubated at 37 °C for 2 h. For adsorption, 30 mg of SBA-15 was dispersed in 15 mL of Tris-HCl buffer containing 6 M urea, 300 μL of denatured RNase A (denoted as D-RNase A) solution (9 mg protein) was then added. The resulting mixture was then shaken at 500 min^{-1}. The amount incorporated was calculated by subtracting the amount calculated from the UV absorbance at 278 nm of the supernatant after centrifugation from that of the D-RNase A at 0.6 mg mL^{-1}. The maximum immobilization of D-RNase A in SBA-15 was reached within 45 h. The amount of denatured protein immobilized was calculated by subtracting the denatured protein concentration determined by UV absorbance at 278 nm of the supernatant after centrifugation from that of the denatured protein solution at the initial concentration. 2 mg protein-entrapped solids were recovered by centrifugation. The leaching test was performed by adding 1 mL of Tris-HCl buffer solution containing 2 M urea. The resulting mixture was then shaken at 500 min^{-1} for 24 h. The protein-loaded SBA-15 exhibited no detectable leaching.

For the refolding of the denatured protein, protein-entrapped solids were recovered by centrifugation and were washed several times with Tris-HCl buffer without urea until no palpable amount of protein was observed in the washing buffer, then re-suspended in Tris-HCl buffer. The resulting suspension with matching buffer was measured from 12 to 120 °C by DSC.

3.5 Differential scanning and pressure perturbation calorimetry

The thermal unfolding of immobilized protein was measured by means of a high precision VP-DSC microcalorimeter from MicroCal, Northampton, MA, USA. The cell volume is ca. 0.514 mL. The reference cell was filled with matching buffer and pure MPSs of the appropriate amount. Both buffer and protein solutions were degassed for 5 minutes with the ThermoVac accessory before being injected into the respective cells. The instrument is also equipped with a pressuring cap that allows application of 1.8 bar to the cells in order to avoid air bubbles at elevated temperatures. The instrument was operated in the high gain mode with a filtering period of 16 seconds at a rate of ca. 40 °C h^{-1}. A prescan thermostat time of 15 minutes was always used to allow for a thorough equilibration of the thermal core of the VP-DSC before beginning the scan. It is important to get the best comparative results in a series of related experiments, thus each sample solution should be treated exactly the same way (*i.e.*, same starting/ending temperature, same scan rate, sample elapsed time between the end of one experiment and the start of next experiment). Results were further improved by having the first scan of the day as a 'dummy scan' with buffer in both cells, since this will put the instrument into the same cycle of thermal history for the first sample scan as for the later sample scans. Baseline subtraction (pure buffer/solvent or buffer/MPSs) and normalization with respect to protein concentration were performed by the instrument software, yielding the temperature-dependent apparent molar heat capacity of the protein, C_p, with respect to the buffer/solvent solution or buffer/MPSs dispersion.

The pressure perturbation (PPC) experiments were performed in the DSC calorimeter using MicroCal PPC accessory. The reference and sample cell volume are identical (0.514 mL) and they open to a common pressure chamber containing a sensor (Fig. 3.3). An equal pressure of 5 bar was applied to both cells in a programmed manner using nitrogen gas. The software then initiates a pressure release to ambient pressure. The temperature is kept constant by active compensation of the heat change caused by the pressure jump. As the solution in the sample and reference cell are identical except for the small amount of dissolved solute in the sample cell (solid ellipses in Fig. 3.3), counterbalanced by the corresponding volume of buffer in the reference cell (dashed ellipses), measured differential heats are quite small. The compensation power returns to the baseline typically within one minute and integration of the supplied power *vs.* time yields the heat consumed or released by the sample. After complete equilibration, an upward pressure jump is applied when the PPC controller reconnects the PPC cells with nitrogen gas. The heat peaks upon compression and decompression agree

within a few % in absolute values; they are of opposite sign, however. For both compression and decompression experiments, temperature, pressure, and heat flow are recorded as a function of time. The calorimeter is then automatically heated or cooled to the next desired temperature and the next two (compression/decompression) pressure jumps are applied (see Fig. 2.3). An earlier debate concerning possible methodological errors with the PPC procedure was referred to by Heerklotz [Heerklotz 2004], Randzio [Randzio 2003] and Brandts [Brandts 2004].

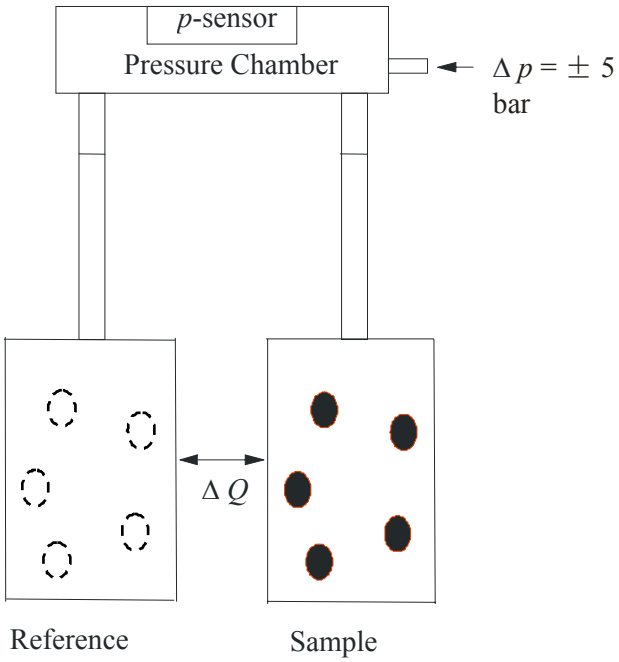

Fig. 3.3. Schematic drawing for the pressure perturbation calorimetry (PPC) experimental setup [adopted from Kujawa 2001]. The open ellipses in the reference cell represent the volume occupied by solvent in this cell, which counterbalances the volume occupied by the solute molecule in the sample (filled ellipses).

Chapter 4

Results and Discussions

4.1 pH-dependent solvation properties and thermal stability of RNase A

The concentration of hydrogen ions (pH) is an important factor that affects protein function and stability in different locations in the cell and in the body [Alberts 1994]. The physiological pH varies in different organs in the human body: the pH in the digestive tract ranges from 1.5 to 7.0, in the kidney it ranges from 4.5 to 8.0, and in body liquids we have a pH of 7.2–7.4 [Davenport 1966]. It was shown that the interstitial fluid of solid tumors have pH 6.5–6.8, which differs from the physiological pH of normal tissue and thus can be used for the design of pH selective drugs [Burger 1999]. The structure and function of most macromolecules are influenced by pH, and most proteins operate optimally at a particular pH (optimum pH) [Boyer 1971]. On the basis of indirect measurements, it has been found that the intracellular pH usually ranges between 4.5 and 7.4 in different cells [Guiton 1976]. The organelles' pH affects protein function and variation of pH away from normal could be responsible for drug resistance [Simon 1999]. Lysosomal enzymes function best at the low pH of 5 found in lysosomes, whereas cytosolic enzymes function best at the close to neutral pH of 7.2 [Alberts 1994]. Experimental studies of pH-dependent properties [Whitten 2000, Pots 1998, Khurana 1995, Pace 1990, Pace 1992] such as stability, solubility and activity, provide the benchmarks for numerical simulation. Experiments revealed that although the net charge of ribonuclease Sa does affect the solubility, it does not affect the pH of maximal stability or activity [Shaw 2001]. Another experimental technique such as acidic or basic denaturation [Acampora 1967, Anderson 1990, Alonso 1991] demonstrates the importance of electrostatic interactions on protein stability. pH-dependent phenomena have been extensively modelled using numerical approaches [Warshel 1981, Warshel 1984, Honig 1995, Schaefer 1997]. It

was shown that the optimum pH results from two factors – amino acid composition and the organization of the titratable groups with the 3D structure [Alexov 2004]. It was demonstrated that the optimum pH and isoelectric point could be quite different. In many cases, the optimum pH was found at a pH corresponding to a large net charge of the protein. At the same time, there was a tendency for proteins having acidic optimum pHs to have a base/acid ratio smaller than one and vice versa. The correlation between the optimum pH and base/acid ratio is significant if only buried groups are taken into account. It was shown that a protein providing a favourable electrostatic environment for acids and disfavouring the bases tends to have high optimum pH and vice versa.

4.1.1 A scenario for the volumetric behavior

Before considering pH effects on solvation properties and the thermal stability of proteins, we discuss a simple scenario, in which the partial specific volume of a protein may be decomposed into three contributions [Chalikian 2003, Chalikian 2001, Likhodi 2000]:

$$V \approx V_{\mathrm{intr}} + \delta V_{\mathrm{hydr}} + V_{\mathrm{therm}} \tag{25}$$

The intrinsic volume, V_{intr}, of the protein results from the van der Waals volume of the atoms plus the volume of water-inaccessible voids in its interior. The hydrational or interaction term, δV_{hydr}, describes the solvent volume changes associated with the hydration of the solvent-accessible hydrophobic, polar or charged protein atomic groups. The thermal volume, V_{therm}, the volume of the void space surrounding the solute molecule, arises from mutual thermally induced vibrations and reorientations of the solute and solvent. Scaled particle theory, by employing statistical mechanical and geometrical arguments to describe the dissolution of a solute, allows one to evaluate the intrinsic and thermal contributions ([Likhodi 2000] and references therein). The sum of the intrinsic (geometrical) volume and the thermal volume thus represents the partial molar volume of the cavity enclosing the solute. In Eq. (25), a minor term taking into account the coefficient of isothermal compressibility of the solvent has been neglected [Chalikian 2003]. Certainly, as there is no rigorous way of disentangling the partial molar volume of a protein into its components, other dissections of V may be conceivable. Owing to the qualitative discussion of the various contributions, this does not affect the conclusions drawn, however.

From the measured partial specific volume and simple models for V_{intr} and V_{therm}, a rough estimate of δV_{hydr} can be given for the native state. Such an analysis, conducted for

RNase A in H_2O, yields as a highly negative value for δV_{hydr}, about $\delta V_{hydr} = -0.2$ cm^3 g^{-1} [Ravindra 2003b]. A negative value implies a smaller partial molar volume, *i.e.* a higher density, of water at the protein surface compared to bulk water. Such a higher density is evidenced by combined neutron and X-ray scattering experiments [Svergun 1998]. Its origin in terms of the property and topology of the protein–water surface has recently been addressed by MD simulations [Merzel 2002].

Eq. (25) implies that a similar dissection may hold for the temperature derivatives of the partial specific volume, *i.e.* the apparent thermal expansion coefficient, α, and its temperature coefficient, $d\alpha/dT$. Only δV_{hydr} and V_{therm} contribute significantly, to α and $d\alpha/dT$, because the intrinsic volume of the native protein does not depend markedly on temperature. In fact, the thermal expansivity of the protein interior has been measured over a limited temperature range, and the changes observed are rather small [Rholam 1984, Frauenfelder 1987, Young 1994, Tilton 1992, Dubins 2003]. The thermal volume is expected to increase with temperature, giving a positive contribution to α. As pointed out by Lin *et al.* [Lin 2002], α and, in particular, $d\alpha/dT$ are primarily controlled by the hydrational contributions, suggesting that $d\alpha/dT$ is a direct measure of the effect of solvation upon volumetric properties of proteins. In fact, the hydrational contribution to the thermal expansibility is known to depend drastically on the nature of the protein–water interface. Hydrophilic groups in contact with water show the characteristic pattern of structure-breakers with large positive values of α, which decrease drastically with increasing temperature. The rationale is that the hydrophilic groups bind more adjacent water at low temperatures, which at higher temperatures are released by thermal agitation, and do no more contribute to α. In contrast, solvent-exposed hydrophobic groups act as structure makers, resulting in a decrease in the water density around hydrophobic groups. In this case α is negative, and the temperature coefficient, $d\alpha/dT$, is positive.

Previous PPC data for RNase A in H_2O indicate high apparent thermal expansion coefficients of the protein and steeply decreasing slopes in their temperature dependence. Thus, they classify RNase A as a protein with a significant number of hydrophilic side groups at the protein surface [Ravindra 2003b]. Even much steeper slopes of $d\alpha/dT$ are found for proteins with more charged side groups, such as SNase [Ravindra 2004a].

4.1.2 Volumetric behavior and protein stability at different pH values

Fig. 4.1(a) shows DSC traces of the apparent molar heat capacity, C_p, of 0.5 wt % RNase A dissolved in 10 mM phosphate buffer at pH values ranging from 2 to 9. From the $C_p(T)$ data, the midpoint temperatures of the thermal unfolding (T_m), the enthalpy changes upon unfolding (ΔH), and ΔC_p, the difference in heat capacities between the unfolded and the native state, were obtained (Table 4.1).

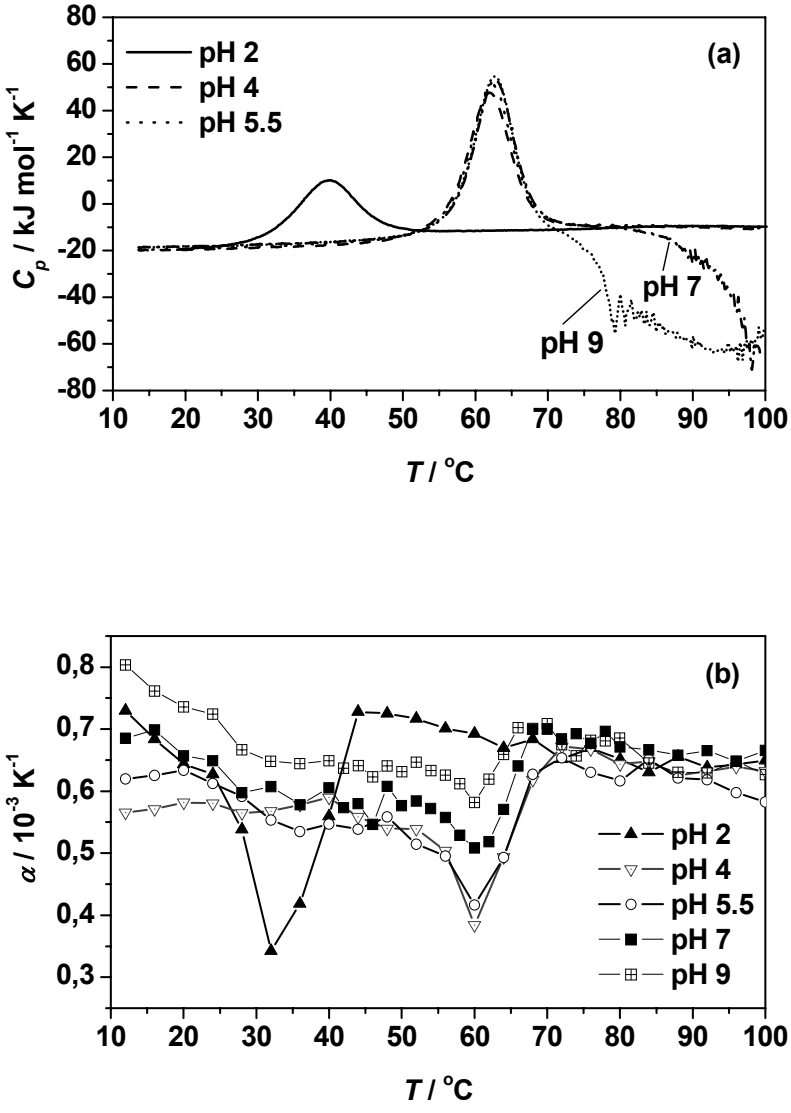

Fig. 4.1. Temperature dependence of the apparent molar heat capacity, C_p, of 0.5 wt % RNase A (a), and of the apparent thermal expansion coefficient, α, of 1.0 wt % RNase A (b), in 10 mM phosphate buffer solution at different pH values.

Thermal unfolding of RNase A at all the pH values investigated is an endothermic process. With the midpoint temperature of unfolding shifting to higher temperatures with increasing pH from 5.5 to 9, the ΔH value as well as T_m increases, indicating a slight and continuous increase in protein stability. The effect of pH on denaturation (*e.g.* T_m is lower at lower pH value) may be explained as follows: As ribonuclease is taken to lower pH values and more carboxyl groups are protonated, the molecule becomes increasingly positively charged and there is a large increase in its electrostatic free energy. Unfolding of the molecule will cause a decrease in the intramolecular Linderstrom-Lang electrostatic interaction parameter, w (known to be a function of the conformation and hydration of globular proteins), by expansion of the molecule or by increased accessible surface area to the solvent, resulting in a decrease in charge density inside the protein and a concomitant decrease in the electrostatic free energy [McPhie 1972]. The ΔC_p value of about 5.5 kJ mol^{-1} K^{-1}, a value typical for proteins, seems to be independent of pH. At pH 7 and 9, the RNase A seems to undergo two calorimetrically detectable transitions: an endothermic unfolding process followed by an exothermic process at higher temperatures, which is probably due to aggregation of unfolded structures, which could be induced by the change in electrostatic interactions, *i.e.*, the reduction of repulsive Coulombic forces between the unfolded protein molecules at pH values close to the PI of the protein.

Table 4.1: PPC and DSC experimental data of the thermal unfolding of RNase A at different pH values (the maximum of the estimated error for T_m is ± 0.2 °C, for ΔH and ΔC_p it is ± 5 %, and for ΔV it is 7 %).

pH	T_m / °C	DSC Results		PPC Results				
		ΔH / kJ mol^{-1}	ΔC_p / kJ mol^{-1} K^{-1}	α_{12} [a] / 10^{-4} K^{-1}	$\Delta\alpha_{12\text{-}40}$ [a] / 10^{-4} K^{-1}	$\Delta V/V$	ΔV_{unf} / mL mol^{-1}	$\Delta\alpha_{unf}$ / 10^{-4} K^{-1}
2.0	39.9	270	5.6	7.3	- [b]	−0.47 %	−43.5	0.9
4.0	61.8	426	5.5	5.7	~ 0	−0.33 %	−31.8	1.2
5.5	62.2	448	5.5	6.2	0.7	−0.31 %	−29.9	1.1
7.0	62.7	462	5.5	6.9	1.0	−0.19 %	−18.3	1.2
9.0	62.8	494	5.4	8.2	1.5	−0.09 %	−8.7	0.8

a: α_T apparent partial expansion coefficient of the protein at temperature T.

b: value not possible to evaluate, but $\Delta\alpha_{12\text{-}24}$ is determined to be 0.8×10^{-4} K^{-1}.

Fig. 4.1(b) represents PPC curves of the apparent thermal expansion coefficient, $\alpha(T)$, of 1.0 wt % RNase A dissolved in 10 mM phosphate buffer at various pH values, from which

α at different temperatures, the midpoint of the thermal unfolding temperature (T_m) and the relative volume changes upon unfolding, $\Delta V/V$, are obtained.

At 12 °C, the order of magnitude of α at different pH is pH 9 > pH 2 ≈ pH 7 > pH 5.5 > pH 4. Before the unfolding, *i.e.* between 12 and 24 °C at pH 2, and between 12 and 40 °C at pH 4, 5.5, 7 and 9, the apparent thermal expansion coefficient of the protein, α, decreases with small positive curvature, upon increasing temperature. RNase A, like other global proteins, contains a large preponderance of hydrophilic sidechains and peptide groups relative to apolar aliphatic sidechains, so it is no surprise that native RNase A exhibits an α vs. temperature behaviour characteristic of structure-breakers, *i.e.*, higher α-values at low temperatures and their decrease up to before unfolding [Lin 2002]. Proteins with highly charged surfaces, such as SNase, exhibit even much larger α-values and steeper negative slopes of $\alpha(T)$ [Ravindra 2003a], and proteins with higher molecular weight such as chymotrysinogen have lower α-values and smaller negative slope of $\alpha(T)$ due, at least partially, to the smaller surface/volume ratio of the larger proteins. The order of $\Delta\alpha_{12\text{-}40}$, which is in the same trend as $-\mathrm{d}\alpha/\mathrm{d}T$ in the pre-transition temperature range, at different pH is pH 9 > pH 7 > pH 5.5 > pH 4. At pH 2, although the $\Delta\alpha_{12\text{-}40}$ is impossible to be determined, it can be clearly seen from Fig. 4.1(b) that the $\mathrm{d}\alpha/\mathrm{d}T$ in the pre-transition temperature range is similar to that at pH 7. The rationale is that the presence of a high charge density tends to accentuate ion-dipole interactions of the individual amino acid (AA) residues but decrease hydrogen bond interactions between water molecules, so that, as ribonuclease is taken to lower pH values (*e.g.* from pH 9 to pH 5.5), both the α-value and its negative slope decrease; on the other hand, extremes of pH, *e.g.* pH 2, cause increased hydration of side chains as well for reasons of enhanced charges.

At T_m, a distinct dip in α is observed. Above that temperature, the solvent accessible surface area (ASA) increases and α increases to a relative constant level in the post-transition temperature range with α values around $0.7\times10^{-3}\,\mathrm{K}^{-1}$, which is larger than that for the native one. After the unfolding, *i.e.* above 50 °C at pH 2, and above 70 °C at pH 4, 5.5, 7 and 9, α decreases slightly. This temperature dependence is explained in terms of suppressed fluctuations in the water molecules in the hydration layers around the protein molecules. It is shown that the thermal expansion coefficient of bound water is larger than bulk water. Interestingly, after unfolding, the apparent thermal expansion coefficient of the protein shows a similar value at different pH, which indicates that, the unfolded structures, irrespective of the pH, exhibit similar hydration conditions. On the other hand, at high temperature, the difference between hydrophilic and hydrophobic hydration vanishes. It has been suggested that at high temperature the apparent expansibility approaches the limit of the intrinsic

expansion of the protein [Hiebl 1991]. The reason for this is twofold: The anomalous contribution to the water expansion caused by order-disorder fluctuations reaches a minimum difference with respect to the normal component. The hydrophobic part of bound water molecules will successively melt as temperature increases and therefore the hydration layer shrinks until hydrophobically bound water does not exist any longer and only the electrostrictively bound water exists.

The relative volume change upon unfolding, $\Delta V/V$, as obtained from the area under the transitional peak, is calculated by integrating the $\alpha(T)$ transition curve (after baseline subtraction). The absolute volume change upon unfolding, ΔV, can be calculated from $\Delta V/V$ using the molar mass of RNase A (13.7 kDa) and its partial specific volume (~0.704 mL g^{-1}). The calculated $\Delta V/V$ and ΔV values are summarized in Table 4.1 and the ΔV values are plotted against the corresponding T_m values in Fig. 4.2. It is shown that the volume change upon unfolding is always relatively small and negative (*i.e.*, the overall volume of water and protein is smaller on denaturation with respect to the bulk solvent) at the pH values investigated. As the transition temperature is shifted to higher temperatures by raising the pH, the value of the volume change becomes less negative. This can be explained as following: upon unfolding, the released nonpolar residues acquire less-dense hydrating water (*e.g.* expanded structures [Tanaka 2000]) at low temperatures, but less able to do so at high temperature. On the other hand, the released polar groups cause a greater increase in density at low temperatures, due to their destruction of the low-density water species (electrostriction effect), than at high temperatures, where there is a lower population of low-density water structures. The progressive development of site-specific hydration algorithms currently allows people to describe biophysically relevant hydration sites on the protein envelope [Durchschlag 2004], and various other approaches using rescaling or water shells are also sufficient to predict molecular parameters quantitively.

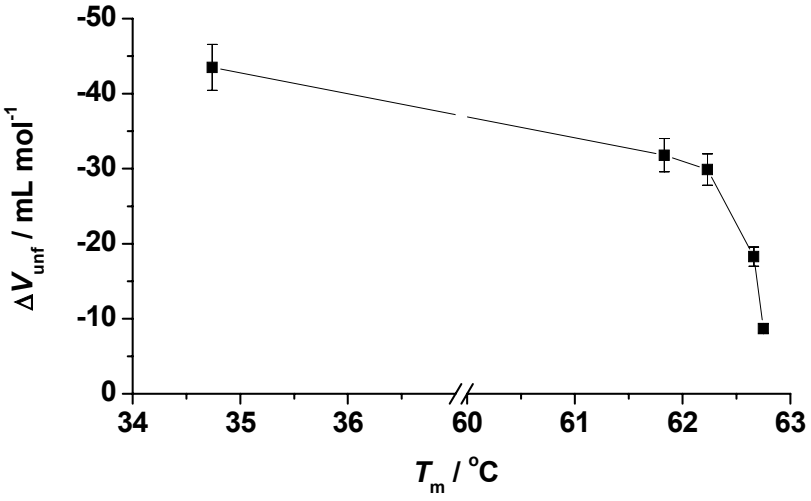

Fig. 4.2. Volume changes upon unfolding of RNase A at different pH values as a function of corresponding T_m.

4.2 Stability of RNase A confined in MCM-48

4.2.1 Immobilization equilibrium

MCM-48 exhibits immobilization of RNase A with a capacity of ca. 117 mg/g (Fig. 4.3), which corresponds to 29 % of the whole protein content, when the mass ratio of RNase A to MCM-48 is 4:10 at pH 5.5. The immobilization equilibrium is reached within 4 h. More than 90 % of the maximum loading is achieved within 1 h, suggesting a high affinity between RNase A and the host. This rate of immobilization is faster than that for the hexagonal phase materials MCM-41 or SBA-15 (Santa Barbara Amorphous No. 15), for which 96 h are required to establish immobilization equilibrium [Hartmann 2005]. This is probably due to the different pore structures. The cubic structure is definitely more beneficial for protein transportation from the entrance to the inner part of the mesopores or mesochannels, which was suggested to be the rate-determining step of the whole immobilization process [Lei 2004]. However, the maximum loading of the protein still corresponds to 8 % of the mesopore volume (assuming the geometrical volume for the space required for a single protein molecule), only, very likely due to the small pore dimensions of the MCM-48 material, which is just comparable to the dimensions of RNase A. The protein molecules are so large that most of them can probably not migrate freely into the inner part of the mesoporous material, but rather accumulate close to the pore entrance region. In fact, it has been suggested that a large diameter of the pore entrance (> 70 Å) is beneficial for fast and efficient immobilization of proteins [Fan 2003b].

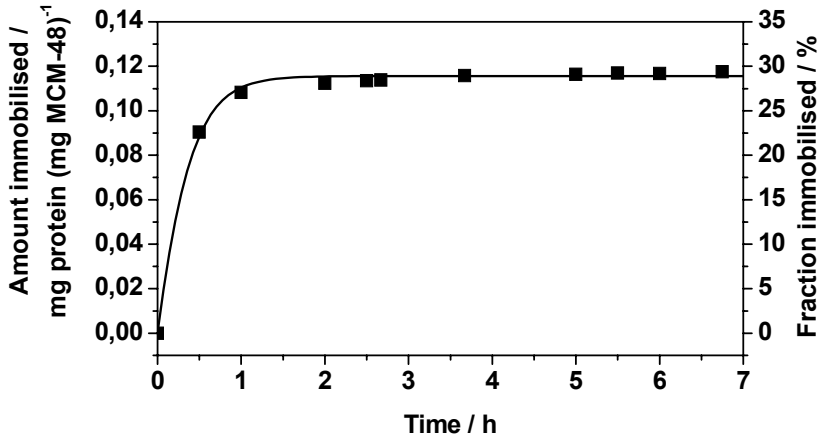

Fig. 4.3. Immobilisation of RNase A in MCM-48 at pH 5.5 (with respect to the initial concentration of RNase A; the mass ratio of RNase A to MCM-48 is 4:10).

As the isoelectric point (PI) of RNase A is 9.6, the protein is positively charged at pH 5.5. The point of zero charge (PZC) of the silica surface of the mesoporous materials is just below 3, hence, the silanol groups of the silicate surface are negatively charged at pH 5.5. As a result, protein migration to the silicate surface may - at least partially - be driven by the electrostatic potential difference. Extended entrapment of protein into the mesopores will require the breaking of Columbic interaction between the mesoporous solid (MPS) and previously entrapped protein, which is an endothermic process [Czeslik 2001]. The silanol groups located on the pore walls of the silicate can promote immobilization through hydrogen bonding interactions with hydrophilic residues of the protein. However, the interaction between the protein and the silica surface is rather weak. Hence, about 10% leaching of the immobilized protein is observed. The protein loading in MCM-48 at different conditions is summarized in Table 4.2.

Table 4.2: Protein loading on MCM-48 at different conditions.

Loading / mg/g	pH		Mass Ratio [a]		Co-solvent / M		
					Urea		Glycerol
	5.5	7.0	4:10	3:10	0.5	3.5	3.5
117	×		×				
108	×			×			
146		×		×			
109	×			×	×		
126	×			×		×	
98	×			×			×

a: mass ratio of RNase A to MCM-48.

It is reasonable to assume that the immobilization equilibrium also changes with the mass ratio of protein to MPS. We found that at pH 5.5, when the ratio of RNase A to MCM-48 was decreased from 4:10 to 3:10, the loading capacity decreases slightly from ca. 117 mg/g to ca. 108 mg/g (the error bar in the loading calculation is smaller than 4 mg/g). We also found that changing the MPS and protein concentration without altering their mass ratio (MPS and protein concentration changed from 10 and 4 to 5 and 2 mg/mL, respectively) did not significantly change either the rate or the equilibrium of the immobilization, indicating that the crucial step influencing immobilization is not the protein diffusion in solution but rather within the MPS, *i.e.*, the migration of the protein into the inner pore channels of the MPS [Lei 2004].

When the pH was increased from pH 5.5 to pH 7 at the same mass ratio of protein to MPS (3:10), the maximum loading drastically increased, from ca. 108 to ca. 146 mg/g. The maximum loading is clearly a function of solution pH. With increasing pH, the net positive charge of the protein surface decreases and the repulsive Coulomb forces between the amino acid residues decrease, probably resulting in a small size reduction of the protein molecule [Hartmann 2005] and a reduction of structure rearrangements [Haynes 1994]. However, the effect of pH on the loading rate may also be satisfactorily explained by a reduction in protein-protein repulsion and thus the formation of close-packed monolayers of protein inside pores is possible.

Noticeably, the maximum loading increases significantly, to 126 mg/g, in the presence of 3.5 M urea, even if the mass ratio of RNase A to MCM-48 is lower (3:10). The destabilizing nature of urea is mainly caused by the weakening of the peptide bonds and as a consequence, the protein (partially) unfolds and attains a more or less random coil like structure [Bennion 2003]. The specific binding of urea to the polypeptide also affects the solvent accessible surface area (ASA) by replacing water molecules and releasing them into the bulk phase, so that an extended hydrogen-bonded water layer around the protein surface is largely absent and the protein is less hydrated [Ravindra 2003a]. As a consequence, the protein molecule becomes highly flexible, hence a closer packing of the protein molecules inside the MPS is possible, so that an increase of the loading capacity is observed. In the presence of 0.5 M urea, the maximum loading was increased by 1 mg/g, only.

On the contrary, in the presence of 3.5 M glycerol, an osmolyte, the maximum loading of RNase A on MCM-48 decreases to 98 mg/g when the mass ratio of RNase A to MCM-48 is 3:10. Glycerol, being a strongly hydrophilic co-solvent, interacts strongly with H_2O and has a weaker affinity for the polar residues on the protein surface, thus leading to preferential hydration of the protein and an increase of the strength of hydration of the protein [Ravindra 2003a]. As a consequence, a close packing of the protein molecules inside the MPS is probably prohibited and the loading capacity decreases.

4.2.2 States of proteins in confined geometry

Depending on the protein concentration, the protein can be adsorbed on the external surface (population represented as P1), and/or diffuse into the pores of the MCM-48 (P2), and there might be an excess protein fraction left without any restricted mobility, *i.e.*, with the bulk-like behavior of the free protein (P3). Fig. 4.4 exhibits the DSC traces of RNase A in MCM-48. The DSC data indicate existence of adsorbed, encapsulated and free states of the protein, which are denoted as P1 ($T_m \approx 52$ °C), P2 ($T_m \approx 90$ °C), and P3 ($T_m \approx 62$ °C), respectively. Protein molecules adsorbed onto the silicate surface (P_1) are susceptible to weak destabilization and hence their unfolding temperature is shifted to slightly smaller values [Deere 2003]. On the contrary, the encapsulated protein (P_2) - owing to severe configurational restrictions [Zhou 2001, Minton 2000a, Minton 2001] - is expected to show an enhanced stability, although the presence of confinement surface would possibly lead to structural rearrangements in the protein molecules [Haynes 1994]. For example, in a rough statistical-mechanical calculation, assuming a random-flight chain model and neglecting intrachain excluded-volume interactions among the amino acid residues, the stability (Gibbs free energy) and temperature of unfolding for a confinement size which is about twice that of the size of the polymer increases by about 10 k_BT and ~20 °C, respectively [Zhou 2001]. The proteins remain in bulk exhibit a similar unfolding temperature to proteins in solution, but it is expected to be slightly more stable due to the presence of MPS particles as a crowding agent.

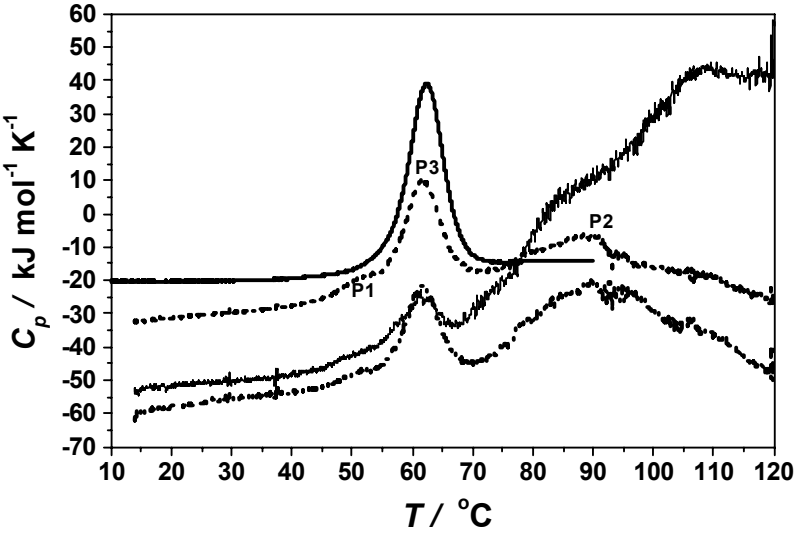

Fig 4.4. DSC traces (background corrected, scan rate 40 °C h^{-1}) of RNase A in MCM-48 at variable concentrations in 10 mM phosphate buffer at pH 5.5. Dashed, dash-dotted, and thin lines represent protein concentrations of 4.5, 2.2, and 1.2 mg/mL dissolved in 10 mg/mL MCM-48. The thick line corresponds to a 5 mg/mL RNase A solution in pure 10 mM phosphate buffer solution at pH 5.5.

As can be clearly seen in the DSC data, the silica-entrapped protein (P2) is in fact significantly more stable against temperature-induced unfolding compared to the protein in bulk solution. The DSC peak for the entrapped species exhibits a maximum around 90 ^{o}C ($\Delta T_m \approx 30$ ^{o}C), and the half width of the peak is ~20 ^{o}C, which is partially due to the variation in pore size diameter in MCM-48, which varies from about 20 - 30 Å with a strong maximum around 25 Å [Gies 2003], but probably also due to the uneven distribution of the protein molecules within the mesopores. The protein molecules are of such size that they are not able to migrate easily into the inner space of the mesopores, but probably rather accumulate close to the pore entrance. It was shown, on one side, that the thermal stability of immobilized protein depends on the pore size of the host and decreases with increased pore size assuming it is large enough to host the protein molecules and the thermal stability is maximized when the pore diameter of the host matches the size of the protein [Hartmann 2005], and on the other side, the protein population in more crowded regions is supposed to have higher stability (and also T_m value) due to the excluded volume effect [Minton 2000a, Minton 2001], and those present in relatively less crowded environments unfold at lower temperatures.

At low protein concentrations, the protein seems to be entrapped essentially in the narrowest pores available in MCM-48, which have about the same dimensions as the protein. Apparently, due to the strong restrictions in conformational space, the protein is not able to unfold markedly in these narrow pores anymore, thus leading to a steady increase of C_p up to the highest temperature measured, only. This is consistent with the observation that the unfolding enthalpy of the immobilized protein is significantly larger than that of the protein in bulk buffer solution (details will be discussed in Section 4.2.3). The DSC trace of a 1.2 mg/mL protein in 10 mg/mL MCM-48 suspension exhibits a very small presence of free protein (P3).

In order to explore whether the hydration properties of the protein change upon entrapping in the MCM, which - in addition to the entropic confinement effect - might play a role in protein stabilization in confined space as well, PPC methods were applied. Since polar groups are present on the surface of both MCM-48 and the protein, their hydration is favourable and dehydration would oppose adsorption. When adsorption occurs, some hydration water is retained between the adsorbed protein layer and the MCM-48 surface. It has been shown recently, that PPC measurements are able to yield valuable information on protein hydration and compactness as well as accurate volume changes in the course of protein unfolding [Ravindra 2003a, Ravindra 2003b, Dzwolak 2003, Lin 2002, Dzwolak 2004, Sasisanker 2004].

Fig. 4.5 shows the PPC data (apparent thermal expansion coefficient, α) of RNase A in pure buffer solution and when confined in MCM-48 at different concentrations. Previous results on cosolvent effects on protein PPC data revealed that the level of hydration contributes significantly to protein stability as can be seen from the absolute value and magnitude of the negative slope of the apparent thermal expansion coefficient, dα/dT [Ravindra 2003a, Ravindra 2003b, Dzwolak 2003, Lin 2002, Dzwolak 2004, Sasisanker 2004]. Surprisingly, Fig. 4.5 shows that the α and dα/dT values measured for a concentration where almost all proteins are incorporated in the MCM-48, are drastically enhanced. For example, at a concentration of 0.7 mg/mL protein, α(10 °C) and dα/dT values of 2.1×10^{-3} K^{-1} and -3.3×10^{-5} K^{-2} are obtained, compared to corresponding values of 0.85×10^{-3} K^{-1} and -4.0×10^{-6} K^{-2} for RNase A in pure buffer solution. The much higher α and dα/dT values of the encapsulated protein indicate that the protein is much stronger hydrated in the silica pores. As a consequence, this is also expected to increase its thermal stability. It is generally believed that Hofmeister ions, and hence also the silanol groups at the silica surface, influence the protein structure indirectly through changes in the hydrogen bonding properties of water, which might lead to the increased hydration of the embedded protein. Part of this effect could also be due to a decrease of the rotational and translational dynamics of the system.

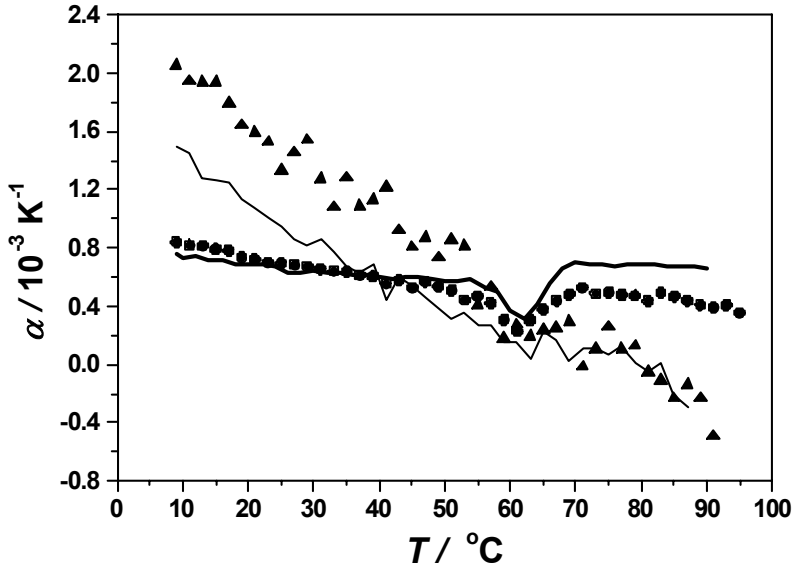

Fig. 4.5. Temperature dependence of the apparent thermal expansion coefficient (background corrected, appromixate scan rate 40 °C/h) of RNase A in MCM-48 at variable concentrations in 10 mM phosphate buffer at pH 5.5. Circles, thin line and triangles, represent 4, 1.2, and 0.7 mg/mL concentrations of RNase A dissolved in 10 mg/mL MCM-48. The thick line corresponds to a 5 mg/mL RNase A solution in pure 10 mM phosphate buffer solution at pH 5.5.

The PPC curves between 50 and 70 °C reflect the unfolding of free RNase A in buffer solution. The volume change upon unfolding, $\Delta V/V$, for free RNase A is negative and amounts 0.27 %, which is in good agreement with literature data (0.29 %) [Ravindra 2003a, Ravindra 2003b, Dzwolak 2003, Lin 2002, Dzwolak 2004, Sasisanker 2004]. With regard to the embedded protein, α is continuously decreasing with temperature, though with decreasing slope at high temperatures. This is in contrast to RNase A in pure buffer solution, whose posttransitional α values are lying above the pretransition baseline, indicating an increase of the expansivity in the unfolded state. A well resolved free protein denaturation transition curve is observed at high protein loadings, only. With regard to the confined protein, the data indicate that inside the silica pores significant unfolding is not feasible anymore and hence must be incomplete. No volume change can be determined even with this sensitive PPC method applied, which allows measuring ΔV values as small as ~0.1 %.

From Fig. 4.4 and Fig. 4.5, it can be inferred: the stability of the protein RNase A confined in the mesoporous silicate system MCM-48 is drastically increased ($\Delta T_m \approx 30$ °C). A similar effect is expected to occur in crowded systems of high protein concentrations, although the effect may be less pronounced as these are soft-matter systems. In dense protein solutions, irreversible protein aggregation often leads to spurious effects, however. No significant volume change upon unfolding of the confined protein is observed even up to temperature as high as 120 °C. It is intriguing that the protein penetrates into the mesopore network despite the fact that the pore size is similar to that of the protein. The increase in stability is probably not only due to a restriction in conformational space (excluded volume effect), but may - at least partially - also be due to an increased strength of hydration of the protein in these narrow silica pores. The latter effect is expected to depend on the surface chemistry of the OMM and be induced by the particular water-structuring properties of the silanol groups of the silica surface, which is in close proximity to the protein surface in our case.

4.2.3 pH-dependent thermal stability of confined RNase A

Fig. 4.6 represents the DSC traces of RNase A in MCM-48 at variable pH ranging from 2 to 9 in 10 mM phosphate buffer. The immobilization was successful at all pH values investigated. At each pH, the DSC peaks for the entrapped species exhibits their maximum at much higher temperatures than that of the free protein (Table 4.3), and the width is also larger than that of the free protein in bulk solution.

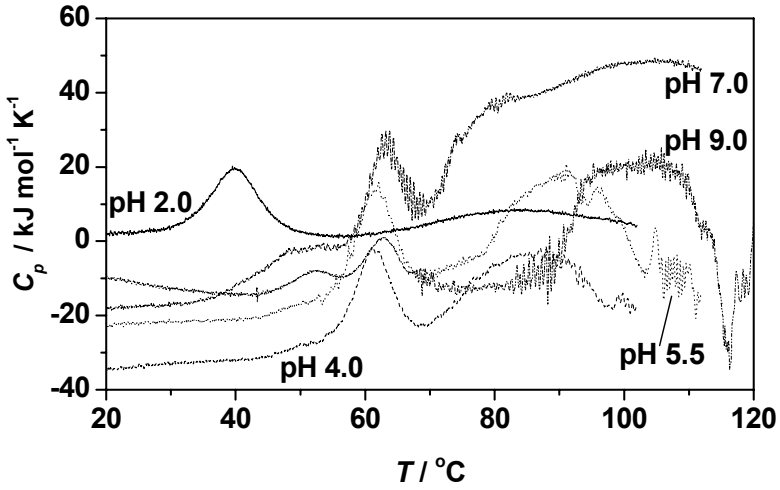

Fig. 4.6. Temperature dependence of the apparent molar heat capacity, C_p, of RNase A in MCM-48 in 10 mM phosphate buffer solution at different pH values. The mass ratio of RNase A to MCM-48 is 3:10 and the RNase A concentration is 3 mg/mL.

The stabilization against temperature-induced unfolding is further enhanced with the protein immobilization at higher pH, *i.e.*, T_m increases with increasing pH also for the confined protein. Interestingly, immobilization was also achieved at pH 2 and pH 11 (data not shown) where the silicate and the protein are both positively or negatively charged, indicating that other driving forces, such as the entropic contributions originating from dehydration of hydrophobic surface areas and adsorption-induced conformational changes of the protein, and the enthalpic van der Waals forces in addition to an attractive electrostatic interaction [Norde 1996, Roth 1993], also contribute to the migration process. The hydrophobic interactions may either originate from attraction of the nonpolar side chains of the amino acids residues on the protein surface by siloxane bridges at the silicate surface or from the interprotein interactions between the hydrophobic side chains of neighboring protein molecules adsorbed on the silicate surface [Vinu 2004b]. It has been reasoned [Norde 1978] and also experimentally

verified [van Dulm 1981] that, simultaneously with protein adsorption, low-molecular-weight ions are transferred between the solution and the adsorbed layer to prevent charge accumulation in the contact region between the protein and the sorbent. Hence, ion association and ion pair formation is expected to occur in that region thus reducing the electrostatic repulsion between the MPS and the protein surface.

Table 4.3: The unfolding temperature of free protein, $T_{m,\,free}$, and of the confined protein, $T_{m,\,conf}$ at different pH values.

pH	$T_{m,\,free}$ / °C	$T_{m,\,conf}$ / °C
2.0	39.9	82.5
4.0	61.8	84.5
5.5	62.2	90.2
7.0	62.7	98.9
9.0	62.8	105.7

The immobilization efficiency is also revealed by comparing the unfolding enthalpy of excess protein in the immobilization suspension, which corresponds to the amount of protein not being immobilized in the MPS, but rather remaining in solution. In Table 4.4, the $1\text{-}\Delta H_{exc}/\Delta H$ values are shown, which are proportional to the relative amount of immobilized protein. They increase with increasing pH, in good agreement with the results obtained from the UV data. The maximum loading of the MPS is achieved at pH 9, which is near the isoelectric point of the protein (9.6 for RNase A), again demonstrating that the protein loading is clearly a function of solution pH. Similarly, the amount of the externally adsorbed population (P1) that unfolds at temperatures lower than the bulk T_m, also increases upon increasing the pH. Furthermore, $(\Delta H_{exc}+\Delta H_{conf})/\Delta H$ is larger than 1, indicating that the unfolding enthalpy of the immobilized protein is significantly larger than that of the protein in bulk buffer solution. This is consistent with the increase in protein stability as reflected by the increase of T_m upon entrapment. The calculated ΔH_{conf} values for the entrapped protein at pH 7 and 9 are not as large, probably due to the fact that the unfolding of RNase A at pH 7 and 9 is followed, at least partially, by aggregation, which is exothermic and reduces the value of enthalpy change for the endothermic unfolding process of the confined protein.

Table 4.4: Comparison of the unfolding enthalpies of RNase A, ΔH, the unfolding enthalpy fractions of the excess and absorbed RNase A, ΔH_{exc}, and the unfolding enthalpy fraction of the confined RNase A, ΔH_{conf}, in the immobilization suspension at different pH values.

pH	ΔH / kJ/mol	ΔH / J/g	ΔH_{exc} / J/g protein dispersed	ΔH_{conf} / J/g protein dispersed	$1-\frac{\Delta H_{exc}}{\Delta H}$	$\frac{\Delta H_{exc}+\Delta H_{conf}}{\Delta H}$	Fraction immobilized
2.0	270	19.7	14.9	15.6	0.24	1.55	0.25
4.0	426	31.1	21.5	57.5	0.31	2.54	0.34
5.5	448	32.7	21.2	62.3	0.35	2.55	0.36
7.0	462	33.7	17.5	72.4	0.48	2.67	0.49
9.0	494	36.1	15.8	90.7	0.56	2.95	0.52

To check for thermal reversibility, consecutive DSC scans were carried out for the samples at pH 5.5 and 7, respectively (Fig. 4.7). In both cases, reheating of the sample revealed the irreversibility of the unfolding reaction, not only of the confined population but also of the free one. The latter finding could be explained by the adsorption of the unfolded protein molecules on the silicate surface, thus reducing the fraction refolding to their native structure upon cooling. Upon unfolding, more amino acids residues (also more hydrophobic groups) are exposed, resulting in a much higher affinity between the protein and MPS. This might lead to a stronger adsorption of the unfolded protein on the MPS surface. Hence, the repeated DSC scans are reflecting essentially the temperature-dependent sum of the heat capacities of the absorbed unfolded protein and that of the unfolded confined protein, which is not able to refold due to the volume restriction in the confined space.

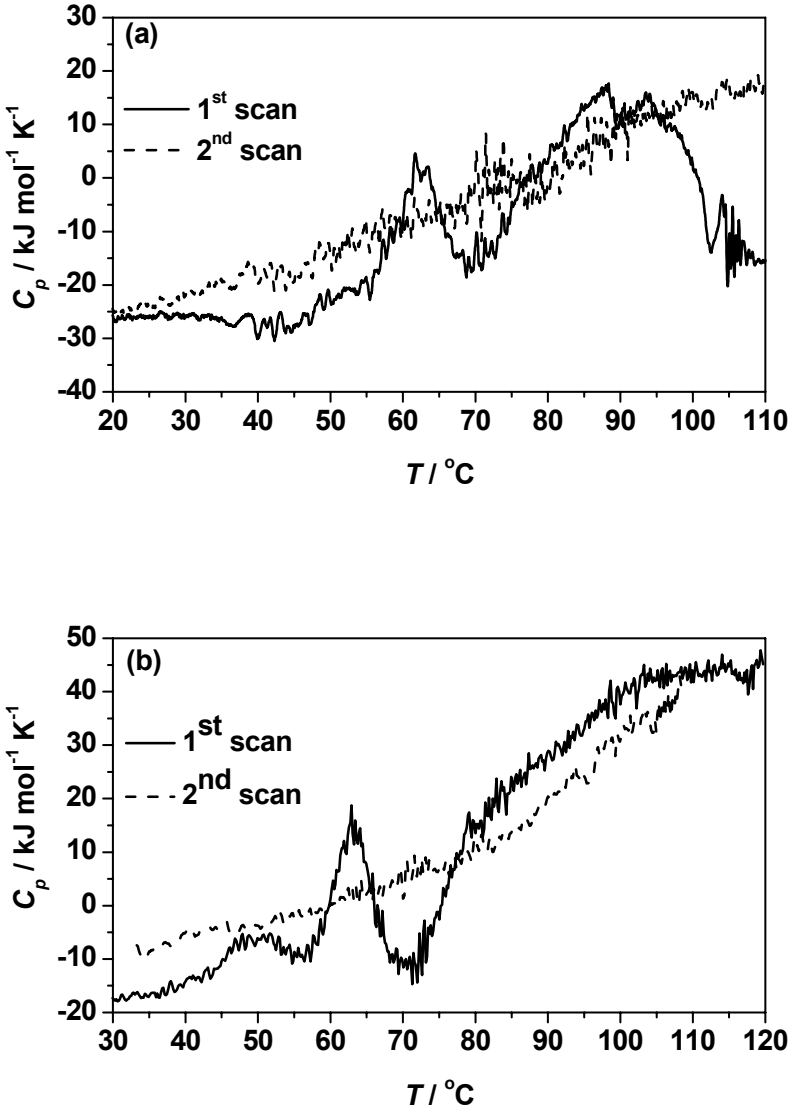

Fig. 4.7. DSC traces of RNase A in MCM-48 dispersion (10 mM phosphate buffer solution) at pH 5.5 (a) and pH 7 (b). The mass ratio of RNase A to MCM-48 is 3:10 and the RNase A concentration is 3 mg/mL. To check for thermal reversibility, two consecutive scans were taken.

4.2.4 The effect of co-solvents, urea and glycerol

The thermal stability and solvational properties of proteins strongly depend on their interaction with the solvent or co-solvent at the protein-solvent interface. For kosmotropic co-solvents, such as glycerol, a continuous increase in hydration strength was observed with increasing glycerol concentration. In addition, glycerol acts as protein stabilizer, which is indicated by the increasing T_m and ΔH values of the protein. On the contrary, the chaotropic agent urea destabilizes proteins by direct ligand binding, which, in turn, is reflected in decreasing T_m and ΔH values [Ravindra 2003b]. Fig. 4.8 depicts DSC curves of RNase A in 10 mM phosphate buffer at pH 5.5 in the presence of a modest urea concentration of 0.5 M in comparison to the DSC trace of RNase A in pure buffer solution. To check for thermal reversibility, consecutive DSC scans were taken. The data indicate that the unfolding temperature, T_m, of RNase in 0.5 M urea is shifted to a slightly lower temperature (61.2 °C) with regard to the enzyme in pure buffer solution, and the reversible unfolding up to ~70 °C is followed by an irreversible aggregation process at higher temperatures. In 3.5 M urea solution, T_m decreases to 53.0 °C ($\Delta T_m = -9.2$ °C).

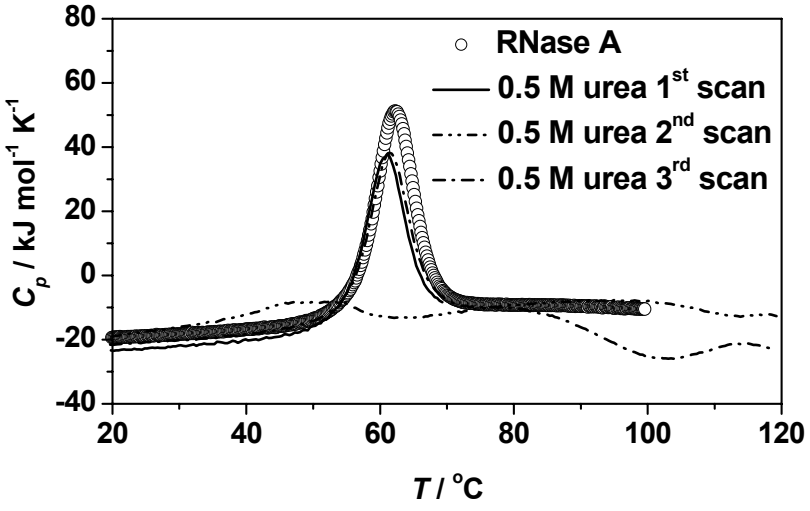

Fig. 4.8. DSC traces of RNase A in 10 mM phosphate buffer solution at pH 5.5 and in the presence of 0.5 M urea. To check for thermal reversibility, three consecutive scans were taken for the urea containing sample (the first scan from 12 to 70 °C, only, the last two runs from 12 to 120 °C).

As mentioned above, the protein loading of the MPS increases to 126 mg/g in the presence of 3.5 M urea at pH 5.5. This effect is also visible in the DSC data (Fig. 4.9). The unfolding of the confined protein leads to much higher integral ΔH values, indicating a higher

protein loading. It has been suggested that even at stirring conditions, there might exist a stagnant solution layer close to the surface of the MPS that must be penetrated by diffusion to allow for loading [Lei 2004]. In the presence of urea, i.e., when the protein is destabilized and partially unfolded, the altered, elongated and more flexible protein conformation probably allows for a more effective penetration into the pores. The unfolding temperatures of the confined protein extend over a wide temperature range, from about 53 to 90 ^{o}C with a maximum at 88.4 ^{o}C ($\Delta T_{m,conf} \approx 35$ ^{o}C). The extended width of transition temperatures probably also reflects the broad distribution of folded and partially unfolded protein structures present under these solvent conditions.

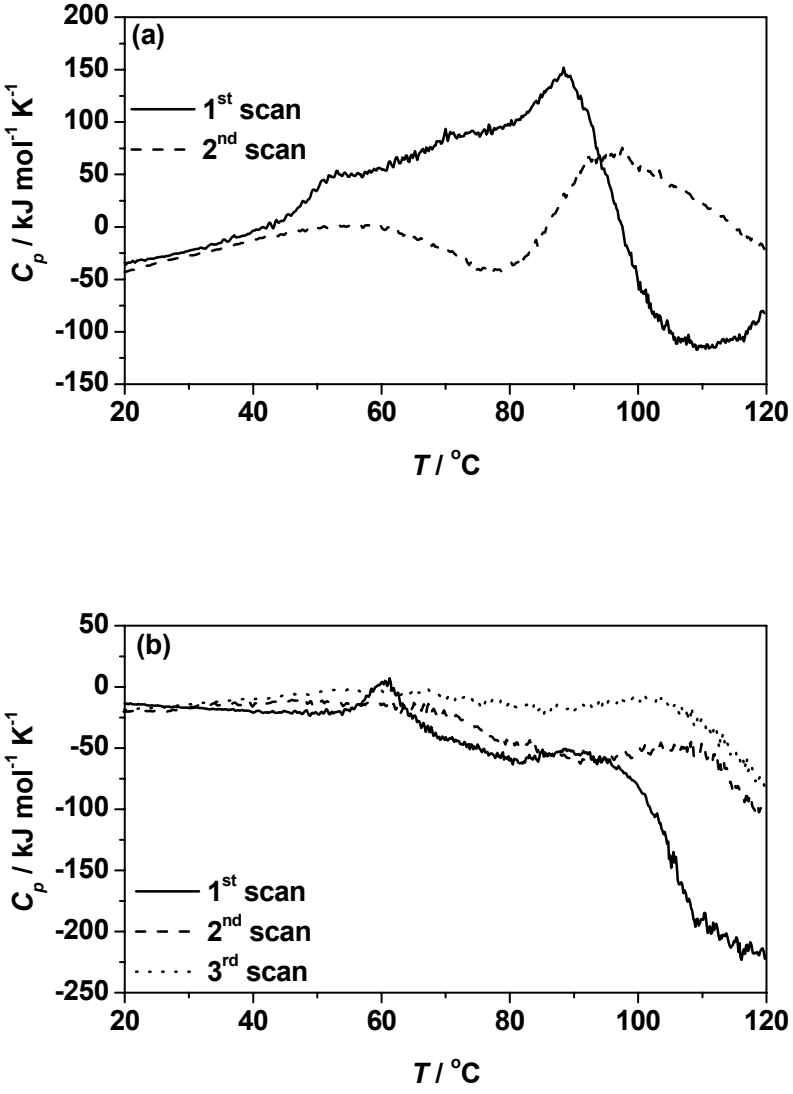

Fig. 4.9. DSC traces of RNase A in MCM-48 in 10 mM phosphate buffer solution at pH 5.5 and in the presence of 3.5 M urea (a) and 0.5 M urea (b). The mass ratio of RNase A to MCM-48 is 3:10, and the RNase A concentration is 3 mg/mL. To check for thermal reversibility, consecutive scans were taken.

To check for thermal reversibility, consecutive DSC scans were taken (Fig. 4.9). Reheating of the 3.5 M urea sample shows a DSC trace indicating that some confined protein population refolds and exhibits an even higher T_m value of about 97.5 °C (ΔT_m = 44.5 °C, see Table 4.5).

Table 4.5: Unfolding temperature T_m of the free and confined protein in the presence of different amount of urea, C_{urea}.

C_{urea} / M	T_m / °C		
	Free protein	Confined protein	
		1st scan	2nd scan
0.5	61.2	88.4	108.3
3.5	53.0	88.4	97.5

On the contrary, the protein loading decreases to 98 mg/g, which corresponds to 33 % of the whole protein content, in the presence of 3.5 M glycerol at pH 5.5. From the DSC results (Fig. 4.10) we calculate 1-$\Delta H_{exc}/\Delta H$ to be 0.32, using ΔH = 460 kJ/mol [Ravindra 2003b]. The T_m of the small amount of confined protein is 101.2 °C, which is 37.4 °C higher than T_m of the free protein (63.8 °C). Furthermore, the C_p value markedly decreases after the unfolding process, probably due to aggregation of adsorbed unfolded protein. In fact, glycerol is able not only to stabilize folded protein structures, but also to enhance hydrophobic interactions between the adsorbed protein molecules, thus fostering aggregation.

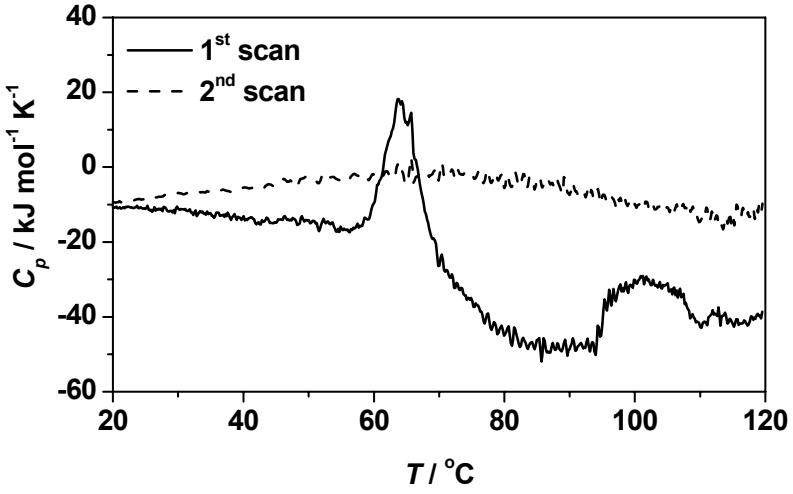

Fig. 4.10. DSC traces of RNase A in MCM-48 in 10 mM phosphate buffer solution at pH 5.5 and in the presence of 3.5 M glycerol at a mass ratio of RNase A to MCM-48 of 3:10, and a RNase A concentration of 3 mg/mL. To check for thermal reversibility, two consecutive scans were carried out.

Reheating of the sample shows no reversibility of both the confined protein population and the free protein, probably, again, due to the strong interaction of the unfolded protein with the silicate's external and internal surface.

4.2.5 Concluding remarks

It has been shown that the cubic phase mesoporous molecular sieve MCM-48 has a higher potential in fast immobilization of proteins compared to hexagonal phase material such as MCM-41 with similar pore diameter (28 Å) [Hartmann 2005]. The cubic, interwoven pore structure is probably more favorable for protein transfer and migration inside the mesopores. The protein loading can be tuned by changing the pH of the protein solution and by introducing co-solvents. The maximum loading was achieved at pH 9, which is close to the PI of RNase A (9.6). The addition of chaotropes such as urea leads to an increased protein loading. On the other hand, low pH and addition of kosmotropes, such as glycerol, leads to lower protein loading.

The protein is partially entrapped in the mesopores upon mixing with the MPS. Some protein fraction still remains in bulk buffer solution and unfolds as normal bulk protein upon heating. The unfolded protein increases the solvent accessible surface area of the protein, resulting in an increased affinity towards adsorption at the silicate surface of the MPS. In the presence of urea, such a major adsorption process does not take place because the unfolded protein's SAS is probably largely bound by the ligand urea. Aggregation of the adsorbed unfolded protein is fostered in the presence of glycerol. The protein RNase A confined in the mesopores of MCM-48 unfolds at much higher temperatures compared to the bulk (e.g., $\Delta T_m \approx 43$ (28) °C at pH 2 (5.5)), probably not only due to the excluded volume effect but also an increased strength of the hydration of the protein in the narrow mesopores as shown in our previous PPC measurements [Ravindra 2004b]. Also for the glycerol and urea containing protein samples, the confinement leads to an increase in unfolding temperature ($\Delta T_m \approx 37$ (35) °C in the presence of 3.5 M glycerol (urea)). It is still not quite clear, if and to what extent, the confined protein forms aggregates, but what is clear is that the support material with a fixed pore size should preclude normal three-dimensional aggregation.

4.3 Stability of RNase A confined in SBA-15

4.3.1 Immobilization equilibrium

The hexagonal phase material SBA-15 exhibits immobilization of RNase A with a capacity of ca. 143 mg/g (Fig. 4.11), which corresponds to 48 % of the whole protein content, when the mass ratio of RNase A to SBA-15 is 3:10 at pH 5.5. This capacity is much higher than that of MCM-48 at the same conditions, which is ca. 108 mg/g (see Section 4.2.1), probably due to larger specific pore volume (see Table 3.1). This is consistent with the observation of Vinu *et al.* that the amount immobilized is mainly a function of the specific pore volume [Vinu 2004b]. Immobilized RNase A molecules which have a dimension of approximately 100 % of the pore size of MCM-48, may hinder further molecules from being immobilized, so that part of the inner pore surface would remain inaccessible. This steric hindrance would be expected to be less significant for the larger pores of SBA-15 resulting in a higher loading. The immobilization equilibrium is reached within 4 h. More than 90 % of the maximum loading is achieved within 1 h, suggesting a high affinity between RNase A and the host. This rate of immobilization is almost the same as that for the cubic phase material MCM-48. Although the cubic structure is definitely more beneficial for protein transportation from the entrance to the inner part of the mesopores or mesochannels, which was suggested to be the rate-determining step of the whole immobilization process [Lei 2004], it has also been suggested that a large diameter of the pore entrance is beneficial for fast and efficient immobilization of proteins [Fan 2003b]. In our case, the pore diameter of SBA-15 is 5.8 nm, which is much larger than that of the MCM-48 investigated, *i.e.*, 2.5 nm, counterbalancing the unfavorable hexagonal pore structure. However, the maximum loading of the protein at pH 5.5 corresponds to 14 % volume of the mesopore volume (assuming the geometrical volume for the space required for a single protein molecule), only. It has been shown that the adsorption isotherms of lysozyme (LYS) on SBA-15 at different solution pH ranging from 6.5 to 10.5 (all lower than the PI of LYS) show a sharp initial rise, suggesting a high affinity between LYS and the adsorbent surface, and finally the isotherms reach a plateau, which are typical L (Langmuir) isotherms [Vinu 2004a]. It was experimentally verified that the protein molecules are well packed in the mesoporous channels of the SBA-15 mesoporous silica as shown in the so-called interdigitated triple molecular model [Miyahara 2006].

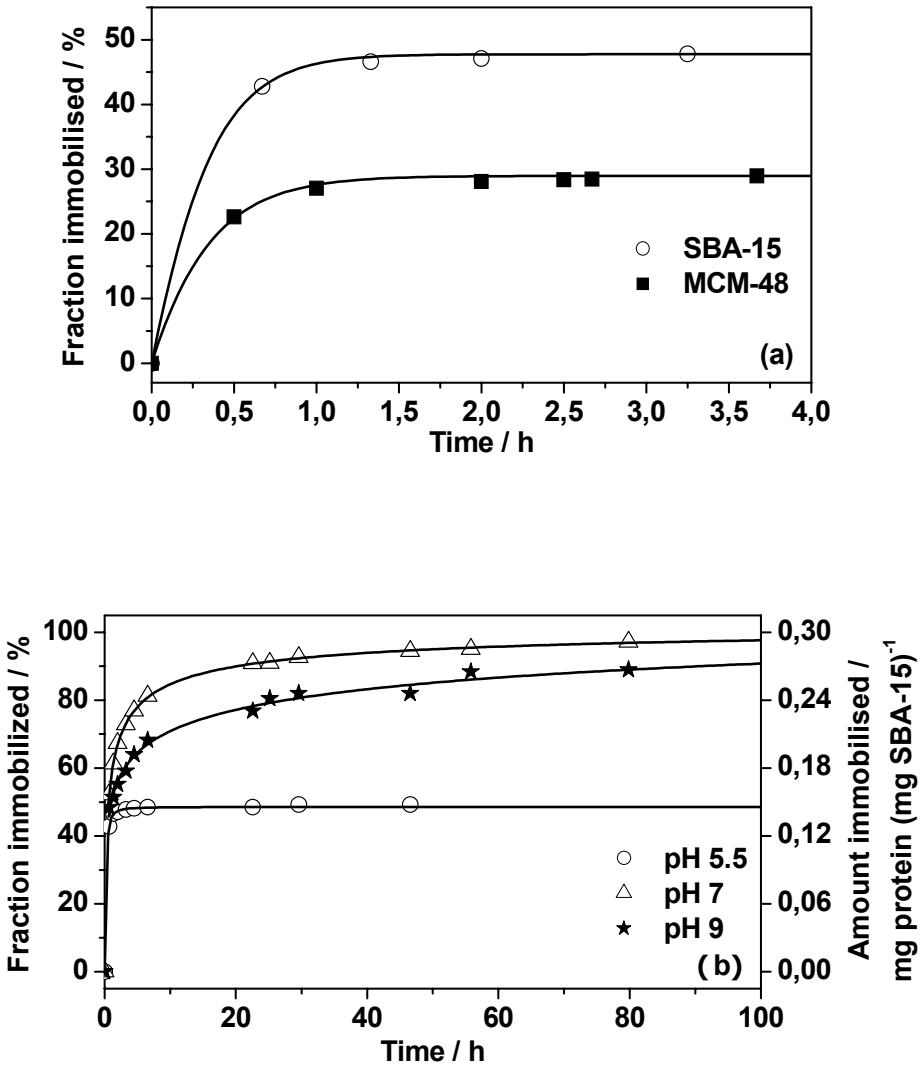

Fig. 4.11. Immobilization of RNase A (a) in SBA-15 and in MCM-48 at pH 5.5 (the mass ratio of RNase A to silicate is 3:10 and 4:10 respectively), and (b) in SBA-15 at different pH values (the mass ratio of RNase A to SBA-15 is 3:10).

As the isoelectric point (PI) of RNase A is 9.6, the protein is positively charged at pH 5.5. The point of zero charge (PZC) of the silica surface of the mesoporous materials is just below 3, hence, the host surface is negatively charged at pH 5.5. As a result, protein migration to the silicate surface may - at least partially - be driven by the electrostatic potential difference. Extended entrapment of protein into the mesopores will require the breaking of Columbic interactions between the mesoporous solid (MPS) and previously entrapped protein, which is an endothermic process [Czeslik 2001], thus one may expect that the amount of immobilization will be increased at elevated temperature, given that the protein structure does not unfold yet. The silanol groups located on the pore walls of the silicate can promote

immobilization through hydrogen bonding interactions with hydrophilic residues of the protein. The protein loading in SBA-15 at different conditions is summarized in Table 4.6.

Table 4.6: Protein loading on SBA-15 at different conditions (the mass ratio of RNase A to SBA-15 is 3:10).

Loading / mg/g	pH			Co-solvent / M		
				Urea		Glycerol
	5.5	7.0	9.0	0.5	3.5	3.5
143	×					
295		×				
277			×			
181	×			×		
214	×				×	
107	×					×

When the pH was increased from pH 5.5 to pH 7 at the same mass ratio of protein to MPS (3:10), the maximum loading drastically increased, from ca. 143 mg/g to ca. 295 mg/g, which, however, required much a longer time, 96 h, to reach. However, this loading of the protein, 98 % of the initial protein concentration, still corresponds to 30 % volume of the mesopore volume (assuming the geometrical volume for the space required for a single protein molecule), only. It is assumed that the amount of immobilization could be further enhanced when higher initial protein concentrations are applied. When the pH was further increased to pH 9, the maximum loading decreased to 277 mg/g, probably due to the too low charge density of the protein surface at this pH.

Noticeably, the maximum loading increases significantly, to 214 mg/g at pH 5.5, in the presence of 3.5 M urea, when the mass ratio of RNase A to SBA-15 is 3:10. The destabilizing nature of urea is mainly caused by a weakening of the peptide bonds and as a consequence, the protein (partially) unfolds and attains a more or less random coil like structure [Bennion 2003]. The specific binding of urea to the polypeptide also affects the solvent accessible surface area (ASA) by replacing water molecules and releasing them into the bulk phase, so that an extended hydrogen-bonded water layer around the protein surface is largely absent and the protein is less hydrated [Ravindra 2003a]. As a consequence, the protein molecule becomes highly flexible, hence a closer packing of the protein molecules inside the MPS is possible, so that an increase of the loading capacity is observed. In the presence of 0.5 M urea, the maximum loading was increased by 38 mg/g.

On the contrary, in the presence of 3.5 M glycerol, an osmolyte, the maximum loading of RNase A on SBA-15 decreases to 107 mg/g when the mass ratio of RNase A to SBA-15 is 3:10. Glycerol, being a strongly hydrophilic co-solvent, interacts strongly with H_2O and has a weaker affinity for the polar residues on the protein surface, thus leading to preferential hydration of the protein and an increase of the strength of hydration of the protein [Ravindra 2003a]. As a consequence, a close packing of the protein molecules inside the MPS is probably prohibited and the loading capacity decreases.

Besides the difference in pore size and pore geometry from the other mesoporous materials investigated in this study, the SBA-15 material possesses a unique property that the mesopores are connected *via* microporous channels [Zhao 1998a, Zhao 1998b]. While not assisting in the transport of proteins themselves, these will facilitate diffusion of substrate and product molecules from the active sites of immobilized enzyme, and thus play a significant role in the application of biocatalysts.

4.3.2 pH-dependent thermal stability of RNase A confined in SBA-15

Fig. 4.12 represents the DSC traces of RNase A in SBA-15 at pH 5.5, 7, and 9 in 10 mM phosphate buffer, respectively. The immobilization was successful at all pH values investigated when the immobilization was realized by shaking of the SBA-15 dispersion instead of stirring it. It seemed that stirring was much less efficient than shaking to the immobilization process. A possible explanation for this could be that stirring with a magnetic stirring bar destroys part of the mesoporous structure while milling the particles. This did not happen to other mesoporous materials, *viz.*, MCM-48 and MCM-41, because they possess rather high mechanical stability as compared to SBA-15, although SBA-15 has thicker walls and is more stable under hydrothermal conditions. It can be explained by a simple mechanical model showing that SBA-15 has an unfavourable ratio between pore diameter and wall thickness. This ratio is more favourable for MCM-41 despite its smaller wall thickness [Hartmann 2002]. The immobilization process was lasting for long enough time so that the equilibrium was reached, *i.e.* 4 h at pH 5.5 and 96 h at pH 7 and 9.

Similar to the MCM-48 result, the DSC peaks for the species entrapped in SBA-15 exhibit their maximum at much higher temperatures than that of the free proteins (Table 4.7), and their widths are also larger than that of the free protein in bulk solution. Interestingly, at pH 5.5, $T_{m,\,conf}$ for the species entrapped in SBA-15 (88.0 °C) is slightly lower than that for the species entrapped in MCM-48, which is probably due to the fact that the pore size of

MCM-48 (2.5 nm) is just comparable to the size of RNase A molecule and hence significantly smaller than that of the SBA-15 (5.8 mm). This is consistent with the observation that the thermal stability is maximized when the pore diameter of the host matches the size of the protein [Hartmann 2005].

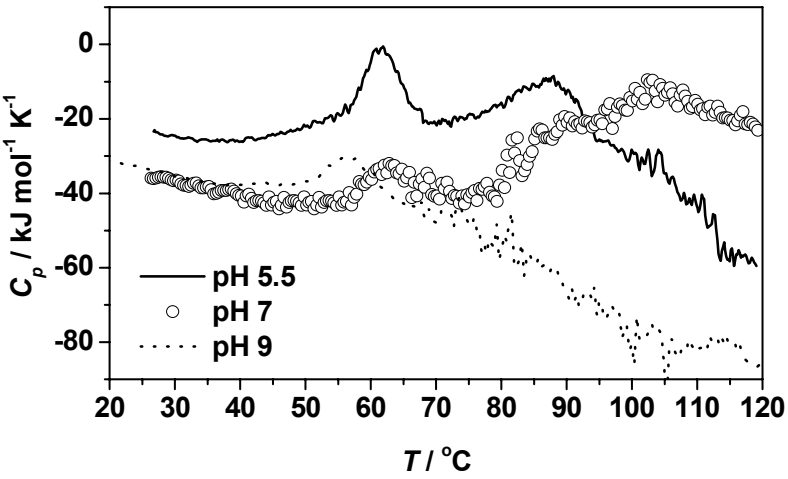

Fig. 4.12. Temperature dependence of the apparent molar heat capacity, C_p, of RNase A in SBA-15 in 10 mM phosphate buffer solution at different pH values. The mass ratio of RNase A to SBA-15 is 3:10 and the RNase A concentration is 3 mg/mL.

It has already been illustrated in Section 4.2.2 that the protein can be adsorbed on the external surface, and/or diffuse into the pores of the silicate, and there might be an excess protein fraction without any restricted mobility, *i.e.* with bulk-like behaviour of free protein. The DSC data in Fig. 4.12 does not indicate - or at least not so pronounced - the existence of adsorbed states of the protein which are susceptible to weak destabilization and whose unfolding temperature is shifted to slightly smaller values [Deere 2003]. This reflects the fact that the ratio of the outer surface area of SBA-15 to its internal surface is smaller than that of MCM-48, which is obviously consistent with the particle's morphology, *i.e.* the spherical MCM-48 material has a larger outer surface area the rod-like SBA-15 material.

Table 4.7: The unfolding temperature of free protein, $T_{m,\,free}$, and of the confined protein, $T_{m,\,conf}$, at different pH values.

pH	$T_{m,\,free}$ / °C	$T_{m,\,conf}$ / °C
5.5	61.9	88.0
7.0	62.8	105.8
9.0	- [a]	- [a]

a: value not possible to evaluate.

At the three pH values investigated, the DSC traces all drop with temperatures before the unfolding of the free protein takes place, very likely due to further adsorption of protein onto the silicate surface, which is exothermic.

At pH 5.5, the DSC trace continuously decreases after the unfolding of immobilized protein (P2), indicating possible aggregation of the unfolded immobilized protein, although, taken a different protein for comparison, it was shown from FT-IR spectra that no serious denaturation accompanies the changes in secondary structure during the immobilization process of myoglobin in SBA-15 mesopores [Miyahara 2006]. This effect was not so pronounced for MCM-48, very likely due to the MCM-48 pore size being just comparable to the size of RNase A molecule and thus preventing aggregation very effectively.

The stabilization against temperature-induced unfolding is further enhanced with the protein immobilization at higher pH, *i.e.*, T_m increases with increasing pH from 5.5 to 7 also for the confined protein. At pH 7, the DSC trace exhibits a very minor presence of free protein (P3) only, which indicates that most of the protein molecules were immobilised in the mesopores. This is in good agreement with the protein immobilization efficiency determined by spectroscopic means (see Section 4.3.1).

At pH 9, however, the DSC trace exhibits only a small peak with its maximum appearing at around 56 °C, a temperature between T_m of the external adsorbed protein (P1, 52 °C) and T_m of the free protein (P3, 63 °C). This peak could thus be assigned to the presence of a minor fraction of the free proteins (P3) and the adsorbed proteins (P1) and a complete absence of the immobilized native structure (P2). This could be due to the fact that the shaking time for immobilization (96 h) was too long for the protein to retain its native structure at pH 9 in the presence of silicate, the protein probably adsorbs on the external/internal surface of the SBA-15 in an already unfolded and/or aggregated state. This is evidenced by the fact that, past the small peak indicating the unfolding of protein adsorbed on the external surface of SBA-15, the DSC curve continuously decreases, which is an indication

for a continuous exothermic aggregation process taking place. Nevertheless, it is unlikely to assume that the protein molecules during the shaking process just form aggregates instead of adsorbing on the silicate surface, so that the concentration measured from the supernatant after centrifugation is so low owing to the fact that the aggregate was also removed by centrifugation. The reason is that the centrifugation speed (6000 rpm) was not high enough to be capable of removing oligomers. RNase A under these conditions can only form oligomers, and amyloid fibers are rarely being formed and under mild acid conditions, only [Liu 2001]. On the other hand, it may be speculated that the RNase A inside the mesopores at pH 9 can form fibers because the local concentration of protein is very high and the protein molecules are partially destabilized by the silicate surface. It has been proposed that every protein may form amyloid fibers at high concentration under partially destabilizing conditions [Chiti 2000] and each protein may be domain-swapped at high concentration under partially destabilizing conditions [Liu 2001].

The immobilization efficiency is also revealed by comparing the unfolding enthalpy of excess protein in the immobilization suspension, which corresponds to the amount of protein not being immobilized in the MPS, but rather remaining in solution. In Table 4.8, the $1-\Delta H_{exc}/\Delta H$ values are shown, which are proportional to the relative amount of immobilized protein. They increase with increasing pH, in agreement with the results obtained from the UV data, although, due to the rather small ΔH_{exc} value and rather noisy baseline, compared with the results from the MCM-48 data, the agreement is less good. The maximum loading of the MPS is achieved at pH 7 and 9 (similar values were obtained), which is near the isoelectric point of the protein (9.6 for RNase A), again demonstrating that the protein loading is clearly a function of solution pH. Similarly, the externally adsorbed population (these protein molecules that adsorb on the external surface of the MPS) that unfolds at temperatures lower than the bulk T_m, also increases upon increasing the pH. It has been shown from the MCM-48 results, that $(\Delta H_{exc}+\Delta H_{conf})/\Delta H$ is larger than 1, indicating that the unfolding enthalpy of the immobilized protein is significantly larger than that of the protein in bulk buffer solution, which is consistent with the increase in protein stability as reflected by the increase of T_m upon entrapment. This is also true for the SBA-15 data, but less pronounced, probably due to the fact that the unfolding of RNase A is, at least partially, followed by aggregation, which is exothermic and reduces the value of enthalpy change for the endothermic unfolding process of the confined protein.

Table 4.8: Comparison of the unfolding enthalpies of RNase A, ΔH, the unfolding enthalpy fractions of the excess and absorbed RNase A, ΔH_{exc}, and the unfolding enthalpy fraction of the confined RNase A, ΔH_{conf}, in the immobilization suspension at different pH values.

pH	ΔH / kJ/mol	ΔH / J/g	ΔH_{exc} / J/g protein dispersed	ΔH_{conf} / J/g protein dispersed	$1-\frac{\Delta H_{exc}}{\Delta H}$	$\frac{\Delta H_{exc}+\Delta H_{conf}}{\Delta H}$	Fraction immobilized
5.5	448	32.7	17.7	15.5	0.46	1.01	0.48
7.0	462	33.7	2.6	41.7	0.92	1.31	0.98
9.0	494	36.1	3.0	- [a]	0.92	- [a]	0.92

a: value not possible to evaluate.

To check for thermal reversibility, consecutive DSC scans were carried out for the samples at pH 5.5, 7 and 9, respectively (Fig. 4.13). In all cases, reheating of the sample revealed the irreversibility of the unfolding reaction, not only of the confined population but also of the free one. The latter finding could be explained by the adsorption of the unfolded protein molecules on the silicate surface, thus reducing the fraction refolding to their native structure upon cooling. Upon unfolding, more amino acids residues (also relatively more hydrophobic groups) are exposed, resulting in a much higher affinity between the protein and MPS. This might lead to a stronger adsorption of the unfolded protein on the MPS surface. Hence, the repeated DSC scans are reflecting essentially the temperature-dependent sum of the heat capacities of the absorbed unfolded protein and that of the unfolded confined protein, which is not able to refold due to the volume restriction in the though larger confined space, and propably also due to the irreversible formation of the aggregates.

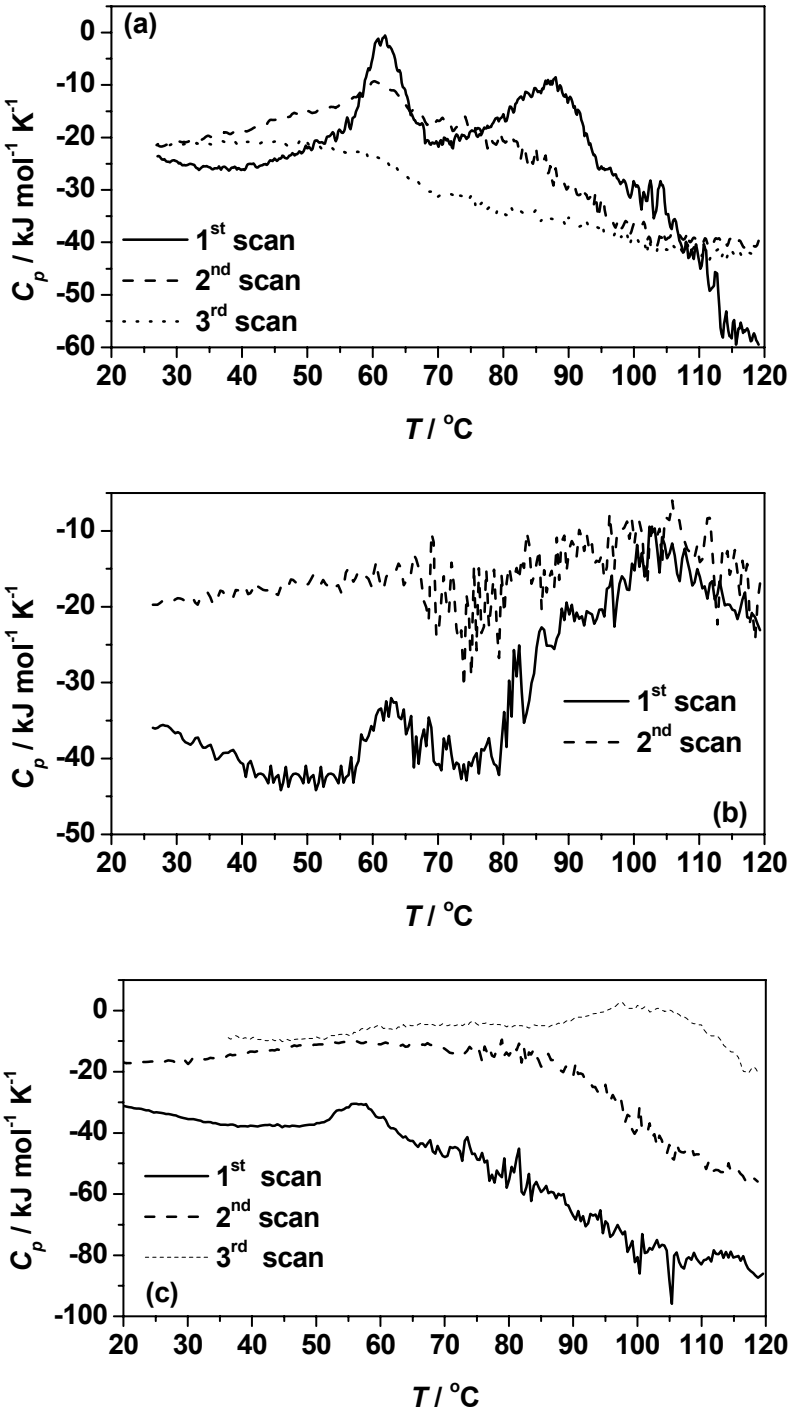

Fig. 4.13. DSC traces of RNase A in SBA-15 dispersion (10 mM phosphate buffer solution) at pH 5.5 (a), pH 7 (b) and pH 9 (c). The mass ratio of RNase A to SBA-15 is 3:10 and the RNase A concentration is 3 mg/mL. To check for thermal reversibility, consecutive scans were taken.

4.3.3 pH-dependent apparent thermal expansion of RNase A confined in SBA-15

In order to explore whether the hydration properties of the protein change upon entrapping in the SBA-15, which - in addition to the entropic confinement effect - might play a role in protein stabilization in confined space as well, PPC methods were applied. PPC measurements are able to yield valuable information on protein hydration and compactness as well as an accurate volume changes in the course of protein unfolding [Ravindra 2003a, Ravindra 2003b, Dzwolak 2003, Lin 2002, Dzwolak 2004, Sasisanker 2004].

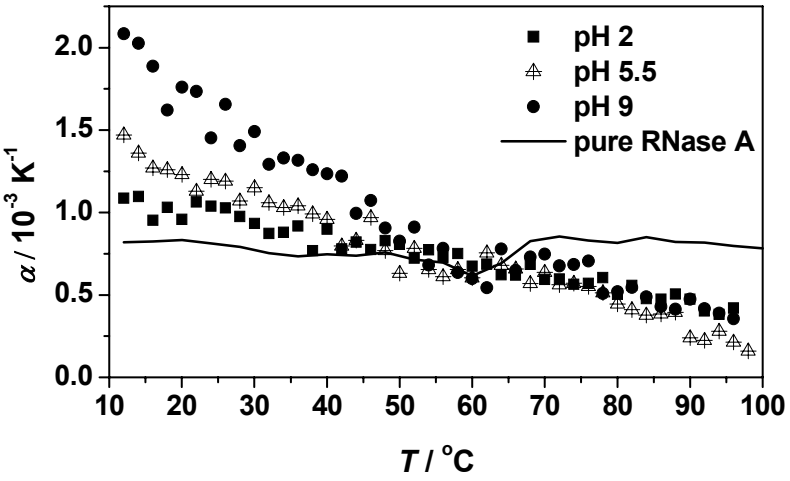

Fig. 4.14. Temperature dependence of the apparent thermal expansion coefficient, α, of RNase A in SBA-15 in 10 mM phosphate buffer solution (the mass ratio of RNase A to SBA-15 is 3:10 and the RNase A concentration is 3 mg/mL) at different pH values and of pure RNase A solution at pH 5.5.

Fig. 4.14 reveals the PPC data (apparent thermal expansion coefficient, α) of RNase A confined in SBA-15 at different pH values. Previous results of cosolvent effects on protein PPC data revealed that the level of hydration contributes significantly to protein stability as can be revealed from the absolute value and magnitude of the negative slope of the apparent thermal expansion coefficient, dα/dT [Ravindra 2003a, Ravindra 2003b, Dzwolak 2003, Lin 2002, Dzwolak 2004, Sasisanker 2004]. Fig. 4.14 shows that the α and dα/dT values measured for the protein incorporated in the SBA-15, are drastically enhanced and pH dependent. For example, at pH 2.0, α(10 °C) and dα/dT values of 1.1×10^{-3} K^{-1} and -8.3×10^{-6} K^{-2}, at pH 5.5, α(10 °C) and dα/dT values of 1.4×10^{-3} K^{-1} and -1.5×10^{-5} K^{-2}, and at pH 9, α(10 °C) and dα/dT values of 2.1×10^{-3} K^{-1} and -2.9×10^{-5} K^{-2}, are obtained, respectively, compared to corresponding values of 0.85×10^{-3} K^{-1} and -4.0×10^{-6} K^{-2} for RNase A in pure buffer solution. The much higher α and negative dα/dT values of the encapsulated protein indicate that the

protein is much stronger hydrated in the silica pores. As a consequence, this is also expected to increase its thermal stability. It is generally believed that Hofmeister ions, and hence also the silanol groups at the silica surface, influence the protein structure indirectly through changes in the hydrogen bonding properties of water, which might lead to the increased hydration of the embedded protein. Part of this effect could also be due to a decrease of the rotational and translational dynamics of the system, however.

The PPC curves at pH 5.5 and 7 between 50 and 70 ^{o}C reflect the unfolding of free RNase A in buffer solution. With regard to the embedded protein, α is continuously decreasing with temperature, though with decreasing slope at high temperatures. This is in contrast to RNase A in pure buffer solution, whose posttransitional α values are lying above the pretransition baseline, indicating an increase of the expansivity in the unfolded state. A well resolved free protein denaturation transition curve is observed at high protein loadings, only. With regard to the confined protein, the data indicate that inside the silica pores significant unfolding is not feasible anymore and hence must be incomplete. No volume change can be determined even with this sensitive PPC method applied, which allows measuring of ΔV values as small as ~0.1 %.

4.3.4 The effect of co-solvents, urea and glycerol

As already mentioned in Section 4.2.3, the thermal stability and solvational properties of proteins strongly depend on their interaction with the solvent or co-solvent at the protein-solvent interface. For kosmotropic co-solvents, such as glycerol, a continuous increase in hydration strength was observed with increasing glycerol concentration. In addition, glycerol acts as protein stabilizer, which is indicated by the increasing T_m and ΔH values of the protein. On the contrary, the chaotropic agent urea destabilizes proteins by direct ligand binding, which, in turn, is reflected in decreasing T_m and ΔH values [Ravindra 2003b]. It has been shown that the unfolding temperature, T_m, of RNase in 0.5 M urea is shifted to a slightly lower temperature with regard to the enzyme in pure buffer solution, and the reversible unfolding up to ~70 ^{o}C is followed by an irreversible aggregation process at higher temperatures. In 3.5 M urea solution, T_m decreases to 52.2 ^{o}C ($\Delta T_m = -10$ ^{o}C).

As mentioned above, the protein loading of the MPS increases to 214 mg/g in the presence of 3.5 M urea at pH 5.5. This effect is also visible in the DSC data (Fig. 4.15).

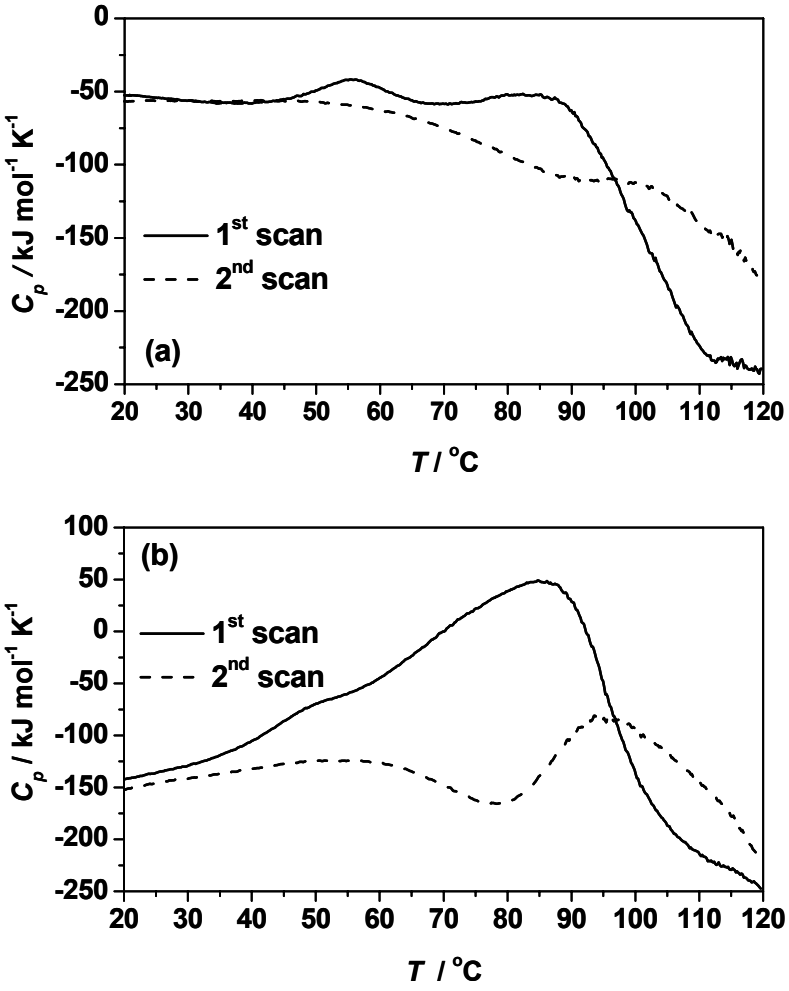

Fig. 4.15. DSC traces of RNase A in SBA-15 in 10 mM phosphate buffer solution at pH 5.5 and in the presence of 0.5 M urea (a) and 3.5 M urea (b). The mass ratio of RNase A to SBA-15 is 3:10, and the RNase A concentration is 3 mg/mL. To check for thermal reversibility, consecutive scans were taken.

The unfolding of the confined protein leads to much higher integral ΔH values, indicating a higher protein loading. It has been suggested that even at stirring conditions, there might exist a stagnant solution layer close to the surface of the MPS that must be penetrated by diffusion to allow for loading [Lei 2004]. In the presence of urea, *i.e.*, when the protein is destabilized and partially unfolded, the altered, elongated and more flexible protein conformation probably allows for a more effective penetration into the pores. When the urea concentration is 3.5 M, the unfolding temperatures of the confined protein extend over a wide temperature range, from about 52 to 94 ^{o}C with a maximum at 85 ^{o}C ($\Delta T_{m,conf} \approx 33$ ^{o}C). The extended width of transition temperatures probably also reflects the broad distribution of folded and partially unfolded protein structures present under these solvent conditions. The unfolding temperatures of the protein confined SBA-15 are slightly lower than that of the

protein confined in MCM-48, which again indicates that the protein stability is maximized when the confinement and the protein molecules are of similar dimensions.

To check for thermal reversibility, consecutive DSC scans were taken (Fig. 4.15). Reheating of the 3.5 M urea sample shows a DSC trace indicating that some confined protein population refolds and exhibits an even higher T_m value of about 94 ^oC (ΔT_m = 42 ^oC, see Table 4.9).

Table 4.9: Unfolding temperature T_m of the free and confined protein in the presence of different amount of urea, C_{urea}.

C_{urea} / M	T_m / °C		
	Free protein	Confined protein	
		1st scan	2nd scan
0.5	55.4	82.4	96.6
3.5	52.2	84.7	94.4

Fig. 4.16 reveals the PPC data (apparent thermal expansion coefficient, α) of RNase A confined in SBA-15 at pH 5.5 and in the presence of urea or glycerol, respectively. It shows that the α and dα/dT values measured for the protein incorporated in the SBA-15 in the presence of cosolvent, are different from those without cosolvent. In the presence of 3.5 M urea, α(10 °C) and dα/dT values of 1.2×10^{-3} K^{-1} and -1.1×10^{-5} K^{-2} are obtained, compared to corresponding values of 1.4×10^{-3} K^{-1} and -1.5×10^{-5} K^{-2} for confined RNase A when urea is absent. The slightly lower α and dα/dT values of the encapsulated protein is probably related to the specific binding of urea to the polypeptide, which affects the solvent accessible surface area by replacing water molecules and releasing them into the bulk phase, so that an extended hydrogen-bonded water layer around the protein surface is largely absent. In the presence of 3.5 M glycerol, α(10 °C) and dα/dT values of 1.3×10^{-3} K^{-1} and -1.8×10^{-5} K^{-2} are obtained, compared to corresponding values of 1.4×10^{-3} K^{-1} and -1.5×10^{-5} K^{-2} for confined RNase A when glycerol is absent. The slightly lower α of the encapsulated protein is probably related to lower protein loading.

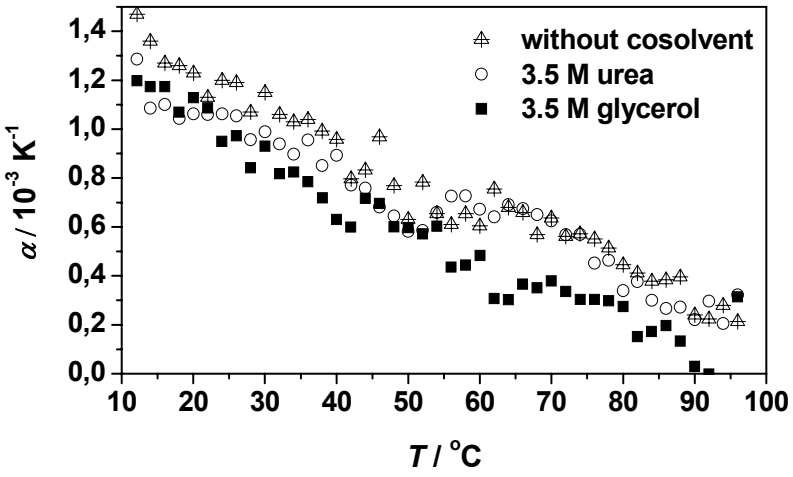

Fig. 4.16. Temperature dependence of the apparent thermal expansion coefficient, α, of RNase A in SBA-15 in 10 mM phosphate buffer solution at pH 5.5 and in the presence of 3.5 M urea and 3.5 M glycerol. The mass ratio of RNase A to SBA-15 is 3:10, and the RNase A concentration is 3 mg/mL.

4.3.5 Concluding remarks

It has been shown that the hexagonal phase mesoporous molecular sieve SBA-15 has a high potential in fast immobilization of proteins. The relatively large diameter of the pore (5.8 nm) is beneficial for protein transfer and migration inside the mesopores. The protein loading can be tuned by changing the pH of the protein solution and by introducing co-solvents. The maximum loading was achieved at pH 7, which is close to the PI of RNase A (9.6). The addition of chaotropes, such as urea, leads to an increased protein loading, whereas, lower pH and addition of kosmotropes, such as glycerol, leads to lower protein loading.

The protein is partially entrapped in the mesopores upon mixing with the MPS. Some protein fraction still remains in bulk buffer solution and unfolds as normal bulk protein upon heating. The unfolded protein increases the solvent accessible surface area of the protein, resulting in an increased affinity towards adsorption at the silicate surface of the MPS. In the presence of urea, such a major adsorption process does not take place because the unfolded protein's SAS is largely bound by the ligand urea. The protein RNase A confined in the mesopores of SBA-15 unfolds at much higher temperature compared to the bulk (e.g., $\Delta T_m \approx$ 26 (43) °C at pH 5.5 (7.0)), probably not only due to the excluded volume effect but also an increased strength of the hydration of the protein in the narrow mesopores as shown in our

PPC measurements. Also for the urea containing protein samples, the confinement leads to an increase in unfolding temperature ($\Delta T_m \approx 34$ °C in the presence of 3.5 M urea). It is clear that the SBA-15 material with it significantly larger pore size precludes normal three-dimensional aggregation not so effectively as MCM-48.

4.4 Stability of RNase A confined in C_{16}-MCM-41

4.4.1 Immobilization equilibrium

Whether high internal loading of proteins can be achieved depends partially on the nature of the protein adsorption on the silicate surface. If the adsorption is reversible, then the pore size needs only to be greater than the protein molecular size, because the relocation of protein molecules inside the mesopores could enable the extended loading. The same criterion applies if rapid, reversible adsorption is followed by slower, irreversible immobilization. However, if the irreversible immobilization is fast, the pore diameter must be at least three times the molecular diameter to enable full access to the internal pores [Yiu 2005]. It is also possible to imagine an intermediate situation, in which the proteins are covalently bonded by tethers present at low concentration within the pores. It would be unlikely for two such tethering points to be present at any one position in the channels, so that a pore diameter of more than twice the biomolecular radius would be required in this case. In any cases where blocking could occur, the hexagonal structure of C_{16}-MCM-41 would possess an inherent disadvantage compared to the cubic structure of MCM-48 with three-dimensional connectivity.

The hexagonal phase material C_{16}-MCM-41 exhibits successful immobilization of RNase A with a capacity of ca. 117 mg/g (Fig. 4.17), which corresponds to 39 % of the whole protein content, when the mass ratio of RNase A to C_{16}-MCM-41 is 4:10 at pH 5.5. This capacity is similar as that of MCM-48 at the same conditions (see Section 4.2.1). Although C_{16}-MCM-41 has a larger pore diameter (4 nm), the hexagonal structure is less beneficial for protein transportation from the entrance to the inner part of the mesopores or mesochannels, which was suggested to be the rate-determining step of the whole immobilization process [Lei 2004]. Compared with SBA-15 which also possesses a hexagonal pore geometry, but a larger pore size, the loading of RNase A in C_{16}-MCM-41 is much less efficient. It has been shown that the adsorption isotherms of lysozyme (LYS) on MCM-41 at different solution pH ranging from 6.5 to 10.5 (all lower than the PI of LYS) show a sharp initial rise, suggesting a high affinity between LYS and the adsorbent surface, and finally the isotherms reach a plateau, which are typical L (Langmuir) isotherms [Vinu 2004a]. Previous study on the adsorption of biomolecules in unfunctionalized MCM-41 shows that there was a significant decrease in adsorption capacity when the molecular mass of the adsorbent increased and molecules with MW higher than 40 kDa cannot enter the pores of MCM-41 but only be adsorbed on the outer

surface [Diaz 1996]. In our study, RNase A has only an MW of 13.7 kDa, and thus is small enough to enter the MCM-41 mesopores and to be successfully immobilized.

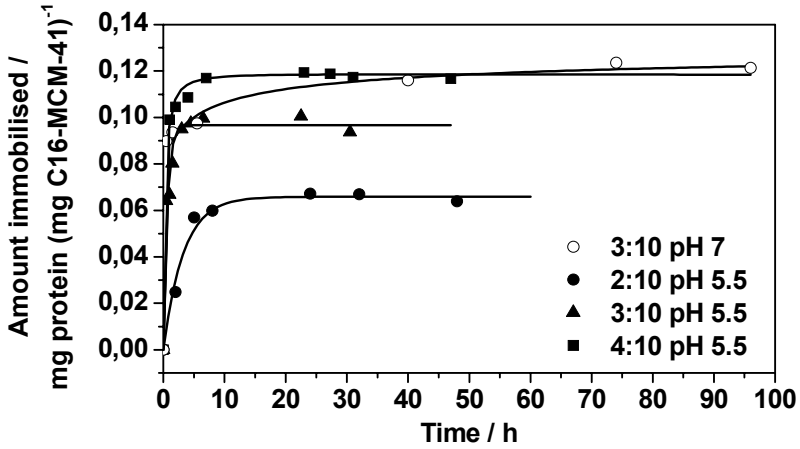

Fig. 4.17. Immobilization of RNase A in C_{16}-MCM-41 at pH 5.5 or 7 (the mass ratio of RNase A to silicate is 2:10, 3:10 and 4:10 respectively).

The forces binding proteins to hydrated silica surfaces may include hydrophobic, electrostatic, hydrogen bonding and weak van der Waals interactions. Eletrostatic protein-surface interactions are likely to be very strong when the immobilization is performed at a pH where the enzyme possesses a positive charge, because the silica surface of the mesoporous materials carries negative charges at pH values above 3. The sign of the overall charge on a surface can readily be predicted on the basis of the isoelectric point (the pH at which the overall charge is zero). This PI value of a protein molecule depends on the balance of surface functional groups (*e.g.* $-NH_2$, –COOH), which may have opposite charges. When the immobilization is performed at a pH lower than the PI of the protein but higher than the PZC of the silica, the protein will be positively charged. As the PI of RNase A is 9.6, the protein is positively charged at pH 5.5. As a result, protein migration to the silicate surface may partially be driven by the electrostatic potential difference. Extended entrapment of protein into the mesopores will require the breaking of Columbic interactions between the mesoporous solid (MPS) and previously entrapped protein, which is an endothermic process [Czeslik 2001], thus one may expect that the amount of immobilization will be increased at elevated temperature, given that the protein structure does not unfold yet. The silanol groups located on the pore walls of the silicate can promote immobilization through hydrogen bonding interactions with hydrophilic residues of the protein. The protein loading in C_{16}-MCM-41 at different conditions is summarized in Table 4.10.

Table 4.10: Protein loading in C16-MCM-41 at different conditions.

Loading / mg/g	Time to reach equilibrium / h	pH		Mass ratio [a]			Co-solvent / M Urea	
		5.5	7.0	2:10	3:10	4:10	0.5	3.5
67	10	×		×				
100	10	×			×			
117	10	×				×		
122	96		×		×			
110	10	×			×		×	
118	10	×						×

a: mass ratio of RNase A to C_{16}-MCM-41.

It is reasonable to assume that the immobilization equilibrium changes with the mass ratio of protein to MPS. We found that at pH 5.5, when the ratio of RNase A to C_{16}-MCM-41 was decreased from 4:10 to 3:10, the loading capacity decreases slightly from ca. 117 mg/g to ca. 100 mg/g (the error bar in the loading calculation is smaller than 4 mg/g), and when the mass ratio was decreased further to 2:10, the loading capacity is only 67 mg/g. Changing the MPS and protein concentration without altering their mass ratio does not significantly change either the rate or the equilibrium of the immobilization, however.

The greater the positive charge of the protein, the stronger the attraction between protein and silicate surface, but the stronger the repulsion between adsorbed molecules. Surface adsorption capacities of proteins are found to vary with the pH of adsorption according to a bell-curve, the maximum of which occurs often at the PI of the protein [Su 1998]. It therefore follows that by judicious variation of the pH, proteins could be adsorbed selectively and possibly be desorbed by changing the pH. When the pH was increased from pH 5.5 to pH 7 at the same mass ratio of protein to MPS (3:10), the maximum loading drastically increased, from ca. 100 mg/g to ca. 122 mg/g, which however required a much longer time, 96 h, to reach. The increased loading may be attributed to the reduced protein-protein repulsion and closer packing or even aggregation. It has been shown from the study of lysozyme immobilization in MPS that, at a higher pH (pH 12) the adsorption is no longer Langmuirian, which indicates that the protein-support interaction is no longer much stronger than the protein-protein interaction, due to the protein picking up negative charge [Vinu 2004a].

Irrespective of the dreadful long time required to reach the maximum loading, about 90 % of the maximum loading was reached within 15 h. On the other hand, as already

discussed in the previous chapter, 96 h was most likely too long for the protein to retain its native structure even at condition as mild as room temperature. Therefore, in all the following experiments, we use 15 h as the loading time instead of 96 h, knowing that the amount of protein loading may be about 10 % lower than the maximum loading. Previous study on the adsorption mechanism of peroxidase into MCM-41 shows that the kinetics is modeled by rapid Langmuir-type physisorption followed by slow chemisorption [Atyaksheva 2004].

The loading of the protein in C_{16}-MCM-14 at pH 7, that is 41 % of the initial protein concentration, was occupying only 18 % of the mesopore volume, assuming the geometrical volume for the space required for a single protein molecule. It is very likely that the amount of immobilization could be further enhanced when higher initial protein concentrations are applied.

Noticeably, the maximum loading increases significantly, to 118 mg/g, when 3.5 M urea was introduced to the loading buffer, and when the mass ratio of RNase A to C_{16}-MCM-41 is 3:10. In the presence of 0.5 M urea, the maximum loading was increased by 10 mg/g.

4.4.2 State distributions of the protein in confined geometry (C_{16}-MCM-41)

At low protein concentrations, the protein seems to be entrapped essentially in the narrowest pores available in C_{16}-MCM-41, which has about the same dimensions as the protein. Apparently, due to the strong restrictions in conformational space, the protein is not able to unfold markedly in these narrow pores anymore, thus leading to a steady increase of C_p up to the highest temperature measured, only (DSC curve for the mass ratio of 1.2 : 10 in Fig. 4.18). This is consistent with the observation that the unfolding enthalpy of the immobilized protein is significantly larger than that of the protein in bulk buffer solution (see Section 4.2.3). The DSC trace of a 1.2 mg/mL protein in 10 mg/mL C_{16}-MCM-41 suspension exhibits only a minor presence of free protein (P3).

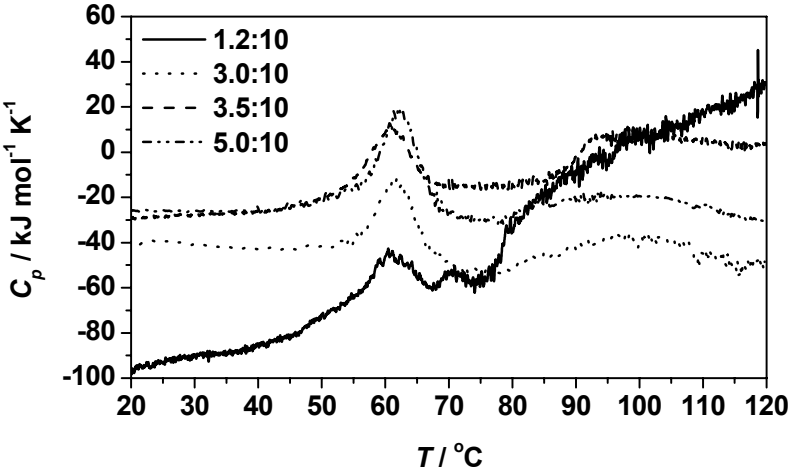

Fig. 4.18. Temperature dependence of the apparent molar heat capacity, C_p, of RNase A in C_{16}-MCM-41 in 10 mM phosphate buffer solution at different mass ratios of RNase A to C_{16}-MCM-41 at pH 5.5.

The immobilization efficiency is also revealed by comparing the unfolding enthalpy of excess protein in the immobilization suspension, which corresponds to the amount of protein not being immobilized in the MPS, but rather remaining in solution. In Table 4.11, the $1\text{-}\Delta H_{exc}/\Delta H$ values are shown, which are proportional to the relative amount of immobilized protein. They increase with increasing mass ratio of protein to C_{16}-MCM-41, in agreement with the results obtained from the UV data. It has been shown from the MCM-48 and SBA-15 result, that $(\Delta H_{exc}+\Delta H_{conf})/\Delta H$ is larger than 1, indicating that the unfolding enthalpy of the immobilized protein is significantly larger than that of the protein in bulk buffer solution, which is consistent with the increase in protein stability as reflected by the increase of T_m upon entrapment. This is also true for the C_{16}-MCM-41 result.

Table 4.11: Comparison of the unfolding enthalpies of RNase A, ΔH, the unfolding enthalpy fractions of the excess and absorbed RNase A, ΔH_{exc}, and the unfolding enthalpy fraction of the confined RNase A, ΔH_{conf}, in the immobilization suspension at different mass ratios of RNase A to C_{16}-MCM-41 at pH 5.5.

Mass ratio[b]	ΔH_{exc} / J/g protein dispersed	ΔH_{conf} / J/g protein dispersed	$1-\frac{\Delta H_{exc}}{\Delta H}$	$\frac{\Delta H_{exc}+\Delta H_{conf}}{\Delta H}$
1.2 : 10	14.4	- [a]	0.56	- [a]
3.0 : 10	22.2	23.8	0.32	1.41
3.5 : 10	25.1	25.7	0.23	1.55
5.0 : 10	26.2	22.7	0.20	1.49

a: value not possible to evaluate.

b: the mass ratio of RNase A to C_{16}-MCM-41.

4.4.3 pH-dependent thermal stability of RNase A confined in C_{16}-MCM-41

The thermal stability of RNase A confined in C_{16}-MCM-41 has been examined in aqueous medium. Fig. 4.19 represents the DSC traces of RNase A in C_{16}-MCM-41 at various pH values in 10 mM phosphate buffer, respectively. The immobilization was successful at all pH values investigated. Similar to the MCM-48 result, the DSC peaks for the species entrapped in C_{16}-MCM-41 exhibit their maximum at much higher temperatures than that of the free proteins (Table 4.12), and their widths are also larger than that of the free protein in bulk solution. $T_{m,\,conf}$ values for the species entrapped in C_{16}-MCM-41 are comparable to those for the species entrapped in MCM-48.

It has already been illustrated in Section 4.2.2 that the protein can be adsorbed on the external surface, and/or diffuse into the pores of the silicate, and there might be an excess protein fraction without any restricted mobility, *i.e.*, with bulk-like behaviour of free protein. The DSC data in Fig. 4.19 do not indicate – or at least not so pronounced – the existence of adsorbed states of the protein attached on the surface which are susceptible to weak destabilization and whose unfolding temperature is generally shifted to slightly smaller values [Deere 2003].

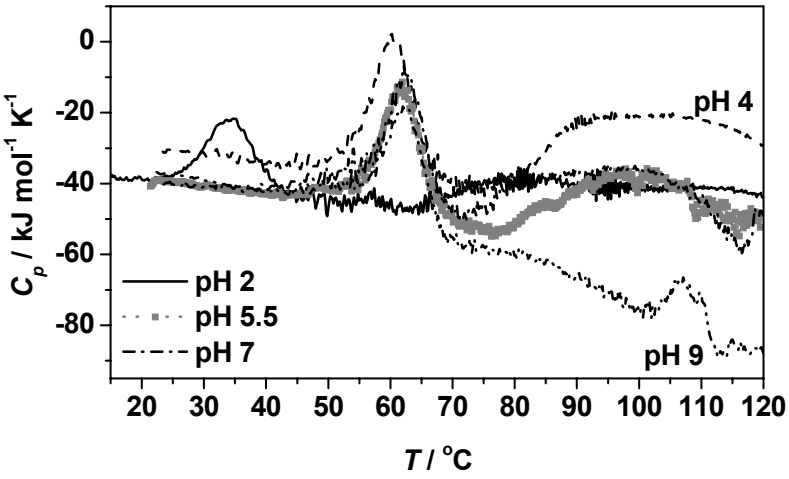

Fig. 4.19. Temperature dependence of the apparent molar heat capacity, C_p, of RNase A in C_{16}-MCM-41 in 10 mM phosphate buffer solution at different pH values. The mass ratio of RNase A to C_{16}-MCM-41 is 3:10 and the RNase A concentration is 3 mg/mL.

At the five pH values investigated, the DSC traces all drop before the unfolding of the free protein takes place, very likely due to further adsorption of protein onto silicate surface, which is exothermic, along with the increase of temperature. It has been shown that, with increasing temperature, the adsorption rate of protein in MPS is increasing over the temperature range from 4 °C to 55 °C [Lei 2004]. The crucial step influencing the adsorption rate is the in-pore diffusion step, and the migration of protein into the inner of mesopores, which is an endothermic process in order to break the Columbic interaction between MPS and the previous entrapped protein. Therefore, increasing temperature may favour a fast immobilization process of protein into MPS. When the immobilization is taken place at room temperature, most of the inner space of C_{16}-MCM-41 is still free of protein and the immobilization capacity is not saturated. Upon heating, further loading of protein is favourable due to the breaking of the Columbic interaction between the MPS and the previous entrapped protein.

Table 4.12: The unfolding temperature of free protein, $T_{m,\,free}$, and of the confined protein, $T_{m,\,conf}$ at different pH values.

pH	$T_{m,\,free}$ / °C	$T_{m,\,conf}$ / °C
2.0	35.2	80.9
4.0	60.3	99.4
5.5	61.9	97.9
7.0	62.2	99.3
9.0	62.0	107.1

The study on the effects of strength nanopore-protein interaction (λ) and temperature (T) on the stability of the protein upon confinement shows that, when there is no interaction between the pore and the protein ($\lambda = 0$ meaning the nanopore is inert), then the effect of pure physical entrapment is to promote stabilization of the native state [Cheung 2006]. Short-lived interactions between the pore wall and the protein side chain destabilize the native configuration but are not strong enough to destabilize the protein permanently. Protein encapsulation with C_{16}-MCM-41 mesopores also offers protection against other denaturing forces, such as extreme pH. A confined protein loses its ability to unfold in response to denaturing forces. As the folded configuration becomes energetically favorable due to confinement, it requires extra energy inputs to undergo denaturation. In Fig. 4.19, it shows that the confined protein at pH 2 exhibits a T_m value at about 81 °C, which is ca. 46 °C higher than the bulk protein. It should be noted that this increase of T_m upon confinement is even higher than those obtained at higher pH values. Another possible explanation for increased pH stability is that, for the encapsulated protein, the layer of water that hydrates the protein molecule within the nanocage is extremely thin, may be only one or two water molecule layer [Frenkel-Mullerad 2005]. If the water surrounding protein within a nanocage contains 100 water molecules, and the external pH is very high, for example pH 0, hydronium ions penetrate the pore so that nominal pH 0 is obtained inside the pore. Only two protons are sufficient to achieve pH 0 inside the pore. Protein can handle two protons in its vicinity, without undergoing denaturation. On the other hand, in solution, pH 0 means that the protein is exposed to a large number of protons, leading to its denaturation. pH is a classical thermodynamics concept that might not be able to explain the observed phenomenon at such a small scale inside the nanocages.

Electrostatic interactions between protein and the pore wall can influence the stability of an entrapped protein to a great extent. The stabilization against temperature-induced

unfolding is further enhanced with the protein immobilization at higher pH, *i.e.*, T_m increases with increasing pH also for the confined protein. At pH 9, however, the DSC trace continuously decreases after the unfolding of free protein (P3), indicating possible aggregation of the unfolded protein, and exhibits only a small peak at around 107 °C (P2), indicating only a very small population of confined native structure. This shows that the shaking time for immobilization was probably too long for the protein to remain its native structure at pH 9 and in the presence of silicate, so that the protein adsorbed on the external/internal surface of C_{16}-MCM-41 is already in its unfolded states or its aggregated states. Similar result was obtained on SBA-15 but even more pronounced, no P2 peak appears, probably because the pore size of SBA-15 (5.8 nm) is larger than that of C_{16}-MCM-41 (4.0 nm). On the other hand, it may be speculated that the RNase A inside the mesopores at pH 9 can form fibers because the local concentration of protein is very high and the protein molecules are partially destabilized by the silicate surface. It has been proposed that every protein may form amyloid fibers at high concentration under partially destabilizing conditions [Chiti 2000] and each protein may be domain-swapped at high concentration under partially destabilizing conditions [Liu 2001]. Furthermore, at pH 9, the RNase A is more likely to form aggregate, which could be induced by the change in electrostatic interactions, *i.e.*, the reduction of repulsive Coulombic forces between the unfolded protein molecules at pH values close to the PI of RNase A (9.6).

The immobilization efficiency is also revealed by comparing the unfolding enthalpy of excess protein in the immobilization suspension, which corresponds to the amount of protein not being immobilized in the MPS, but rather remaining in solution. In Table 4.13, the $1-\Delta H_{exc}/\Delta H$ values are shown, which are proportional to the relative amount of immobilized protein. They increase with increasing pH, in agreement with the results obtained from the UV data. The maximum loading of the MPS is achieved at pH 7 and 9 (similar values were obtained), which are near the isoelectric point of the protein (9.6 for RNase A), again demonstrating that the protein loading is clearly a function of solution pH.

Table 4.13: Comparison of the unfolding enthalpies of RNase A, ΔH, the unfolding enthalpy fractions of the excess and absorbed RNase A, ΔH_{exc}, and the unfolding enthalpy fraction of the confined RNase A, ΔH_{conf}, in the immobilization suspension at different pH values.

pH	ΔH / kJ/mol	ΔH / J/g	ΔH_{exc} / J/g protein dispersed	ΔH_{conf} / J/g protein dispersed	$1-\frac{\Delta H_{exc}}{\Delta H}$	$\frac{\Delta H_{exc}+\Delta H_{conf}}{\Delta H}$	Fraction immobilized
2.0	270	19.7	14.9	25.0	0.24	2.03	0.25
4.0	426	31.1	20.5	42.6	0.34	2.03	0.34
5.5	448	32.7	21.6	48.3	0.34	2.13	0.33
7.0	462	33.7	20.3	57.3	0.40	2.30	0.41
9.0	494	36.1	20.2	- [a]	0.44	- [a]	0.42

a: value not possible to evaluate.

The $(\Delta H_{exc}+\Delta H_{conf})/\Delta H$ values when RNase A is immobilized in MCM-48, SBA-15 and C_{16}-MCM-41, respectively, are plotted against the corresponding pH in Fig. 4.20. The $(\Delta H_{exc}+\Delta H_{conf})/\Delta H$ values are all larger than 1, indicating that the unfolding enthalpy of the immobilized protein is significantly larger than that of the protein in bulk buffer solution. This is consistent with the increase in protein stability as reflected by the increase of T_m upon entrapment. The $(\Delta H_{exc}+\Delta H_{conf})/\Delta H$ values for the SBA-15 are much lower than MCM-48 and C_{16}-MCM-41, probably due to the fact that the unfolding of RNase A is, at least partially, followed by aggregation, which is exothermic and reduces the value of enthalpy change for the endothermic unfolding process of the confined protein. In the case of MCM-48 and C_{16}-MCM-41, the mesopores are smaller, thus protect the protein from aggregation more effectively. The $(\Delta H_{exc}+\Delta H_{conf})/\Delta H$ values for C_{16}-MCM-41 are generally lower than MCM-48, due to the fact that the amount of protein loading in MCM-48 is slightly higher.

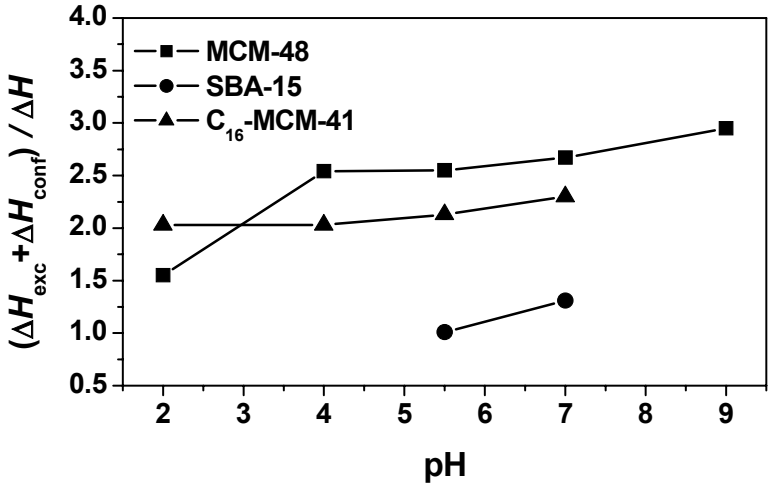

Fig. 4.20. Comparison of the $(\Delta H_{exc}+\Delta H_{conf})/\Delta H$ values at different pH in the case of MCM-48, SBA-15 and C_{16}-MCM-41.

It has been suggested that a strong interaction between the protein and the internal surface of the mesopore takes place upon unfolding [Droghetti 2005]. The unfolding process mainly depends on the interaction between the exposed positive charges of the unfolded protein and the negatively charged functional groups of the silica surfaces. To check for thermal reversibility, consecutive DSC scans were carried out for the samples at pH 5.5 and 7, respectively (Fig. 4.21). In both cases, reheating of the sample revealed the irreversibility of the unfolding reaction, not only of the confined population but also of the free one, probably due to the adsorption of the unfolded protein molecules on the silicate surface, thus reducing the fraction refolding to their native structure upon cooling. Upon unfolding, more amino acids residues (also more hydrophobic groups) are exposed, resulting in a much higher affinity between the protein and MPS. This might lead to a stronger adsorption of the unfolded protein on the MPS surface. Hence, the repeated DSC scans are reflecting essentially the temperature-dependent sum of the heat capacities of the absorbed unfolded protein and that of the unfolded confined protein, which is not able to refold due to the volume restriction in the confined space, and propably also due to irreversible formation of aggregates.

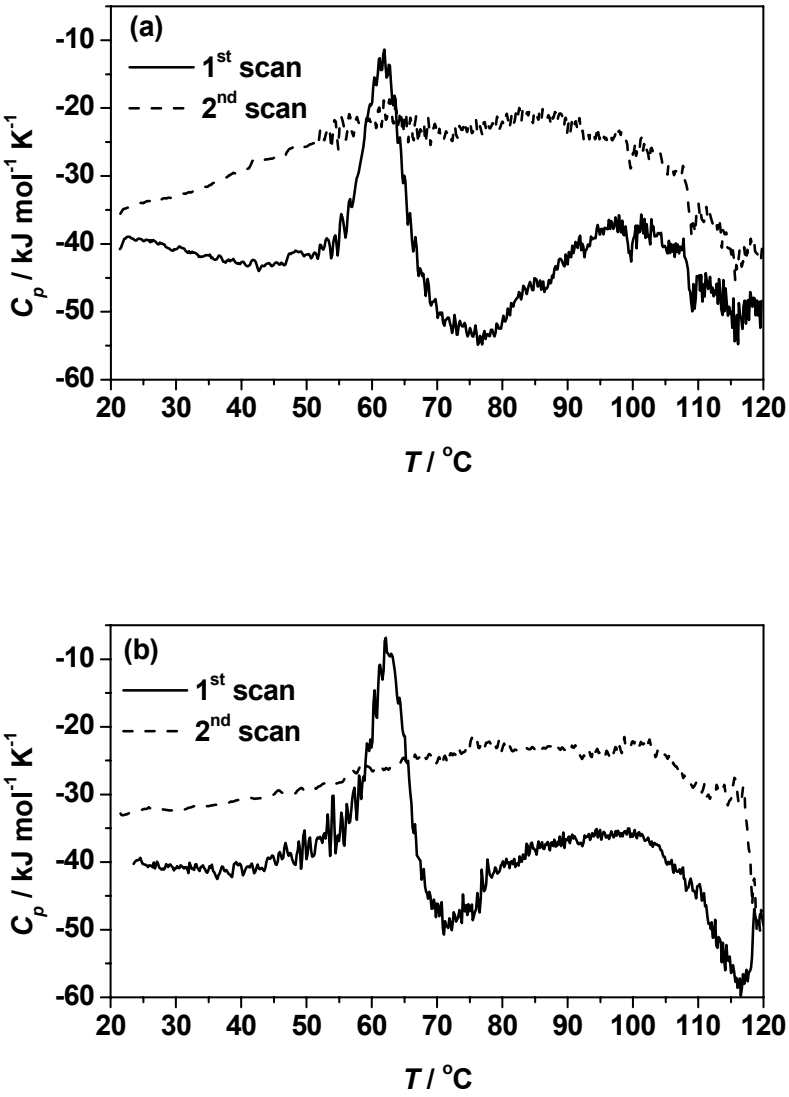

Fig. 4.21. DSC traces of RNase A in C_{16}-MCM-41 dispersion (10 mM phosphate buffer solution) at pH 5.5 (a) and pH 7 (b). The mass ratio of RNase A to C_{16}-MCM-41 is 3:10 and the RNase A concentration is 3 mg/mL. To check for thermal reversibility, consecutive scans were taken.

For applications in chemical industries, establishing their stability and activity in non-aqueous media would be an important step forward for enzyme immobilization [Carrea 2000]. Additionally, once supported, the solubility of an enzyme in an organic solvent may be very low, and leaching is avoided in this way. Accordingly, examination of thermal stability of immobilized protein in organic solvent would be of great interest for the future study.

4.4.4 pH-dependent apparent thermal expansion of RNase A confined in C_{16}-MCM-41

Once entrapped within the nanopores, the dynamics of protein molecule such as rotational mobility or diffusional ability will be altered as a result of steric hindrance. If the pores are filled with a solvent, then the microviscosity with the encapsulation site will be the additional constraint on the dynamics of the molecule with the pore. The solvent residing with the nanopores is likely to become perturbed due to interactions with the pore walls. The solvent confined within the nanopores might behave differently than bulk solvent [Bellissent-Funel 2003]. Polar solvents interact with polar surface groups of the silica matrix, which results in increased viscosity with the layer of the solvent adjacent to the pore walls. The depth of this perturbed layer and increase in viscosity depend upon the strength of interaction and dimension of the pore that confines the solvent. Such surface interaction effects on the viscosity of confined solvents are inversely proportional to the pore radius. As the pore radius decreases, the surface area to volume ratio increases, leading to increased surface interactions. Non-polar solvents, on the other hand, due to lack of any interaction with the surrounding silica matrix, remain relatively unperturbed with the pores [Klafter 1989]. The change in the solvent viscosity affects the rate of conformational changes of proteins [Beece 1980]. Obviously, the protein molecule residing in the mesochannel has restricted freedom. Molecular dynamics simulation of a model protein within a solvent of high and low viscosity showed no dependence of protein equilibrium properties on solvent viscosity [Walser 2001]. The secondary structure of protein is the same as in both viscosity domains. However, the dynamic properties of protein are dependent on solvent viscosity. High viscosity affects the motion of protein atoms on the surface as well as in the centre of the protein. Solvent dielectric constant also affects protein motion: protein dynamics is faster when the solvent has a high dielectric constant [Affleck 1992].

In order to explore whether the hydration properties of the protein change upon entrapping in the C_{16}-MCM-41, which - in addition to the entropic confinement effect - might play a role in protein stabilization in confined space as well, the PPC method was applied. Fig. 4.22 reveals the PPC data (apparent thermal expansion coefficient, α) of RNase A confined in C_{16}-MCM-41 at different pH values. Volumetric data derive from the PPC curves are summarized in Table 4.14. For RNase A incorporated in the C_{16}-MCM-41, both the absolute values of the thermal expansion coefficient α at low temperature, as well as their temperature coefficient $d\alpha/dT$, are markedly higher than in pure buffer solution. These volumetric effects of confinement are in the same direction as obtained by H_2O-D_2O substitution, and also

observed by addition of kosmotropic co-solvents such as glycerol or sorbitol [Ravindra 2003b]. This evidences a prime role of the enhanced solvation of the hydrophilic amino acid groups by water in mesochannels, and clearly points towards a stabilization of the native form upon entrapping. Part of this effect could also be due to a decrease of the rotational and translational dynamics of the system. It also shows that there is a continuous increase in α(10 °C) and $-\mathrm{d}\alpha/\mathrm{d}T$ with increasing pH values, which indicates an increase of the degree of solvation of the protein and an increase of the fraction of protein loading. With regard to the embedded protein, α is continuously decreasing with temperature. At pH 2 and pH 5.5, the volume change upon unfolding of the free protein is still visible at the corresponding T_m, ca. 40 °C and 60 °C, respectively. At pH 9, however, the unfolding of the free protein is not observable, possibly due to the fact that a large fraction of the protein is confined in the mesopores.

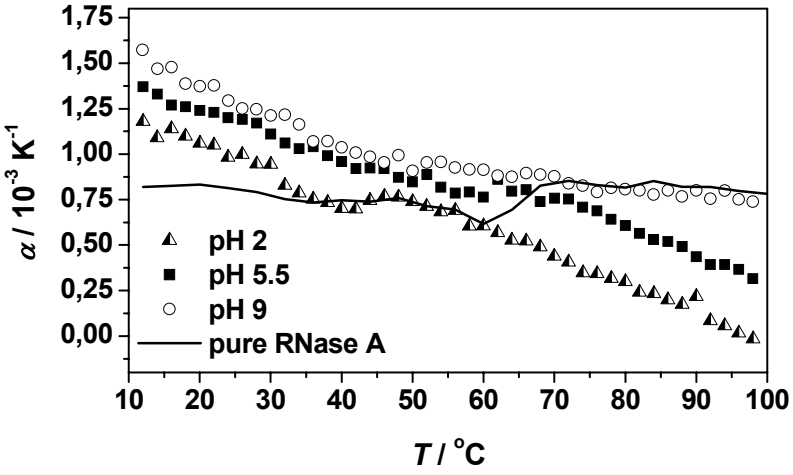

Fig. 4.22. Temperature dependence of the apparent thermal expansion coefficient, α, of RNase A in C_{16}-MCM-41 in 10 mM phosphate buffer solution (mass ratio of RNase A to C_{16}-MCM-41 is 1:10 and the RNase A concentration is 5 mg/mL) at different pH values and of pure RNase A solution at pH 5.5.

Table 4.14: Volumetric data obtained from the PPC experiments on RNase A in C_{16}-MCM-41 in 10 mM phosphate buffer solution (mass ratio of RNase A to C_{16}-MCM-41 is 1:10 and the RNase A concentration is 5 mg/mL) at different pH values and on pure RNase A solution at pH 5.5.

	pH 2	pH 5.5	pH 9	Pure RNase A
α(10 °C) / 10^{-3} K^{-1}	1.2	1.4	1.6	0.85
$\mathrm{d}\alpha/\mathrm{d}T$ / 10^{-5} K^{-2}	−1.3	−1.5	−1.7	−0.4

4.4.5 The effect of co-solvent, urea

Chaotropes, which are substances that disrupt the structure of water interactions, may help to solubilize hydrophobic residues of protein molecules. For example, hydrophobic peptides and proteins often may be dissolved in coupling buffer containing either 6 M Guanidine•HCl or 4 M urea. In addition to increasing solubility of hydrophobic residues, urea is general protein denaturant, unfolding proteins and altering their three-dimensional structures. Consequently, some proteins will be irreversibly altered upon action of these compounds and may lose their enzymatic activity.

However, protein encapsulation within the mesopores of MPS has been shown to offer protection against denaturants, such as urea. Fig. 4.23 depicts the DSC traces of RNase A in C_{16}-MCM-41 in 10 mM phosphate buffer solution at pH 5.5 and in the presence of 0.5 M urea and 3.5 M urea, respectively. Even when the urea concentration is as high as 3.5 M, the confined protein exhibits a T_m value of ca. 83 °C. The peaks for the entrapped species are relatively broader, which probably reflects, in addition to the variation in the mesopore size and the uneven protein distribution inside the mesopore, also a difference in the cooperativity of protein unfolding. The width of the calorimetric transition at half peak height, $\Delta T_{1/2}$, is indicative of the cooperativity of protein unfolding [Privalov 1971]. If the peak presents a low $\Delta T_{1/2}$ the transition is considered highly cooperative. Upon encapsulation, a loss of cooperativity (high $\Delta T_{1/2}$) of protein unfolding is detected. This effect is magnified at high concentrations of urea.

In addition, urea has been shown to be able to promote protein immobilization in mesoporous materials. This effect is also visible in the DSC data (Fig. 4.23). The enthalpy change of the unfolding for the entrapped species in the presence of urea is much higher than without urea, and increases further with increasing urea concentration, which indicates that the amount of protein loading increases also with increasing urea concentration.

The unfolding temperature T_m of the free protein and the protein confined in C_{16}-MCM-41 in the presence of different amount of urea, C_{urea}, is summarized in Table 4.15. Reheating of the sample shows a DSC trace (Fig. 4.23), which indicates some confined protein population refolds and exhibits an even higher T_m value, for example 95 ^oC in the presence of 3.5 M urea.

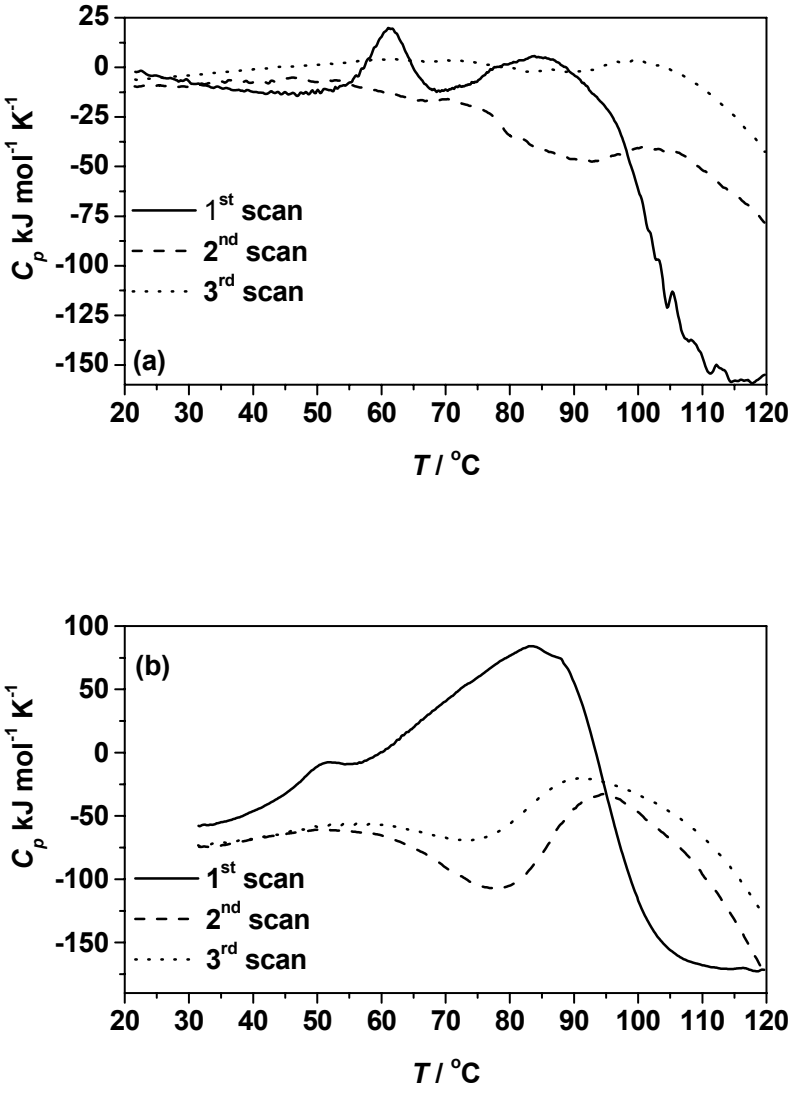

Fig. 4.23. DSC traces of RNase A in C_{16}-MCM-41 in 10 mM phosphate buffer solution at pH 5.5 and in the presence of 0.5 M urea (a) and 3.5 M urea (b). The mass ratio of RNase A to SBA-15 is 3:10, and the RNase A concentration is 3 mg/mL. To check for thermal reversibility, consecutive scans were taken.

Table 4.15: Unfolding temperature T_m of the free and confined protein in the presence of different amount of urea, C_{urea}.

C_{urea} / M	T_m / °C		
	Free protein	Confined protein	
		1st scan	2nd scan
0.5	61.0	83.8	100.4
3.5	51.8	83.3	94.7

A comparison of the unfolding temperatures of the protein confined in different MPSs in the presence of urea is summarized in Fig. 4.24. T_m values for the protein confined in C_{16}-MCM-41are slightly lower than those of the protein confined in MCM-48 with a smaller pore size (2.5 nm), and slightly higher than SBA-15 with a larger pore size (5.8 nm), which indicates that the protein stability is maximized when the confinement and the protein molecules are of similar dimensions.

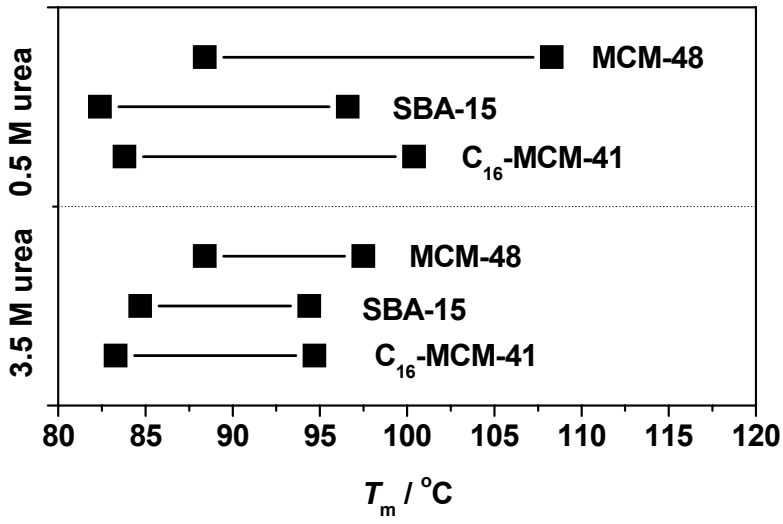

Fig. 4.24. Comparison of the unfolding temperatures (determined from 1st and 2nd DSC heating-scans) of the protein confined in different MPSs in the presence of 0.5 M and 3.5 M urea.

4.4.6 Concluding remarks

The immobilization behavior of RNase A in the hexagonal phase mesoporous silica (MPS) C_{16}-MCM-41 with mesochannel diameter of 4 nm has been studied. It is revealed that the solution pH and the addition of chaotrope, urea, plays an important role in the immobilization performance of enzyme: both the increase of pH from 5.5 to 7, and the introduction of urea into the protein solution, lead to a significant improvement of immobilization ability. The immobilization capacity of C_{16}-MCM-41 is generally similar as that of MCM-48 at the same conditions. Although C_{16}-MCM-41 has a larger pore diameter (4 nm), the hexagonal structure is less beneficial for protein transportation from the entrance to the inner part of the mesopores or mesochannels, which was suggested to be the rate-determining step of the whole immobilization process [Lei 2004]. Compared with SBA-15 which also possesses a

hexagonal pore geometry but a larger pore size, the loading of RNase A in C_{16}-MCM-41 is much less efficient.

Once entrapped within the nanopores, the dynamics of protein molecule such as rotational mobility or diffusional ability will be altered as a result of steric hindrance. Consequently, protein encapsulated within C_{16}-MCM-41 offers protection against thermal denaturation and other denaturing forces, such as the presence of a denaturant or extreme pH. As the folded configuration becomes energetically favourable due to confinement, it requires extra energy inputs to undergo denaturation. RNase A confined in C_{16}-MCM-41 with mesochannel diameter of 4 nm, exhibits T_m value of 98 °C at pH 5.5, 81 °C at pH 2, and 83 °C in the presence of 3.5 M urea.

It has been suggested that a strong interaction between the protein and the internal surface of the mesopore takes place upon unfolding [Droghetti 2005]. The unfolding process mainly depends on the interaction between the exposed positive charges of the unfolded protein and the negatively charged functional groups of the silica surfaces. The unfolded protein increases the solvent accessible surface area of the protein, resulting in an increased affinity towards adsorption at the silicate surface of the MPS. As a consequence, reheating of the sample revealed the irreversibility of the unfolding reaction, not only of the confined population but also of the free one. However, in the presence of urea, such a major adsorption process does not take place because the unfolded protein's SAS is largely bound by the ligand urea.

For RNase A incorporated in the C_{16}-MCM-41, both the absolute values of the thermal expansion coefficient α at low temperature, as well as their temperature coefficient $d\alpha/dT$, are markedly higher than in pure buffer solution. This evidences a prime role of the enhanced solvation of the hydrophilic amino acid groups by water in mesochannels, and clearly points towards a stabilization of the native form upon entrapping. Part of this effect could also be due to a decrease of the rotational and translational dynamics of the system.

4.5 Stability of RNase A confined in C_{12}-MCM-41

4.5.1 Immobilization equilibrium

The hexagonal phase material C_{12}-MCM-41 is almost identical to C_{16}-MCM-41, except the smaller pore diameter (3 nm). C_{12}-MCM-41 exhibits immobilization of RNase A with a capacity of ca. 83 mg/g (Fig. 4.25), which corresponds to 28 % of the whole protein content, when the mass ratio of RNase A to C_{12}-MCM-41 is 3:10 at pH 5.5. It has been shown that the adsorption isotherms of lysozyme (LYS) on MCM-41 at different solution pH ranging from 6.5 to 10.5 (all lower than PI of LYS) show a sharp initial rise, suggesting a high affinity between LYS and the adsorbent surface, and finally the isotherms reach a plateau, which are typical L (Langmuir) isotherms [Vinu 2004b]. This capacity is lower than that of C_{16}-MCM-41 at the same condition (100 mg/g, see Section 4.4.1), due to smaller pore size and smaller specific pore volume. This capacity is also lower than that of MCM-48 at the same condition (108 mg/g, see Section 4.2.1), although C_{12}-MCM-48 has a slightly larger pore diameter, the hexagonal structure is less beneficial for protein transportation from the entrance to the inner part of the mesopores or mesochannels, which was suggested to be the rate-determining step of the whole immobilization process [Lei 2004].

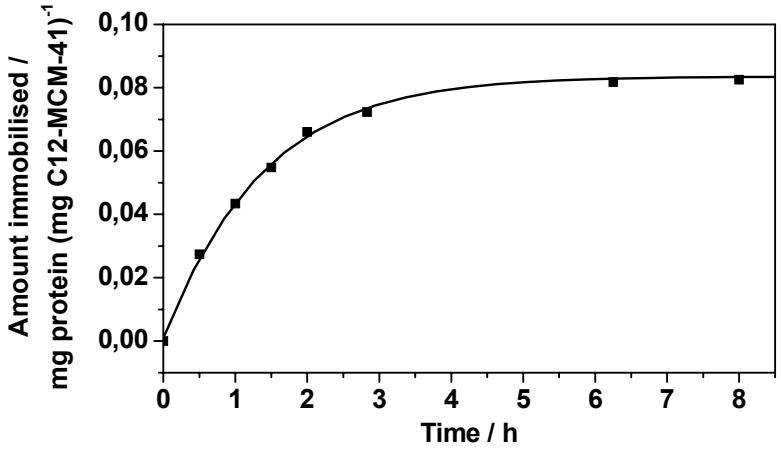

Fig. 4.25. Immobilization of RNase A in C_{12}-MCM-41 at pH 5.5 (the mass ratio of RNase A to silicate is 3:10).

In summary, the maximal loading of RNase A in MPSs seems to increase with increasing specific pore volume of the mesoporous adsorbent. It can be seen from Table 3.1 that the pore volume decreases in the following order: SBA-15 > MCM-48 > C_{16}-MCM-41 > C_{12}-MCM-41. At pH 5.5 and when the mass ratio of RNase A to MPS is 3:10, the maximal

loading of RNase A in C_{12}-MCM-41 is 83 mg/g, whereas 100, 108 and 143 mg/g were observed for C_{16}-MCM-41, MCM-48 and SBA-15, respectively. It should be noted that the corresponding volumes occupied by the RNase A molecule are 12 % (C_{12}-MCM-41), 15 % (C_{16}-MCM-41), 7 % (MCM-48) and 14 % (SBA-15) of the specific pore volumes of the MPSs (assuming the geometrical volume for the space required for a single protein molecule). Fig. 4.26 shows the relation between specific pore volume of the MPSs and the amount of protein immobilized at pH 5.5. Not surprisingly, a clearly linear correlation is observed.

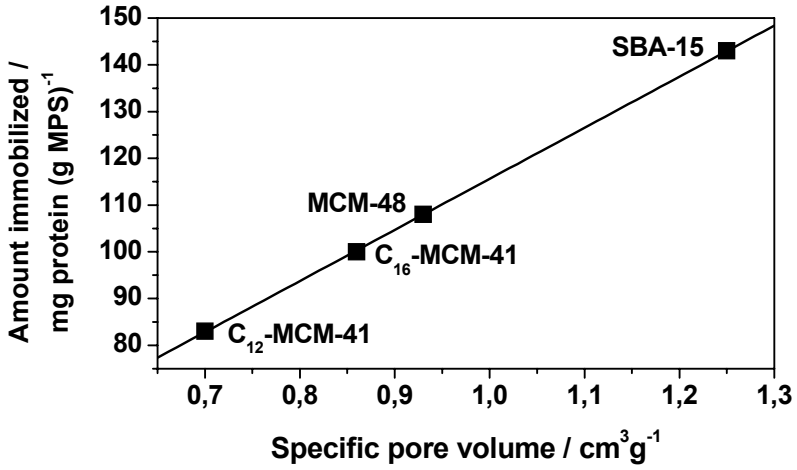

Fig. 4.26. Effect of specific pore volume of MPS on the RNase A immobilization efficiency at pH 5.5 in 10 mM phosphate buffer (the mass ration of RNase A to MPS is 3:10).

Back to the case of C_{12}-MCM-41, when the pH was increased from pH 5.5 to pH 9 at the same mass ratio of protein to MPS (3:10), the maximum loading drastically increased, from ca. 83 mg/g to ca. 110 mg/g, which, however, required a longer time to reach. This loading of the protein, 37 % of the initial protein concentration, corresponds to 15 % volume of the mesopore volume (assuming the geometrical volume for the space required for a single protein molecule), only. The amount of immobilization could be further enhanced when higher initial protein concentrations are applied.

Various biological molecules have been immobilized in C_{12}-MCM-41 in some previous studies. When tested as drug delivery system for the controlled released of ibuprofen (size = 1.0×0.6 nm), a maximum uptake of 300 mg/g was observed [Vallet-Regi 2001]. The maximal amount of lysozyme, whose molecular dimensions are slightly larger than RNase A, immobilized in C_{12}-MCM-41 at pH 10.5 is 193 mg/g, while the maximum loading of cyt c, which is of similar molecular size as RNase A, at pH 9.6 is 124 mg/g [Vinu 2004a].

4.5.2 pH-dependent thermal stability of RNase A confined in C_{12}-MCM-41

RNase A was successfully immobilized in C_{12}-MCM-41 at both pH 5.5 and pH 9. The protein molecules confined in the mesopores were stabilized according to temperature change by the protective environment. Such a mesoporous support with high protein immobilization capacity, possibly high protein activity, and enhanced protein thermal stability will be attractive for practical applications.

Fig. 4.27 represents the DSC traces of RNase A in C_{12}-MCM-41 in 10 mM phosphate buffer. The DSC peaks for the species entrapped in C_{12}-MCM-41 exhibit their maximum at much higher temperatures ($T_{m,\,conf}$ = 94 °C at pH 5.5, 108 °C at pH 9) than that of the free proteins, and their widths are also broader. $T_{m,\,conf}$ for the species entrapped in C_{12}-MCM-41 are comparable to those for the species entrapped in C_{16}-MCM-48.

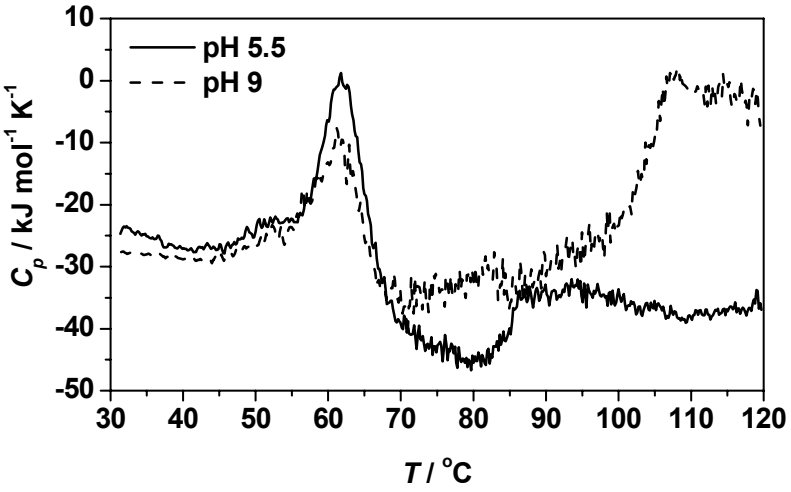

Fig. 4.27. Temperature dependence of the apparent molar heat capacity, C_p, of RNase A in C_{12}-MCM-41 in 10 mM phosphate buffer solution at different pH 5.5 and pH 9. The mass ratio of RNase A to C12-MCM-41 is 3:10 and the RNase A concentration is 3 mg/mL.

It has already been illustrated in Section 4.2.2 from the MCM-48 result, that the protein can be adsorbed on the external surface, and/or diffuse into the pores of the silicate, and there might be an excess protein fraction without any restricted mobility, *i.e.*, with bulk-like behaviour of free protein. The DSC data in Fig. 4.27 indicates existence of adsorbed states of the protein which are susceptible to weak destabilization and whose unfolding temperature is shifted to slightly smaller values (52 °C) [Deere 2003]. On the contrary, the protein adsorbed on the external surface of C_{16}-MCM-41 and SBA-15 is not so pronouncedly

visible, possibly due to the fact that their pore size is large enough for the protein to enter freely and consequently only very small amount of protein adsorbed on the external surface.

The immobilization efficiency is also revealed by comparing the unfolding enthalpy of excess protein in the immobilization suspension, which corresponds to the amount of protein not being immobilized in the MPS, but rather remaining in solution. The P2 peak increases with increasing pH, in agreement with the results obtained from the UV data.

To check for thermal reversibility, consecutive DSC scans were carried out for the samples at pH 5.5 and 9, respectively (Fig. 4.28).

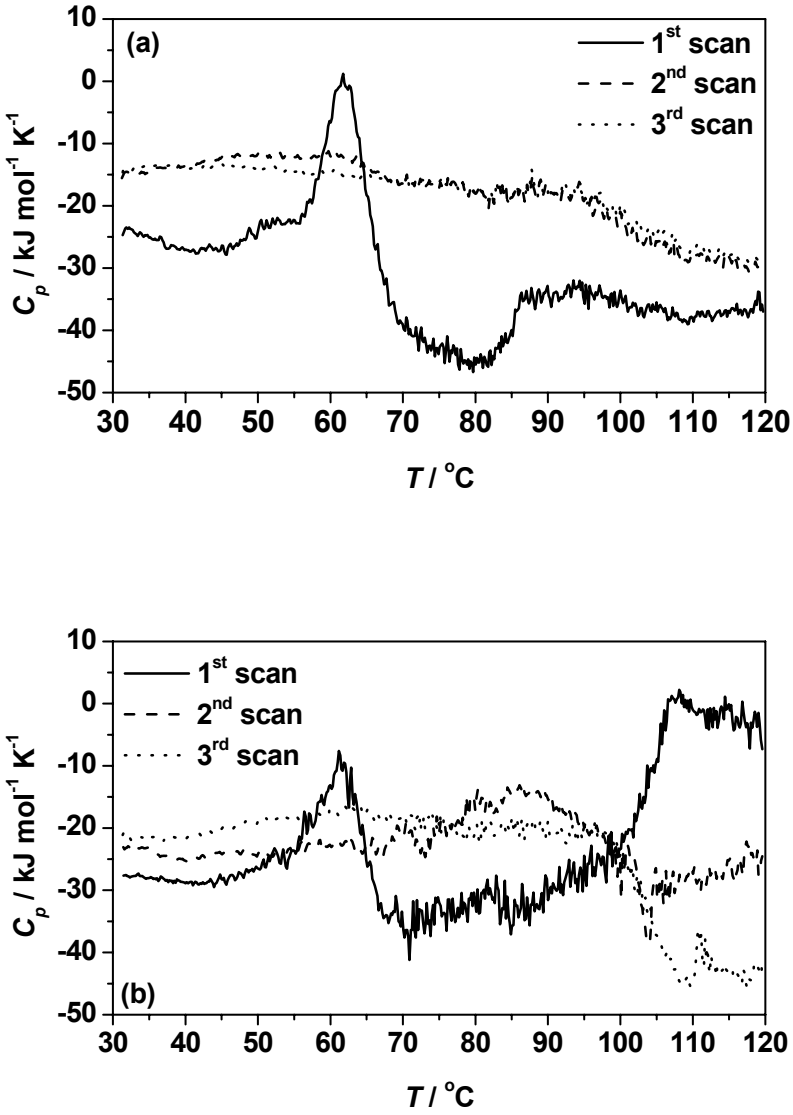

Fig. 4.28. DSC traces of RNase A in C_{12}-MCM-41 dispersion (10 mM phosphate buffer solution) at pH 5.5 (a) and pH 9 (b). The mass ratio of RNase A to C_{12}-MCM-41 is 3:10 and the RNase A concentration is 3 mg/mL. To check for thermal reversibility consecutive scans were taken.

Reheating of the sample at pH 5.5 revealed the irreversibility of the unfolding reaction, not only of the confined population but also of the free one. The second and the third heating scans are more or less identical, indicating that all the protein content, both the free protein and the confined one, losses the native structure almost completely upon the first heating run. However, at pH 9, the second heating scan shows a clear endothermic transition with its maximum at around 85 °C. This indicates that some of the confined protein molecules are able to refold upon cooling after being heated up to even 120 °C, whereas the free bulk protein not. It has been proposed that confinement of denatured protein in the narrow space results in acceleration of folding compared to that in free solution [Brinker 2001]. On the other hand, the refolding of denatured structure in the mesopores was not feasible at pH 5.5, because the highly positively charged amino acid residues and consequently their high affinity towards the negatively charged silicate surface, leads to a strong adsorption of the unfolded structure on the mesopore wall. At pH 9, which is very close to the PI of RNase A (9.6), the protein is only slightly charged, thus the interaction between protein and silicate is very weak.

4.5.3 Apparent thermal expansion of RNase A confined in C_{12}-MCM-41

Pressure perturbation calorimetric measurements on the RNase A/C12-MCM-41 sample confirm the previous observation that the hydration properties of the protein change upon entrapping in the MPS. Fig. 4.29 reveals the PPC data (apparent thermal expansion coefficient, α) of RNase A confined in C_{12}-MCM-41. The α and $d\alpha/dT$ values measured for the protein incorporated in the C_{12}-MCM-41, are drastically enhanced. For example, α(10 °C) and $d\alpha/dT$ values of 0.98×10^{-3} K^{-1} and -8.75×10^{-6} K^{-2} are obtained, compared to corresponding values of 0.85×10^{-3} K^{-1} and -4.0×10^{-6} K^{-2} for RNase A in pure buffer solution. The much higher α and $-d\alpha/dT$ values of the encapsulated protein indicate that the protein is much stronger hydrated in the silica pores. However, the α and $-d\alpha/dT$ values measured for the protein incorporated in the SBA-15 are even higher, due to its higher capacity in immobilizing RNase A.

The PPC curves between 50 and 70 ^{o}C reflect the unfolding of free RNase A in buffer solution. With regard to the embedded protein, α is continuously decreasing with temperature. A well resolved free protein denaturation transition curve is observed. This is in contrast to the PPC curves obtained from the RNase A/SBA-15 and RNase A/C_{16}-MCM-41 samples, which shows no visible volume change upon unfolding of the free protein, possibly due to their higher protein immobilization capacity. The relative volume change upon unfolding,

$\Delta V/V$, for the free protein faction is −0.20 %, whereas for pure protein in buffer is −0.31 %. The ratio of these two values, 0.67, indicates roughly the protein fraction remains in bulk phase. This ratio deviates only slightly (5 %) from the result calculated from UV data that 28 % of the whole protein content is immobilized in the mesopores.

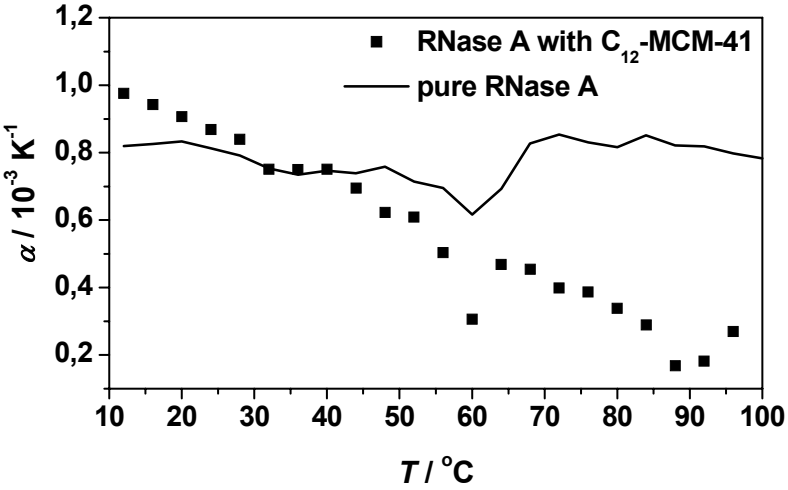

Fig. 4.29. Temperature dependence of the apparent thermal expansion coefficient, α, of RNase A in C_{12}-MCM-41 in 10 mM phosphate buffer solution (the mass ratio of RNase A to C_{12}-MCM-41 is 1:10 and the RNase A concentration is 5 mg/mL) at pH 5.5 and of pure RNase A solution at pH 5.5.

4.5.4 Concluding remarks

The hexagonal phase material C_{12}-MCM-41 is almost identical to C_{16}-MCM-41, except the smaller pore diameter (3 nm). C_{12}-MCM-41 exhibits immobilization of RNase A with a capacity of ca. 83 mg/g, when the mass ratio of RNase A to C_{12}-MCM-41 is 3:10 at pH 5.5. This capacity is lower than that of C_{16}-MCM-41 and MCM-48. The maximal loading of RNase A in MPSs seems to increase with increasing specific pore volume of the mesoporous adsorbent. Both the specific pore volume and the protein immobilization ability of the MPS decrease in the following order: SBA-15 > MCM-48 > C_{16}-MCM-41 > C_{12}-MCM-41.

The protein RNase A confined in the mesopores of C_{12}-MCM-41 unfolds at much higher temperature compared to the bulk (*e.g.*, $\Delta T_m \approx 32$ (45) °C at pH 5.5 (9.0)). Heating of the samples up to 120 °C at pH 5.5 and pH 9 shows different unfolding/refolding scenario, and the refolding of the heat-denatured RNase A in the confinement is feasible at pH value close to PI of the protein. The α and $d\alpha/dT$ values measured for the protein incorporated in the

C_{12}-MCM-41, are drastically enhanced. A well resolved free protein denaturation transition curve is observed. The relative volume change upon unfolding, $\Delta V/V$, for free RNase A faction is calculated to be −0.20 %, from which the free protein fraction was calculated to be 0.67. This deviates only slightly from the result calculated from UV data that 28 % of the whole protein content is immobilized in the mesopores.

4.6 Immobilization of urea-denatured RNase A into SBA-15

For different purposes, some researchers have attempted to immobilize protein molecules on solid surfaces or in confined space. Heat-denatured carbonic anhydrase and acid-denatured urease have been adsorptively immobilized on a hydrophobic surface, providing a convenient method of immobilization for proteins, which are not normally adsorbed on this surface [Azari 1999, Azari 2001]. Fusion protein of monomeric α-glucosidase was denatured and noncovalently immobilized on a polyanionic solid support, and shows an improved refolding behaviour upon removal of the denaturant [Stempfer 1996]. Upon unfolding, more amino acids residues (also more hydrophobic groups) of the protein molecule are exposed, resulting in a much higher affinity towards the solid surface. This might lead to a stronger adsorption of the unfolded protein on the surface, thus is supposed to improve the immobilization efficiency.

We report here a method to immobilize the urea-denatured RNase A in the SBA-15 mesopores, and test the refolding behavior of the confined protein upon the removal of urea. During the refolding process, the mesoporous structure may offer protection of the denatured protein against aggregation and accelerate the protein refolding due to the volume exclusion effect [Brinker 2001].

4.6.1 Immobilization equilibrium

SBA-15 showed a rapid adsorption of denatured RNase A (denoted as D-RNase A) with a capacity of ca. 215 mg/g (Fig. 4.30), which corresponds to 71.6 % of the whole protein content. The maximum immobilization of D-RNase A into SBA-15 was reached within 45 h. Considering the small external surface area of SBA-15 (10 m^2/g) based on a *t*-plot calculation [Fan 2003a], we conclude that almost all D-RNase A was adsorbed on the internal surface. Interestingly, the protein-loaded SBA-15 exhibited no detectable leaching over a period of 24 h in a Tris-HCl buffer containing 2 M urea, as monitored by UV absorbance at 278 nm. This result suggests a strong affinity of D-RNase A on the surface of SBA-15, which can be attributed to a close match of both hydrophilic-hydrophilic and hydrophobic-hydrophobic interactions between D-RNase A and the surface of SBA-15.

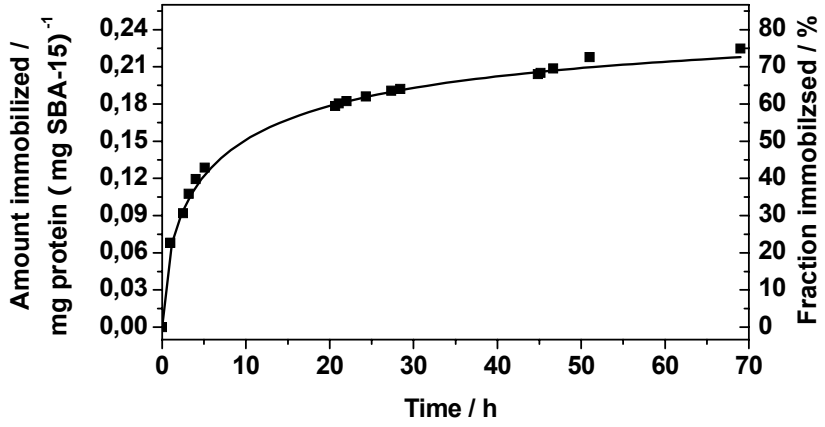

Fig. 4.30. Immobilization of D-RNase A into SBA-15 when the mass ratio of D-RNase A to SBA-15 is 3:10.

4.6.2 Refolding of D-RNase A inside SBA-15 mesopores

Protein-entrapped solids were recovered by centrifugation and washed several times with Tris-HCl buffer without urea until no palpable amount of protein was observed in the washing buffer, then re-suspended in Tris-HCl buffer. The resulting suspension with matching buffer was measured from 12 to 120 °C by DSC (Fig. 4.31). The DSC trace shows its maximum at around 79 °C, which corresponds to the thermal unfolding of the native RNase A confined in SBA-15. This population of native RNase A was refolded from the D-RNase A immobilized in the mesopores of SBA-15. It shows that upon the elimination of urea from the buffer, the

confined protein can refold and remain in the SBA-15 mesopores. The confinement should speed up the process of refolding.

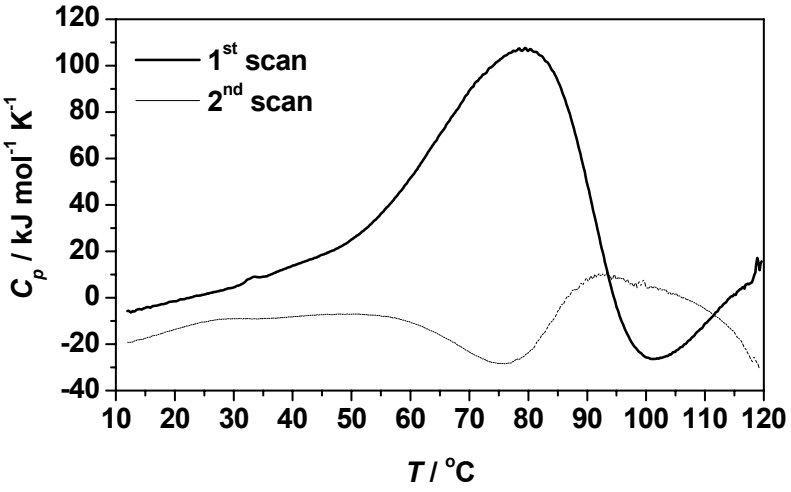

Fig. 4.31. DSC traces of the refolded confined RNase A in SBA-15.

4.6.3 Concluding remarks

The entrapment of protein RNase A was illustrated by entrapment of D-RNase A in SBA-15 and by subsequent refolding of the entrapped D-RNase A when the urea content was washed out from the system. This allows the high-yield entrapment of proteins if high enough concentration is provided. It also shows that the refolding behaviour of protein can be improved upon confinement.

Chapter 5

Conclusions

In this work, our approach was to encapsulate the model protein RNase A in various mesoporous silica materials, such as MCM-48, SBA-15, C_{16}-MCM-41, and C_{12}-MCM-41, with glasslike wall structure and well-defined pores to create a confined hydrophilic microenvironment. The average pore sizes of these materials are 25 Å, 58 Å, 40 Å, and 30 Å, respectively; and the specific pore volumes are 0.93 $cm^3\ g^{-1}$, 1.25 $cm^3\ g^{-1}$, 0.86 $cm^3\ g^{-1}$, and 0.70 $cm^3\ g^{-1}$, respectively.

It has been shown that all the mesoporous molecular sieves investigated have a high potential in fast immobilization of proteins. For the hexagonal phase materials MCM-41 and SBA-15, the amount of immobilized protein is a function of the pore size and specific pore volume, *i.e.*, SBA-15 > C_{16}-MCM-41 > C_{12}-MCM-41. The cubic, interwoven pore structure MCM-48 is probably more favorable for protein transfer and migration inside the mesopores. Although the pore size of cubic MCM-48 (2.5 nm) is smaller than that of hexagonal C_{12}-MCM-41 (3 nm), the amount of protein immobilized in MCM-48 is higher. For all the four materials investigated, the amount of immobilized protein decreases linearly with decreasing specific pore volume, *i.e.*, SBA-15 > C_{16}-MCM-41 > MCM-48 > C_{12}-MCM-41. The amount of immobilized protein can also be influenced by the electrical charge, the hydrophobicity, and the protein structure's stability. The protein loading was tuned by changing the pH of the protein solution and by introducing co-solvents. The maximum loading was achieved at pH 7 and 9, which is close to the PI of RNase A (9.6). The addition of chaotropes, such as urea, leads to an increased protein loading, *e.g.*, from 108 mg/g to 126 mg/g for 3.5 M urea in the case of MCM-48. On the other hand, low pH and addition of kosmotropes, such as glycerol, leads to lower protein loading, *e.g.*, from 108 mg/g to 98 mg/g for 3.5 M glycerol in the case of MCM-48. The main driving force for protein migration into MPS pores is probably

hydrophobic dehydration, however electrostatic interactions, hydrogen bonding, dipolar interactions and dispersive interactions also contribute to the adsorption affinity [Norde 1996, Roth 1993].

The differential scanning calorimetric (DSC) and pressure perturbation calorimetric (PPC) method was employed to evaluate the stability and volumetric as well as hydrational properties of the confined protein as a function of pH and at various co-solvent conditions. Due to a significant stabilization effect, the immobilized protein exhibits a large shift (about 30 °C at pH 5.5) in the unfolding temperature in confined space of 25-58 Å. The stabilization against temperature-induced unfolding is further enhanced with the protein immobilized at higher pH, *i.e.*, T_m for the confined protein increases from 98 °C at pH 5.5 to 107 °C at pH 9 in the case of C_{16}-MCM-41. Entrapping protein in MPS mesopores also offer protection from pH-denaturation and urea-denaturation.

The protein is partially entrapped in the mesopores upon mixing with the MPS. Some protein fraction still remains in bulk buffer solution and unfolds as normal bulk protein upon heating. The unfolded protein increases the solvent accessible surface area of the protein, resulting in an increased affinity towards adsorption at the silicate surface of the MPS. In the presence of urea, such a major adsorption process does not take place because the unfolded protein's SAS is largely bound by the ligand urea. Aggregation of the adsorbed unfolded protein is fostered in the presence of glycerol. The protein RNase A confined in the mesopores of MPS unfolds at much higher temperature compared to the bulk, probably not only due to the excluded volume effect but also an increased strength of the hydration of the protein in the narrow mesopores as shown in the PPC measurements. It was shown that the α and $d\alpha/dT$ values measured for the protein incorporated in the SBA-15, are drastically enhanced and pH dependent. For example, at pH 2.0, α(10 °C) and $d\alpha/dT$ values of 1.1×10^{-3} K^{-1} and -8.3×10^{-6} K^{-2}, at pH 5.5, α(10 °C) and $d\alpha/dT$ values of 1.4×10^{-3} K^{-1} and -1.5×10^{-5} K^{-2}, and at pH 9, α(10 °C) and $d\alpha/dT$ values of 2.1×10^{-3} K^{-1} and -2.9×10^{-5} K^{-2}, are obtained respectively, compared to corresponding values of 0.85×10^{-3} K^{-1} and -4.0×10^{-6} K^{-2} for RNase A in pure buffer solution. The much higher α and negative $d\alpha/dT$ values of the encapsulated protein indicate that the protein is much stronger hydrated in the silica pores. Also for the glycerol and urea containing protein samples, the confinement leads to an increase in unfolding temperature compared to bulk, *e.g.*, $\Delta T_m \approx 37$ °C in the presence of 3.5 M glycerol and $\Delta T_m \approx 35$ °C in the presence of 3.5 M urea.

The entrapment of protein RNase A was also illustrated by entrapment of D-RNase A in SBA-15 and by subsequent refolding of the entrapped D-RNase A when the urea content

was washed out from the system. This allows the high-yield entrapment of proteins if high enough concentration is provided. It also shows that the refolding behaviour of protein can be improved upon confinement.

In summary, confining protein in various MPS mesopores offers protection from denaturation forces, such as heat, pH and denaturant. Although it is still speculated that the confined protein forms aggregates, the support material with a fixed pore size should preclude normal three-dimensional aggregation.

Chapter 6

Zusammenfassung

In dieser Arbeit wurde das Modelprotein RNase A in verschiedene mesoporöse Silikatmaterialien, wie MCM-48, SBA-15, C_{16}-MCM-41 und C_{12}-MCM-41 eingekapselt. Diese Materialien besitzen eine glasähnliche Wandstruktur und definierte Poren, so dass sie eine begrenzte hydrophile Mikroumgebung bilden. Die durchschnittliche Porengröße dieser Materialien ist entsprechend 25 Å, 58 Å, 40 Å bzw. 30 Å.; die spezifischen Porenvolumina betragen 0.93 $cm^3\ g^{-1}$, 1.25 $cm^3\ g^{-1}$, 0.86 $cm^3\ g^{-1}$ bzw. 0.70 $cm^3\ g^{-1}$.

Es hat sich gezeigt, daß alle untersuchten mesoporösen Molekularsiebe ein hohes Potential aufweisen Proteine sehr schnell zu immobilisieren. Für die hexagonalen Phasenmaterialien MCM-41 und SBA-15 entspricht die Menge des immobilisierten Proteins einer Funktion aus Porengröße und dem spezifischen Porenvolumen (z.B. SBA-15 > C_{16}-MCM-41 > C_{12}-MCM-41). Die kubische, miteinanderverwobene Porenstruktur von MCM-48 scheint günstiger für den Proteintransfer und die Migration im Inneren der Mesoporen zu sein. Obwohl die Porengröße des kubischen MCM-48 (2.5 nm) kleiner ist als die des hexagonalen C_{12}-MCM-41 (3 nm), ist die Menge an immobilisiertem Protein im MCM-48 höher. Für alle vier untersuchten Materialien nimmt die Menge an immobilisiertem Protein mit abnehmendem spezifischem Porenvolumen ab (z.B. SBA-15 > C_{16}-MCM-41 > MCM-48 > C_{12}-MCM-41). Die Menge an immobilisiertem Protein kann ebenfalls durch die elektrische Ladung, die Hydrophobizität und der Stabilität der Proteinstruktur beeinflußt werden. Die Proteinbeladung wurde durch eine Veränderung des pH-Wertes der Proteinlösung und durch das Einführen von Co-Solventien eingestellt. Die maximale Beladung wurde bei pH 7 und 9 erreicht, was nahe am isoelektrischen Punkt der RNase A (9.6) ist. Das Hinzufügen von chaotropen Co-Solventien wie Urea, führt zu einer höheren Proteinbeladung, z.B. von 108 mg/g zu 126 mg/g für 3.5 M Urea im Falle von MCM-48. Andererseits führen ein geringerer

pH-Wert und das Hinzufügen von kosmotropen Co-Solventien wie Glycerol, zu einer geringeren Proteinbeladung, z.B. von 108 mg/g zu 98 mg/g für 3.5 M Glycerol bei Verwendung von MCM-48. Die hauptsächliche Antriebskraft für die Proteinmigration in die MPS Poren ist wahrscheinlich die hydrophobe Dehydratation, doch auch elektrostatische, dipolare und dispersive Wechselwirkungen sowie Wasserstoffbrückenbindungen tragen zur Adsorptionsaffinität bei [Norde 1996, Roth 1993].

Die "difference scanning calorimetry" (DSC) und die "pressure perturbation calorimetry" (PPC) wurden hier angewendet, um die Stabilität und die Volumenveränderung ebenso wie die Hydratationseigenschaften des eingeschlossenen Proteins als eine Funktion des pH-Wertes und verschiedener Co-Solventien zu evaluieren. Aufgrund eines signifikanten stabilisierenden Effekts, weist das immobilisierte Protein eine große Verschiebung (über 30°C bei pH 5.5) in der Entfaltungstemperatur im Raum von 25-58 Å auf. Diese Stabilisierung wird gegenüber der temperatur-induzierten Entfaltung weiterhin mit einem Protein verstärkt, welches bei höherem pH-Wert immobilisiert wird. Die Übergangstemperatur T_m für ein eingeschlossenes Protein z.B. steigt von 98°C bei pH 5.5 auf 107°C bei pH 9 im Falle von C_{16}-MCM-41; die maximale Proteinbeladung wurde nahe des isoelektrischen Punkts beobachtet. Es wurde ebenfalls herausgefunden, daß das Hinzufügen von kosmotropen (Glycerol) und chaotropen (Urea) Co-Solventien unterschiedliche Einflüsse auf die Proteinimmobilität und auf das Entfaltungsszenario hat.

In Verbindung mit MPS ist das Protein teilweise eingeschlossen. Jedoch ein Teil der Proteinfraktion verbleibt in der Pufferlösung und entfaltet wie ein freies, nicht eingeschlossenes Protein. Das entfaltete Protein vergrößert die für das Lösungsmittel zugängliche Oberfläche ("accessible surface area", ASA) des Proteins, was zu einer höheren Affinität der Adsorption an die Silikatoberfläche des MPS führt. Bei der Verwendung von Urea findet ein Adsorptionsprozess solchen Maßes nicht statt, da die ASA des entfalteten Proteins größtenteils von Urea gebunden wird. Eine Aggregation des adsorbierten entfalteten Proteins wird durch die Präsenz von Glycerol begünstigt. Das Protein RNase A, eingeschlossen in die Mesoporen des MPS, entfaltet bei sehr viel höheren Temperaturen im Vergleich zum freien Protein. Dies geschieht wahrscheinlich nicht nur wegen des ausgeschlossenen Volumens sondern auch wegen der Zunahme der Hydratation des Proteins in den engen Mesoporen, wie es die PPC Ergebnisse veranschaulichen. Es wurde gezeigt, dass α und $d\alpha/dT$ Werte für das Protein, eingebaut in SBA-15, sich drastisch verstärken und pH abhängig sind. Beispielsweise betrugen bei pH 2 die Werte für α(10°C) und $d\alpha/dT$ 1.1×10^{-3} K^{-1} und -8.3×10^{-6} K^{-2}, bei pH 5.5 α(10°C) und $d\alpha/dT$ 1.4×10^{-3} K^{-1} und -1.5×10^{-5} K^{-2} und bei

pH 9 α(10°C) und dα/dT 2.1×10^{-3} K^{-1} und -2.9×10^{-5} K^{-2}, verglichen mit den korrespondierenden Werten von 0.85×10^{-3} K^{-1} und -4×10^{-6} K^{-2} für RNase A in reiner Pufferlösung. Die sehr viel höheren α und niedrigeren dα/dT Werte für das eingekapselte Protein indizieren, dass das Protein in den Silikatporen stärker hydratisiert ist. Auch für die mit Glycerol und Urea beinhaltenden Proteinproben, führt das Einschließen zu einer Zunahme der Entfaltungstemperatur im Vergleich zum freien Protein. So beträgt z.B. $\Delta T_m \approx 37$°C bei Präsenz von 3.5 M Glycerol und ungefähr 35°C bei 3.5 M Urea. Doch immer noch ist es nicht ganz klar, ob und in welchem Maße, das eingeschlossene Protein Aggregate bildet. Was aber klar ist, ist dass das unterstützende Material mit einer festen Porenanzahl eine normale dreidimensionale Aggregation ausschließen sollte.

References

Acampora, G. and Hermans, J., J. Am. Chem. Soc. **89** (1967) 1543.

Affleck, R., Haynes, C. A. and Clark, D. S., Proc. Natl. Acad. Sci. USA **89** (1992) 5167.

Alberts, B., Bray, D., Lewis, J., Raff, M., Roberts, K. and Watson, J., Molecular Biology of the Cell, 3rd Edn., Garland Publishing, New York (1994).

Alexov, E., Eur. J. Biochem. **271** (2004) 173.

Alonso, D., Dill, K. and Stigter, D., Biopolymers **31** (1991) 1631.

Anderson, D. E., Becktel, W. J. and Dahlquist, F. W., Biochemistry **29** (1990) 2403.

Atyaksheva, L. F., Knyazeva, E. E., Poltorak, O. M., Chukhrai, E. S., Khomich, A. S. and Medved'ko, A. V., Russ. J. Phys. Chem. **78** (2004) 1849.

Avnir, D., Braun, S., Lev, O. and Ottolenghi, M., Chem. Mater. **6** (1994) 1605.

Azari, F. And Nemat-Gorgani, M., Biotech. Bioeng. **62** (1999) 193.

Azari, F., Hosseinkhani, S., Nemat-Gorgani, M., Appl. Biochem. Biotech. **94** (2001) 265.

Barrett, E. P., Joyner, L. G. and Halenda, P. P., J. Am. Chem. Soc. **73** (1951) 373.

Beck, J. S., Vartuli, J. C., Roth, W. J., Leonowicz, M. E., Kresge, C. T., Schmitt, K. D., Chu, C. T. W., Olson, D. H., Sheppard, E. W., McCullen, B. B., Higgins, J. B. and Schlenker, J. L., J. Am. Chem. Soc. **114** (1992) 10834.

Becktel, W. J. and Schellman, J. A., Biopolymers **16** (1987) 115.

Beece, D., Eisenstein, L., Frauenfelder, H., Good, D., Marden, M. C., Reinisch, L., Reynoids, A. S., Sorensen, L. B. and Yue, K. T., Biochemistry **19** (1980) 5147.

Behrens, P. and Stucky, G. D., Angew. Chem., Int. Ed. Engl. **32** (1993) 696.

Bellissent-Funel, M. C., Eur. Phys. J. E. **12** (2003) 83.

Bennion, B. J. and Daggett, V., Proc. Natl. Acad. Sci. USA **100** (2003) 5142.

van den Berg, B., Ellis, R. J. and Dobson, C. M., EMBO J. **18** (1999) 6927.

Bhatia, R. B., Brinker, C. J., Gupta, A. K. and Singh, A. K., Chem. Mater. **12** (2000) 2434.

Bookchin, R. M., Balasz, T., Wang, Z., Josephs, R. and Lew, V. L., J. Biol. Chem. **274** (1999) 6689.

Boyer, P., Hydrolysis: Peptide Bonds, Vol. III., Academic Press, New York (1971).

Brandts, J. F. And Hunt, L., J. Am. Chem. Soc. **89** (1967) 4826.

Brandts, J. F., Oliveira, R. J. and Westort, C., Biochemistry **9** (1970) 1038.

Brandts, J. F. and Lin, L.-N., Thermochim. Acta **414** (2004) 95.

Brinker, A., Pfeifer, G., Kerner, M. J., Nayloe, D. J., Hartl, F. U. And Hayer-Hartl, M., Cell **107** (2001) 223.

Brunauer, S., Emmett, P. H. and Teller, E., J. Am. Chem. Soc. **60** (1938) 309.

Bull, H. B. and Breese, K., J. Phys. Chem. **72** (1968) 1817.

Burger, A. M., Steidle, C., Fiebig, H. H., Frick, E., Scholmerich, J. and Kreutz, W., Clin. Cancer Res. **5** (1999) 10 78.

Burova, T. V., Grinberg, N. V. Grinberg, V. Y., Rariy, R. Y. and Klibanov, A. M., Biochim. Biophys. Acta **1478** (2000) 309.

Carrea, G. and Riva, S., Angew. Chem., Int. Ed. Engl. **39** (2000) 2226.

Chalikian, T. V. and Breslauer, K. J., Biopolymers **39** (1996) 619.

Chalikian, T. V., J. Phys. Chem. B **105** (2001) 12566.

Chalikian, T. V., Ann. Rev. Biophys. Biomol. Struct. **32** (2003) 207.

Chebotareva, N. A., Kurganov, B. I. and Livanova, N. B., Biochemistry (Moscow) **69** (2004) 1239.

Cheung, M. S. and Thirumalai, D., J. Mol. Biol. **357** (2006) 632.

Chiti, F., Taddei, N., Bucciantini, M., White, P., Ramponi, G. and Dobson, C. M., EMBO J. **19** (2000) 1441.

Chothia, C., Annu. Rev. Biochem. **53** (1984) 537.

Cole, N. and Ralston, G. B., Int. J. Biochem. **26** (1994) 799.

Cooper, A., Proc. Natl. Acad. Sci. USA **73** (1976) 2740.

Cooper, A., Prog. Biophys. Mol. Biol. **44** (1984) 181.

Corma, A., Navarro, M. T. and Pariente, J. P., J. Chem. Soc., Chem Commun. (1994) 147.

Czeslik, C. and Winter, R., Phys. Chem. Chem. Phys. **3** (2001) 235.

Dave, B. C., Dunn, B., Valentine, J. S. and Zink, J. I., Anal. Chem. **66** (1994) 1120A.

Davenport, H. W., Physiology of the Digestive Tract., Medical Publishers Incorporated, Chicago, IL (1966).

Davis, M. E., Saldarriaga, C., Montes, C., Garces, J. and Crowder, C., Nature **331** (1988) 698.

Diaz, J. F. and Balkus, K. J., J. Mol. Catal. B: Enzym. **2** (1996) 115.

Deere, J., Magner, E., Wall, J. G. and Hodnett, B. K., Chem. Commun. (2001) 465.

Deere, J., Magner, E., Wall, J. G. and Hodnett, B. K., J. Phys. Chem. B **106** (2002) 7340.

Deere, J., Magner, E., Wall, J. G. and Hodnett, B. K., Biotechnol. Prog. **19** (2003) 1238.

Dessau, R. M., Schlenkar, J. L. and Higgins, J. B., Zeolites **10** (1990) 522.

Dubins, D. N., Filfil, R., Macgregor, R. B. and Chalikian, T. V., Biochemistry **42** (2003) 8671.

Dubois, M., Gulik-Krzywicki, T. H. and Cabane, B., Langmuir **9** (1993) 673.

van Dulm, P., Norde, W. and Lyklema, J., J. Colloid Interface Sci. **82** (1981) 77.

Dunbar, J, Yennawar, H. P., Banerjee, S., Luo, J. and Farber, G. K., Prot. Sci. **6** (1997) 1727.

Durchschlag, H. and Zipper, P., Progr. Colliod Polym. Sci. **127** (2004) 98.

Dzwolak, W., Ravindra, R. and Winter, R., Biochemistry **42** (2003) 11347.

Dzwolak, W., Ravindra, R., Nicolini, C., Jansen, R. and Winter, R., J. Am. Chem. Sci. **126** (2004) 3762.

Estermann, M., McCusker, L. B., Baerlocher, C., Merrouche, A. and Kessler, H., Nature **352** (1991) 320.

Eggers, D. K. and Valentine, J. S., J. Mol. Biol. **314** (2001a) 911.

Eggers, D. K. and Valentine, J. S., Protein Sci. **10** (2001b) 250.

Ellis, R. J., Trends Biochem. Sci. **26** (2001) 597.

Fadnavis, N. W., Bhaskar, V., Kantam, M. L. and Choudary, B. M., Biotech. Prog. **19** (2003) 46.

Fan, J., Lei, J., Wang, L. M., Yu, C. Z., Tu, B. and Zhao, D. Y., Chem. Commun. (2003a) 2140.

Fan, J., Yu, C. Z., Gao, T., Lei, J., Tian, B. Z., Wang, L. M., Luo, Q., Tu, B., Zhou, W. Z. and Zhao, D. Y., Angew. Chem., Int. Ed. **42** (2003b) 3146.

Fenimore, P. W., Frauenfeder, H., McMahon, B. H. and Parak, F. G., Proc. Natl. Acad. Sci. USA **99** (2002) 16047.

Fersht, A., Structure and Mechanism in Protein Science, W. H. Freeman and Company, New York (1999).

Frauenfelder, H., Hartmann, H., Karplus, M., Kuntz, I. D., Kuriyan, J., Parak, F., Petsko, G. A., Ringe, D., Tilton, R. F., Conolly, M. I. and Max, N., Biochemistry **26** (1987) 254.

Frenkel-Mullerad, H. and Avnir, D., J. Am. Chem. Soc. **127** (2005) 8077.

Galan, A., Sot, B., Llorca, O., Carrascosa, J. L., Valpuesta, J. M. and Muga, A., J. Biol. Chem. **276** (2001) 957.

Gekko, K. and Timasheff, S. N., Biochemistry **20** (1981) 4667.

Giddings, J. C., Kucera, E., Russell, C. P. and Myers, M. N., J. Phys. Chem. **72** (1968) 4397.

Gies, H., Grabowski, S., Bandyopadhyay, M., Grünert, W., Tkachermko, O. P., Klementiev, K. V. and Birkner, A., Micropor. Mesopor. Mater. **60** (2003) 31.

Gregory, R. B. (Ed.), Protein-Solvent Interactions, Marcel Dekker, New York (1995).

Guiton, A., Textbook of Medical Physiology, W. B. Saunders Company, Philadelphia (1976).

Han, Y.-J., Stucky, G. D. and Butler, A., J. Am. Chem. Soc. **121** (1999) 9897.

Han, Y.-J., Watson, J. T., Stucky, G. D. and Butler, A., J. Mol. Catal. B: Enzym. **17** (2002) 1.

Harding, S. E., Rowe, A. J. and Horton, J. C. (Ed.), Analytical Unltracentrifugation in Biochemistry and Polymer Science, Royal Society of Chemistry, Cambridge (1992).

Hall, D. and Minton, A. P., Biochim. Biophys. Acta **1649** (2003) 127.

Haque, I., Singh, R., Moosavi-Movahedi, A. A. and Ahmad, F., Biophys. Chem. **117** (2005) 1.

Harrison, B. and Zimmermann, S. B., Nucleic Acids Res. **14** (1986) 1863.

Hartmann, M. and Vinu, A., Langmuir **18** (2002) 8010.

Hartmann, M., Chem. Mater. **17** (2005) 4577.

Haynes, C. A. and Norde, W., Colloid Surfaces B: Biointerfaces **2** (1994) 517.

Heerklotz, H. and Seelig, J., Biophys. J. **82** (2002) 1445.

Heerklotz, H., J. Phys.: Condens. Matter **16** (2004) R441.

Heilmann, A., Teuscher, N., Kiesow, A., Janasek, D. and Spohn, U., J. Nanosci. Nanotech. **3** (2003) 375.

Hiebl, M. and Maksymiw, R., Biopolymers **31** (1991) 161.

Hill, T. L., An Introduction to Statistical Thermodynamics, Addison-Wesley, Reading (1962).

Hinz, H. J. and Meyer, R., Biophys. Chem. **52** (1994) 275.

Honig, B. and Nicholls, A., Science **268** (1995) 1144.

Hoppert, M. and Mayer, F., Am. Sci. **87** (1999) 518.

Hou, Q., Margolese, D. I., Ciesla, U., Feng, P., Gier, T. E., Sieger, P., Leon, R., Petroff, P. M., Schüth, F. and Stucky, G. D., Nature 368 (1994) 317.

Iler, R. K., The Chemistry of Silica, Wiley, New York (1979).

Jackler, G., Steitz, R. and Czeslik, C., Langmuir **18** (2002) 6565.

Jie, L., Jie, F., Yu, C.-Z., Zhang, L.-Y., Jiang, S.-Y., Bo, T. and Zhao, D.-Y., Micropor. Mesopor. Mater. **73** (2004) 121.

Kauzmann, W., *Nature* **325** (1987) 763.

Khurana, R., Hate, A., Nath, U. and Udgaonkar, B., Protein Sci. **4** (1995) 1133.

Kidoaki, S. and Yoshikawa, K., Biophys. Chem. **76** (1999) 133.

Kim, J., Grate, J. W. and Wang, P., Chem. Eng. Sci. **61** (2006) 1017.

Kisler, J. M., Dähler, A., Stevens, G. W. and O'Connor, A. J., Micropor. Mesopor. Mater. **44** (2001a) 769.

Kisler, J. M., Stevens, G. W. and O'Connor, A. J., Mater. Phys. Mech. **4** (2001b) 89.

Klafter, J. and Drake, J. M. (Ed.), Molecular Dynamics in Restricted Geometries, John Wiley, New York (1989).

Klibanov, A. M., Science **219** (1983) 722.

Klibanov, A. M., Trends Biotechnol. **15** (1997) 97.

Klibanov, A. M., Nature **409** (2001) 241.

Knubovels, T. and Osterhout, J. J., Connoly, P. J., and Klibanov, A. M., Proc. Natl. Acad. Sci. USA **96** (1999) 1262.

Kresge, C. T., Leonowicz, M. E., Roth, W. J., Vartuli, J. C. and Beck, J. S., Nature **359** (1992) 710.

Kujawa, P. and Winnik, F. M., Macromolecules **34** (2001) 4130.

Kuntz I. D. Jr and Kauzmann W., Adv. Prot. Chem. **28** (1974) 239.

Landis, M. E., Aufdembrink, B. A., Chu, P., Johnson, I. D., Kirker, G. W. and Rubin, M. K., J. Am. Chem. Soc. **113** (1991) 3189.

Lei, C. H., Shin, Y. S., Liu, J. and Ackerman, E. J., J. Am. Chem. Soc. **124** (2002) 11242.

Lei, J., Fan, J., Yu, C.-Z., Zhang, L.-Y., Jiang, S.-Y., Tu, B. and Zhao, D.-Y., Micropor. Mesopor. Mater. **73** (2004) 121.

Likhodi, O. and Chalikian, T. V., J. Am. Chem. Soc. **122** (2000) 7860.

Lin, L. N., Brandts, J. F., Brandts, J. M. and Plotnikov, V., Anal. Biochem. **302** (2002) 144.

Lindner, R. and Ralston, G., Biophys. Chem. **57** (1995) 15.

Lindner, R. and Ralston, G., Biophys. Chem. **66** (1997) 57.

Liu, B., Hu, R. and Deng, J., Anal. Chem. **69** (1997a) 2343.

Liu, B., Hu, R. and Deng, J., Analyst **122** (1997b) 821.

Liu, Y.-S, Gotte, G., Libonati, M. and Eisenberg, D., Nat. Struct. Biol. **8** (2001) 211.

Liu, B., Cao, Y., Chen, D., Kong, J. and Deng, J., Anal. Chim. Acta **478** (2003) 59.

Makhatadze, G. I., Medvedkin, V. N. and Privalov, P. L., Biopolymers **30** (1990) 1001.

McPhie, P., Biochemistry **11** (1972) 879.

Meier, W. M. and Olson, D. H., Atlas of Zeolite Structure Types, 2nd Edn, Butterworths, London (1988).

Merzel, F. and Smith, J. C., Proc. Natl. Acad. Sci. USA **99** (2002) 5378.

Minton, A. P., Biochemistry **20** (1981a) 4821.

Minton, A. P., Biopolymers **20** (1981b) 2093.

Minton, A. P., Biophys. J. **63** (1992) 1090.

Minton, A. P., Biophys. J. **68** (1995) 1311.

Minton, A. P., Methods Enzymol. **295** (1998) 127.

Minton, A. P., Biophys. J. **78** (2000a) 101.

Minton, A. P., Curr. Opin. Struct. Biol. **10** (2000b) 34.

Minton, A. P., J. Mol. Biol. Chem. **276** (2001) 10577.

Minton, A. P., Curr. Biol. **16** (2006) R270.

Miyahara, M., Vinu, A., Hossain, K. Z., Nakanishi, T and Ariga, K., Thin Solid Film **499** (2006) 13.

Moore, P. B. and Shen, J., Nature **306** (1983) 356.

Muramatsu, N. and Minton, A. P., Proc. Natl. Acad. Sci. USA **85** (1988) 2984.

Murphy, L. D. and Zimmermann, S. B., Biochim. Biophys. Acta **1219** (1994) 277.

Murphy, L. D. and Zimmermann, S. B., Biophys. Chem. **57** (1995) 71.

Naimushin, A. N., Quach, N., Fujimoto, B. S. and Schurr, J. M., Biopolymers **58** (2001) 204.

Nir, S., Prog., Surface Sci. **8** (1977) 1.

Nocek, J. M., Hatch, S. L., Seifert, J. L., Hunter, G. W., Thomas, D. D. and Hoffman, B. M., J. Am. Chem. Soc. **124** (2002) 9404.

Norde, W. and Lyklema, J., J. Colloid Interface Sci. **66** (1981) 285.

Norde, W. and Favier, J. P., Colloids and Surfaces **66** (1992) 299.

Norde, W., Macromol. Symp. **103** (1996) 5.

Ogston, A. G., Preston, B. N. and Wells, J. D., Proc. R. Soc. Lond. A **353** (1973) 297.

Pace, C.N., Laurents, D.V. and Thomson, J.A., Biochemistry **29** (1990) 2564.

Pace, C.N., Laurents, D.V. and Erickson, R.E., Biochemistry **31** (1992) 2728.

Panick, G. and Winter, R., Biochemistry **39** (2000) 1862.

Ping, G., Yuan, J.-M., Vallieres, M., Dong, H., Sun, Z., Wei, Y., Li, F.-Y. and Lin, S.-H., J. Chem. Phys. **118** (2003) 8042.

Ping, G., Yuan, J.-M., Sun, Z.-F. and Wei, Y., J. Mol. Recog. **17** (2004) 433.

Pinnavaia, T. J., Science **220** (1983) 365.

Pohl, F. M., J. Biochem. **7** (1969) 146.

Pots, A., Jongh, H., Gruppen, H., Hessing, M. and Voragen, A. J., Agric. Food Chem. **46** (1998) 2546.

Privalov, P. L., Khechinashvili, N. N. And Atanasov, B. P., Biopolumers **10** (1971) 1875.

Privalov, P. L., Adv. Prot. Chem. **33** (1979) 167.

Ralston, G. B., J. Chem. Educ. **67** (1990) 857.

Randzio, S. L., Thermochim. Acta **398** (2003) 75.

Rariy, R. V. and Klibanov, A. M., Proc. Natl. Acad. Sci. USA **94** (1997) 13520.

Ravindra, R. and Winter, R., Chem. Phys. Chem. **4** (2003a) 359.

Ravindra, R. and Winter, R., Z. Phys. Chem. **217** (2003b) 1221.

Ravindra, R., Royer, C. and Winter, R., Phys. Chem. Chem. Phys. **6** (2004a) 1952.

Ravindra, R., Zhao, S., Gies, H. and Winter, R., J. Am. Chem. Soc. **126** (2004b) 12224.

Reddy, K. M., Moudralovski, I. and Sayari, A., J. Chem. Soc., Chem. Commun. (1994) 1059.

Rholam, M., Scarlata, S. and Weber, G., Biochemistry **23** (1984) 6793.

Richards, F. M., Annu. Rev. Biophys. Bioeng. **6** (1977) 151.

Richards, F. M., Methods Enzymol. **115** (1985) 440.

Richards, F. M., Protein Folding (Ed. Creighton, T. E.), New York, Freeman (1992) 1.

Richards, F. M. and Lim, F. A., Q. Rev. Biophys. **26** (1994) 423.

Rivas, G., Fernández, J. A. and Minton, A. P., Biochemistry **38** (1999) 9379.

Rivas, G., Fernández, J. A., and Minton, A. P., Proc. Natl. Acad. Sci. USA **98** (2001) 3150.

Rivas, G. and Minton, A. P., Biochem. Soc. Trans. **31** (2003) 1015.

Roth, C. M. and Lenhoff, A. M., Langmuir **9** (1993) 962.

Rösgen, J. and Hinz, H. J., J. Biophys. Chem. **83** (2000) 61.

Rupley, J. A. and Careri, G., Adv. Prot. Chem. **41** (1991) 37.

Sasaki, T., Kajino, T., Li, B., Sugiyama, H. and Takahashi, H., App. Env. Microbiol. **67** (2001) 2208.

Sasisanker, P., Oleinikova, A., Weingärtner, H., Ravindra, R. and Winter, R., Phys. Chem. Chem. Phys. **6** (2004) 1899.

Schaefer, M., Sommer, M. and Karplus, M., J. Phys. Chem. **101** (1997) 1663.

Shaw, K., Grimsley, G., Yakovlev, G., Makarov, A. and Pace, N., Protein Sci. **10** (2001) 1206.

Simon, S., Drug Discovery Today **4** (1999) 32.

Smith, P. E., J. Phys. Chem. B **103** (1999) 525.

Steadman, B. L., Thompson, K. C., Middaugh, C. R., Matsun, K., Vrona, S., Lawson, E. Q. and Lewis, R. V., Biotechnol. Bioeng. **40** (1992) 8.

Stempfer, G., Höll-Neugebauer, B. and Rudolph, R., Nat. Biotech. **14** (1996) 329.

Su, T. J., Green, R. J., Wang, Y., Murphy, E. F., Lu, J. R., Ivkov, R. and Satija, S. K., Langmuir **16** (1998) 4999.

Svergun, D. I., Richard, S., Koch, M. H. J., Sayers, Z., Kuprin, S. and Zaccai, G., Proc. Natl. Acad. Sci. USA **95** (1998) 2267.

Takahashi, H., Li, B., Sasaki, T., Miyazaki, C., Kajino, T. and Inagaki, S., Chem. Mater. **12** (2000) 3301.

Takahashi, H., Li, B., Sasaki, T., Miyazaki, C., Kajino, T. and Inagaki, S., Micropor. Mesopor. Mater. **44** (2001) 755.

Tanaka, H., J. Chem. Phys. **112** (2000) 799.

Tilton, R. F., Dewan, J. C. and Petskp, G. A., Biochemistry **31** (1992) 2469.

Timasheff, S. N., Annu. Rev. Biophys. Biomol. Struct. **22** (1993) 67.

Timasheff, S. N., Adv. Prot. Chem. **51** (1998) 355.

Tindwa, R. M., Ellis, D. K., Peng, G. Z. and Clearfield, A., J. chem. Soc. Faraday Trans. 1, **81** (1985) 545.

Uversky, V. N., Gillespie, J. R., Fink, A. L., Prot. Struct. Funct. Genet. **41** (2000) 415.

Uversky, V. N., Prot. Sci. **11** (2002a) 739.

Uversky, V. N., Eur. J. Biochem. **269** (2002b) 2.

Vallet-Regi, M., Ramila, A., del Real, R. P. And Perez-Pariente, J., Chem. Mater. **13** (2001) 308.

Vanderkooi, J. M., Biochim. Biophys. Acta **1386** (1998) 241.

Vartuli, J. C., Schmitt, K. D. and Kresge, C. T., Chem. Mater. **6** (1994) 2317.

Vaughan, D. E. W. and Lussier, R. J., Proc. 5th int. Conf. Zeolites (Ed. L. V. C. Rees), Heyden, London (1980) 94.

Vaughan, D. E. W., Am. Chem. Soc. Symp. Series **368** (1988) 308.

Vidugiris, G. J. A., Markley, J. L. and Royer, C. A., Biochemistry **34** (1995) 4909.

Vinu, A., Murugesan, V. and Hartmann, M., J. Phys. Chem. B **108** (2004a) 7323.

Vinu, A., Murugesan, V., Tangermann, O. and Hartmann, M., Chem Mater. **16** (2004b) 3056.

Walser, R. and van Gunsteren, W. F., Proteins-Struct. Funct. Genet. **42** (2001) 414.

Warshel, A., Biochemistry **20** (1981) 3167.

Warshel, A. and Russell, S., Quart. Rev. Biophys. **17** (1984) 283.

Washmon-Kriel, L., Jimenez, V. L., and Balkus, K. J., Jr., J. Mol. Catal. B **10** (2000) 453.

Weetall, H. H., Appl. Biochem. Biotech. **41** (1993) 157.

Weetall, H. H., Biosens. Bioelectron. **11** (1996) 327.

Whitten, S. and Garcia-Moreno, B., Biochemistry 39 (2000) 14292.

Wright, P. E. and Dyson, H. J., J. Mol. Biol. **293** (1999) 321.

Xing, G.-W., Li, X.-W., Tian, G.-L. and Ye, Y.-H., Tetrahedron **56** (2000) 3517.

Yanagisawa, T., Shimizu, Kazuyuki, T., K. and Kato, C., Bull. Chem. Soc. Jpn. **63** (1990) 988.

Yang, P., Zhao, D., Margolese, D., Chmelka, B. F. and Stucky, G. D., Nature **396** (1998) 152.

Yiu, H. H. P., Wright, P. A. and Botting, N. P., J. Mol. Catal. B: Enzym. **15** (2001) 81.

Yiu, H. H. P. and Wright, P. A., J. Mater. Chem. **15** (2005) 3690.

Young, A. C., Tilton, R. F. and Dewan, J. C., J. Mol. Biol. **235** (1984) 302.

Yu, C., Fan, J., Tian, B., Zhao, D. and Stucky, G. D., Adv. Mater. **14** (2002) 1742.

Zhao, D., Huo, Q., Feng, J., Chmelka, B. F. and Stucky, G. D., J. Am. Chem. Soc. **120** (1998a) 6024.

Zhao, D., Feng, J., Huo, Q., Melosh, N., Fredrikson, G., Chmelka, B. F. and Stucky, G. D., Science **279** (1998b) 548.

Zhou, H.-X. and Dill, K. A., Biochemistry **38** (2001) 11289.

Zhou, H.-X., Acc. Chem. Res. **37** (2004a) 123.

Zhou, H.-X., J. Mol. Recognit. **17** (2004b) 368.

Zimmerman, S. B. and Minton, A. P., J. Mol. Biol. **222** (1991) 599.

Zimmerman, S. B. and Minton, A. P., Annu. Rev. Biophys. Biomol. Struct. **22** (1993) 27.

List of Abbreviations:

AA	Amino acid
CD	Circular dichroism
CPG	Controlled porous glass
cyt c	Cytochrome c
DNA	Deoxyribonucleic acid
DSC	Differetial scanning calorimetry
DTT	Dithiothreitol
E. coli	*Escherichia coli*
EDTA	Ethylenediaminetetraacetic acid
FT-IR	Fourier transform infrared
ITC	Isothermal titration calorimetry
IUPAC	International union of pure and applied chemistry
LYS	Lysozyme
MCM	Mobile composition of matter
MPS	Mesoporous silicate
PEG	Polyethylene glycol
PI	Isoelectric point
PPC	Pressure perturbation calorimetry
PZC	Point of zero charge
RNase A	Ribonuclease A
SAS	Surface accessible area
SBA	Santa barbara material
UV	Ultraviolet
ZPC	Point of zero charge

Acknowledgements

From experience I can tell that the last pages of a Ph.D. thesis may be the most widely read pages of the entire publication. It is here where you think you will find out whether you have meant something in the life of the Ph.D. candidate.

This work would not have been possible without the contributions of many, many people and, organizations, which, if are all listed here, could possibly need another hundred pages. So if you do not find your name below but feel you deserve my appreciation – just take it without hesitate!

My deepest gratitude goes first and foremost to Prof. Dr. Roland Winter, my supervisor, for allowing me do my dissertation here in Dortmund (not far from my husband!), for giving me this interesting research topic, and for the constant encouragement and guidance. He has walked me through all the stages of my Ph.D. study, given me so much support and advice, put in me large trust, and shown me contagious enthusiasm and numerous bright ideas**.** I would like to thank him also for providing the best possible working conditions, both socially and instrumentally. There are not so many people in the world who have the opportunity to work with PPC, I am lucky enough to be among them.

I thank also Prof. J. P. Pohl and PD. Dr. C. Czeslik for being my examination committee.

I thank Prof. Dr. H. Gies (Institute of Geology, Mineralogy & Geophysics**,** Ruhr-Universität-Bochum) and Prof. Dr. M. Hartmann (Institute of Physics, Universität Augsburg) for providing the MPS samples.

I would like to thank International Max Planck Research School in Chemical Biology for the financial assistance.

I always feel how important it is to work together with the people you like and how lucky I am that I spent the most significant three years of my life together with all colleagues in the group of Prof. Dr. Roland Winter's, who made these years so enjoyable and memorable for me. I love the equally healthy and international mix of people in PC I. Firstly, Ravi (Dr. Revanur Ravindra) was my first office mate and I thank him for introducing me to the DSC and PPC instrument and for sharing with me so much interesting things about India. Lally,

most of the time I work together with her and she is really my happy fairy. I especially thank her for writing Zusammenfassung. I am also grateful to Claus who seems to be omnipotent. Whenever I had troubles I went to him, and he was always of help. I also acknowledge Andrea, our secretary, Dr. Horstmann, Mr. Saskovic, and Berti, for their kind help. I would like to specially mention my office mates, Vytautas and Micheal, I thank them for sharing with me so much happy time. I also thank Ewa, Nadeem, Karsten and Dahabada for their help and friendship. In all, the staff members in PC I (for the whole list, refer to our website please!) all deserve my appreciation.

I would like to thank all my Chinese friends in Dortmund for their pure-hearted friendship.

Last but not least, I thank
my parents and grandparents, for their endless and selfless love and support, and
my husband for loving me so much.

Shuang Zhao, Dortmund, February 2007